UCLA
UCLA Electronic Theses and Dissertations

Title

An Assessment of Glioblastoma Metabolism Reveals Pathway-Specific Targets for Therapy

Permalink

https://escholarship.org/uc/item/5f1919rc

Author

Sperry, Jantzen

Publication Date

2019

Peer reviewed|Thesis/dissertation

UNIVERSITY OF CALIFORNIA

Los Angeles

An Assessment of Glioblastoma Metabolism Reveals Pathway-Specific Targets for Therapy

A dissertation submitted in partial satisfaction of

the requirements for the degree Doctor of Philosophy in

Molecular and Medical Pharmacology

by

Jantzen Sperry

2019

ABSTRACT OF THE DISSERTATION

An Assessment of Glioblastoma Metabolism Reveals Pathway-Specific Targets for Therapy

by

Jantzen Sperry

Doctor of Philosophy in Molecular and Medical Pharmacology

University of California, Los Angeles, 2019

Professor Harley I. Kornblum, Chair

Glioblastoma (GBM) remains the most common and lethal primary brain tumor in adults despite concerted efforts to establish more effective treatments. The oncogenic-associated alterations that make GBM cells metabolically distinct from surrounding tissue also represent prime targets for the development of novel therapies. Due to the interconnectivity of signaling networks and the overall heterogeneity of the disease, identifying key metabolic pathways that drive neoplastic pathogenesis is essential to establishing more effective therapeutic strategies. In this dissertation, we performed expression analysis and unbiased metabolomics to better characterize metabolic differences between a cohort of patient-derived isocitrate dehydrogenase 1 (IDH1) mutant and wildtype gliomasphere cultures. This analysis revealed clear, cell type-specific differences in glucose metabolism, nucleotide synthesis utilization, and DNA repair capacity following radiation that could be exploited for therapy. Furthermore, we investigated the ability of GBM cells to oxidize fatty acids (FAO) and ketone bodies to support tumor growth, while also interrogating the effectiveness of the ketogenic diet (KD) as an adjuvant therapy for GBM. We

ii

discovered extensive FAO utilization throughout the GBM metabolome, identified CPT1A as a potential therapeutic target, and determined that the KD can have adverse effects on tumor growth.

The dissertation of Jantzen Sperry is approved.

Heather R. Christofk

Albert Lai

Robert M. Prins

Harley I. Kornblum, Committee Chair

University of California, Los Angeles

2019

Dedication

This work is dedicated to my wife, Mia Brett, who has been an unwavering source of love, support, patience, and encouragement. You are my inspiration. I cannot express how truly grateful I am to have you in my life.

Table of Contents

List of Figures

Chapter 3 (continued)

List of Tables

Acknowledgements

This work was generated under the thoughtful guidance, support, and creative scientific insight of Dr. Harley Kornblum. It was a both a pleasure and privilege to have him as a mentor and collaborator on this work.

I would like to acknowledge the invaluable insight and training provided by my thesis committee members: Dr. Heather Christofk, Dr. Robert Prins, and Dr. Albert Lai. I am grateful for their knowledge, support, and gracious participation in bringing this dissertation to fruition.

Chapter 2 of this dissertation contains an adapted version of the published work: Metabolic characterization of isocitrate dehydrogenase (IDH) mutant and IDH wildtype gliomaspheres uncovers cell type-specific vulnerabilities. Matthew Garrett and Jantzen Sperry, Daniel Braas, Weihong Yan, Thuc M. Le, Jack Mottahedeh, Kirsten Ludwig, Ascia Eskin, Yue Qin, Rachelle Levy, Joshua J. Breunig, Frank Pajonk, Thomas G. Graeber, Caius G. Radu, Heather Christofk, Robert M. Prins, Albert Lai, Linda M. Liau, Giovanni Coppola, and Harley I. Kornblum[1].

Chapter 3 of this dissertation is a version of a manuscript in preparation for publication: Metabolism of fatty acids and ketone bodies for growth by glioblastoma: Implications for Ketogenic Diet Therapy. Jantzen Sperry, Janel E. Le Belle, Michael C. Condro, Lea Guo, Daniel Braas, Nathan Vanderveer-Harris, Kristen K.O. Kim, Whitney B. Pope, Ajit S. Divakaruni, Albert Lai, Heather Christofk, Harley I. Kornblum.

I would like to acknowledge the contribution of these scientists and collaborators:

Daniel Braas: Assistance and analysis of labeled-substrate LC-MS experiments.

Joshua J. Breunig: Generated and provided the IDH1 mutant overexpression vector.

Michael C. Condro: Culture maintenance, xenotransplantation experiments, virus production.

Biographical Sketch

Jantzen Sperry

Education

2013-2019 University of California, Los Angeles, Los Angeles, CA

PhD Candidate, Department of Molecular and Medical Pharmacology

2004-2008 Brigham Young University, Hawaii, Laie, HI

B.S. Pre-Professional Biology

Academic and Professional Honors

Certificate of Distinction in Teaching, UCLA Life Sciences Core Education, 2015-2016

Graduated with Honors, Brigham Young University, Hawaii, 2008.

Selected Peer-Reviewed Publications

Garrett, M and J Sperry, Braas D, Yan W, Le TM, Mottahedeh J, Ludwig K, Eskin A, Qin Y, Levy R, Breunig JJ, Pajonk F, Graeber TG, Radu CG, Christofk H, Prins RM, Lai A, Liau LM, Coppola G, and Kornblum HI. Metabolic characterization of isocitrate dehydrogenase (IDH) mutant and IDH wildtype gliomaspheres uncovers cell type-specific vulnerabilities. Cancer Metabolism, 2018; 6(4).

Laks DR, Oses-Prieto JA, Alvarado AG, Nakashima J, Chand S, Azzam DB, Gholkar AA, Sperry J, Ludwig K, Condro MC, Nazarian S, Cardenas A, Shih MYS, Damoiseaux R, France B,

Orozco N, Visnyei K, Crisman TJ, Gao F, Torres JZ, Coppola G, Burlingame AL, Kornblum HI. A molecular cascade modulates MAP1B and confers resistance to mTOR inhibition in human glioblastoma. Neuro Oncology, 2018; 20(6):764-775.

Laks DR, Crisman TJ, Shih MY, Mottahedeh J, Gao F, Sperry J, Garrett MC, Yong WH, Cloughesy TF, Liau LM, Lai A, Coppola G, and Kornblum HI. Large-scale assessment of the gliomasphere model system. Neuro Oncology, 2016; 18(10):1367-78.

Le Belle JE, Sperry J, Ngo A, Ghochani Y, Laks DR, López-Aranda M, Silva AJ, and Kornblum HI. Maternal inflammation contributes to brain overgrowth and autism-associated behaviors through altered redox signaling in stem and progenitor cells. Stem Cell Reports, 2014; 3(5):725-34.

Chapter 1

Introduction

Hallmarks of Cancer

Oncogenesis is the process through which normal cells of the body transform into cancer cells. This multifactorial progression includes a series of genetic alterations, such as oncogene activation or tumor suppressor inactivation, followed by complex cellular changes that result in unrestricted cell growth. With more than 100 distinct types of cancer, a far greater number of associated cancer subtypes, and an estimated 1.7 million new cases of cancer diagnosed in 2018 in the United States alone, cancer is at the forefront of health concerns facing modern society[2]. In an effort to elucidate the essential characteristics of cancer and to help "the complexities of the disease […] become understandable in terms of a small number of underlying principles," Hanahan and Weinberg outlined six fundamental physiologic changes that regulate malignant progression[3]. These changes include self-sufficiency in growth signals, limitless replicative potential, evasion of programmed cell death, insensitivity to growth-inhibitory signals, sustained angiogenesis, and tissue invasion and metastasis. Over a decade later, these *Hallmarks of Cancer* were amended to include two additional emerging hallmarks: reprogramming of energy metabolism and evading immune destruction[4]. Understanding the mechanisms through which cancer cells reprogram their metabolism, a process referred to as metabolic transformation and the primary focus of the work presented here, represents a critical step to developing and improving precision cancer therapies.

Glioma

One particular type of cancer that epitomizes the hallmarks set forth by Hanahan and Weinberg is glioma. Glioma comprises a broad category of brain tumors that develop from the supportive cells of the central nervous system (CNS). Gliomas make up nearly 30% of all primary CNS tumors and approximately 80% of malignant brain tumors[5, 6]. Gliomas are classified by regional location of the tumor, histologic characterization according to the cell type with which they share defined characteristics, and by pathologic criteria defined by the World Health Organization (WHO)[7, 8]. Low grade gliomas (grades 1 and 2) are well-differentiated, slow-growing or benign tumors that are associated with better prognoses. High grade gliomas (grades 3 and 4) are anaplastic, malignant tumors characterized histologically by increased cellularity, necrosis, and vascular proliferation[9, 10]. Glioblastoma (GBM), a grade IV astrocytoma, comprises 54% of all gliomas making it the most common, aggressive, and therapy-resistant form of malignant brain cancer in adults[5].5/16/19 2:36:00 PM Despite aggressive treatment which includes surgical resection followed by combined radiation and chemotherapy with temozolomide (TMZ), GBM remains incurable. This standard of care therapy only marginally extends life expectancy, leaving those diagnosed with the bleak prognosis of a 15 month median survival[11]. Thus, new treatment strategies for GBM are desperately needed.

Glioblastoma: A Metabolic Disease

Like many other aggressive and therapy resistant cancers, GBM can be characterized as a formidable and multifaceted tumor system that rivals the complexity of organs[8, 12]. A fundamental contributor to this complexity is GBM's unique metabolism that can be attributed to the numerous oncogenic signaling pathways activated during gliomagenesis. By definition, oncogenes and tumor

suppressors regulate tumor growth. The majority of these essential regulators also impact the expression and activity of metabolic enzymes. Likewise, there are examples of mutations to metabolic genes that also drive tumorigenicity. Cancer-associated alterations to these genes result in metabolic transformation that promotes the growth of actively dividing cells while simultaneously inhibiting signals responsible for growth suppression. GBM, therefore, can be characterized as a highly intricate and adaptable metabolic disease resulting from a series of interconnected and often redundant signaling pathways that drive neoplastic pathogenesis.

PI3Kinase/Akt Signaling Network

The phosphoinositide 3-kinase (PI3K)/protein kinase B (Akt) pathway is one of the major signaling networks associated with GBM and is activated in over 90% of all GBMs[13]. Activation of this pathway and its downstream target molecules functions as a central regulator of many cellular processes including, but not limited to, cell cycle progression, apoptosis, and metabolism[13, 14]. PI3K is recruited to the cell membrane and activated through phosphorylation by receptor tyrosine kinases (RTKs) such as epidermal growth factor receptor (EGFR), the first protein linked to oncogenesis in GBM[15]. EGFR is amplified in ~40% of all GBMs with about half of those tumors expressing the constitutively active EGFRviii form[16]. It is estimated that over 60% of GBM patients have some form of genomic alteration to the EGFR/PI3K pathway[17, 18]. Another prominent regulator of this pathway, the tumor suppressor phosphatase and tensin homolog (PTEN), is significantly altered in 30-40% of GBMs[19]. Similar to EGFR, loss of PTEN function by either deletion or mutation results in hyperactivation of PI3K signaling pathway.

The Warburg Effect

Elevated PI3K/Akt signaling results in a number of metabolic changes that are fundamental to tumor physiology. Most prominently, this signaling cascade serves as a key driver behind the most documented metabolic phenotype in GBM, the Warburg effect[20, 21, 22]. The Warburg effect is the observation that cancer cells predominantly meet bioenergetic demands by utilizing a high rate of aerobic glycolysis followed by lactic acid fermentation in the cytosol. This is in contrast to the comparatively low rate of glycolysis occurring in most healthy differentiated tissues, which depend instead on oxidation of pyruvate in the mitochondria. Hyperactivation of PI3K/Akt and other similar cancer-associated signaling networks cause GBM cells to shift their metabolism away from oxidative phosphorylation (OxPhos), making them highly reliant on elevated glucose flux instead[23]. Phosphorylation of Akt results in increased expression and activation of GLUT1, a protein localized to the plasma membrane that mediates transport of glucose into the cell[24]. Pathway activation also promotes the binding of hexokinase 2 (HK2) to voltage-dependent ion channels, once again stimulating increased glucose uptake and aerobic glycolysis[25]. Aerobic glycolysis is further promoted through increased phosphofructokinase 1 (PKFP1) activity and stability as a direct result of Akt activation resulting from PTEN loss and EGFR-dependent PI3K induction[26].

The metabolic adaptation of GBM cells to utilize the Warburg effect extends far beyond simply the production of ATP for bioenergetic demands. In fact, aerobic glycolysis represents a less efficient means of generating ATP than mitochondrial respiration on a per mole of glucose basis[27]. Although, because glycolysis rates are significantly elevated in cancer, the total amount of ATP generated over any given period of time is comparable to that of OxPhos[22, 28]. In addition to ATP production, the Warburg effect may play a number of other important roles. Glucose acts as

a carbon source for the *de novo* production of lipids, nucleotides, and proteins that are essential for supporting sustained proliferation[29, 30, 31]. Increased glucose uptake also elicits excess production of reducing equivalents such as NADPH that are required for *de novo* biosynthetic processes[32]. Finally, it has been proposed that the Warburg effect may promote enhanced invasiveness[33], immune evasion[34], and angiogenesis[35] through the production and release of lactate into the tumor microenvironment, and may also play a key role in the regulation of reactive oxygen species (ROS) levels[28, 36].

Despite knowledge of this metabolic phenomenon for nearly a century, little progress has been made in establishing an effective therapeutic strategy targeting glucose metabolism in GBM. Several approaches for targeting EGFR have yielded underwhelming results in clinical trials. Receptor tyrosine kinase (RTK) inhibitors for EGFR such as erlotinib, gefitinib, lapatinib, afatinib have all been investigated, but none of these have demonstrated efficacy either alone or in combination with other drugs or small molecule inhibitors[37, 38, 39, 40]. Most of these studies site poor brain penetrance, lack of specificity, and activation of redundant RTK pathways as reasons for the ineffectiveness. Similar trials with EGFR-specific monoclonal antibodies such as Cetuximab and Nimotuzumab have also failed to result in large-scale benefits, although Nimotuzumab has shown more promising results in patients with GBMs that are O-6-methylguanine-DNA methyltransferase (MGMT) non-methylated[41]. Early clinical trials investigating first generation pan-PI3K inhibitors (wortmannin and LY294002) were also ineffective due to poor solubility, off-target effects, and toxicity[42]. However, newer generation inhibitors targeting the PI3K/Akt/mTOR signaling axis have shown increased specificity and efficacy and have thus entered into clinical trials for GBM[43]. Due to the adaptability of GBM metabolism and the overlapping signaling

pathways that regulate it, it has yet to be determined if glucose metabolism can be a beneficial target in GBM.

Isocitrate Dehydrogenase 1 (IDH)

In addition to oncogenic signaling pathways such as EGFR/PI3K/Akt that drive tumorigenesis by altering tumor metabolism, there are also examples of mutations to metabolic genes that cause tumorigenicity. The most prominent example of this in GBM are isocitrate dehydrogenases (IDH1/2). IDH1 is a homodimeric enzyme localized to the cytoplasm and peroxisomes of cells, whose wildtype function is to produce alpha-ketoglutarate through the oxidative decarboxylation of isocitrate as part of the TCA or citric acid cycle. A mutation in IDH1 at the arginine 132 residue (R132H), however, causes a neomorphic gain of function that further converts alpha-ketoglutarate to the proposed oncometabolite 2-hydroxyglutarate (2-HG)[44]. This particular IDH1 mutation is present in nearly 80% of grade II-III gliomas[45, 46, 47], but also occurs in a smaller subset of GBMs[48, 49]. With regard to clinical prognosis, IDH mutations serve as favorable prognostic biomarkers for both overall and progression-free survival[50, 46]. An analogous but mutually exclusive mutation at residue R172 in IDH2, a member of the IDH gene family localized to the mitochondria, is also found in glioma. This mutation similarly results in gain-of-function production of 2-HG, although it is far less common than that of IDH1[50]. Recently, several compelling studies indicate IDH mutations occur early in gliomagensis[51, 50, 52]. This fact, combined with the overall prevalence of these mutations throughout gliomas, would seem to suggest IDH mutations are key events in tumorigenesis while reinforcing the significance of metabolic transformation in this process. However, determining whether oncogenic transformation is a result

of the IDH mutation itself, the resulting 2-HG production, or a combination of both has yet to be fully established.

In addition to 2-HG production, IDH mutations are also often associated with genome-wide DNA hypermethylation called Glioma CpG Island Methylation Phenotype (G-CIMP)[53], a valuable determinant of tumor pathogenicity. G-CIMP can result in the reorganization of both the methylome and transcriptome of these mutant tumors, although the comprehensive effects of this process are still being investigated[54]. In addition to being a major enzyme in the citric acid cycle, IDH may also serve several other important functions. Wildtype activity of IDH, the production of alpha-ketoglutarate from isocitrate, also results in the generation of nicotinamide adenine dinucleotide phosphate (NADPH) from NADP+, a critical reducing agent shown to regulate certain aspects of macromolecular biosynthesis, glutathione (GSH) production, ROS generation, and DNA repair in glioma[55, 56, 57]. The manner in which the IDH1 mutation and 2-HG production alter these processes will be covered in a later chapter, however, two things have become increasingly apparent. The IDH1 mutation serves a role extending far beyond TCA-mediated metabolism, and studies involving IDH1 mutant tumors reinforce the idea that brain tumors are, in fact, metabolic diseases.

Fatty acid Metabolism

The role of glucose metabolism in brain tumors has been extensively documented over the past two decades. Yet more recent evidence has made it abundantly clear that gliomas utilize other metabolic substrates to meet bioenergetic demands and produce the raw materials required to sustain uncontrolled proliferation. One particular type of substrate that has drawn interest of late are fatty acids (FAs). FAs are a diverse class of molecules performing an equally diverse set of

functions within the cell. Some of the roles of FAs include: serving as molecular building blocks for membrane biosynthesis, acting as storage reservoirs for energy production, and assisting in both inter- and intracellular signaling. Similar to what is observed with other metabolic substrates, however, the rates and manner of FA utilization can differ significantly when comparing healthy tissue to that of a rapidly dividing tumor.

FA Synthesis: GBM vs. Healthy Brain

Fatty acid synthesis is the anabolic process of generating FAs from acetyl-CoA and NADPH. This process takes place in the cytoplasm where the majority of acetyl-CoA is derived from glucose via glycolytic flux through the TCA cycle. Glucose-derived acetyl-CoA cannot be exported directly to the cytoplasm for FA synthesis, however. It must first be condensed with oxaloacetate to produce citrate in the TCA cycle. Excess citrate in the TCA cycle is converted to acetyl-CoA by ATP citrate lyase (ACLY), an enzyme directly phosphorylated and activated by Akt[32], followed by decarboxylation of acetyl-CoA into malonyl-CoA. Malonyl-CoA is an important molecule because it functions as both a substrate for FA synthesis and as an inhibitor of fatty acid oxidation, a process that will be covered shortly[58]. When glucose is prevalent in GBM, excess acetyl-CoA can be used to generate high levels of malonyl-CoA that drive fatty acid synthesis for use in membranes to support proliferation. When malonyl-CoA levels drop, FA synthesis slows, allowing GBM cells to compensate for decreased glucose availability by shifting toward FA catabolism in support of survival. This process, which is significantly amplified in GBM relative to surrounding brain tissue, bestows an adaptable advantage to changing nutrient levels in the tumor microenvironment[59]. In addition to acting as a metabolic switch, malonyl-CoA represents the molecular building block by which fatty acid synthase (FASN) generates palmitate,

the first fatty acid produced which also serves as the precursor for synthesis of longer chain fatty acid molecules[60, 59]. FASN is therefore a critical enzyme regulating *de novo* FA synthesis, and indeed, increased expression of this enzyme correlates with malignancy in glioma[61].

As mentioned previously, GBMs are highly versatile malignancies that rival the complexity of organs[12]. Thus, cellular processes such as FA synthesis can only occur if they are supported by GBM's innate metabolic machinery and are conducive to the tumor microenvironment. Due to the abnormal vascularization present in GBM, persistence of FA synthesis under conditions of metabolic stress is key to supporting the unmitigated proliferative potential of these tumors. Importantly, FA metabolism has been shown to persist under conditions of hypoxia and low nutrient availability[62]. Low oxygen levels result in hypoxia inducible factor 1 (Hif1)-mediated activation of sterol regulatory element-binding protein (SREBP)-1, the major transcriptional regulator of fatty acid synthase (FASN)[63]. Hypoxia also induces storage of FAs in lipid-rich cellular organelles called lipid droplets. Upon reoxygenation, the sequestered fatty acids are then used for ATP production through β-oxidation[64]. Because of the elevated rate of FA synthesis in GBM, the ability to store intracellular FAs has the added benefit of circumventing lipotoxicity and endoplasmic reticulum (ER) stress[65].

FA Beta-Oxidation: GBM vs. Healthy Brain

In contrast to fatty acid synthesis, fatty acid oxidation (FAO) is the catabolic process through which long-chain FAs are broken down in the mitochondria to generate acetyl-CoA. This process was largely overlooked in GBM until recently, likely due to misconceptions that fatty acids are unable to cross the blood brain barrier (BBB) and that the extent to which FAO takes place in the brain is negligible. It has been demonstrated that non-esterified fatty acids such as palmitic

acid and arachidonic acid are able to cross the BBB by simple diffusion while other fatty acids enter through passive diffusion[66, 67]. It is true that very little FAO takes place in neurons. Several hypotheses for this have been proposed: 1) generating ATP through FAO demands more oxygen than glucose which risks hypoxia in neurons[68, 69], 2) FAO generates superoxide to which neurons have poor antioxidative defenses[70] and 3) the process of ATP generation from tissue-derived fatty acids is slower than that of blood glucose[71]. A more recent study estimates that FAO may actually account for 15-20% of total brain oxidative energy production, but that this process occurs primarily in glial cells rather than in neurons[72]. Unlike neurons and other healthy brain cells, however, GBMs thrive under hypoxic conditions. FAs are also easily stored within tumor cells for use during nutrient deprivation. And given the highly invasive nature of GBM, these FAs also represent an alternative energy source as tumor cells migrate away from vascular supplies of glucose.

Several additional lines of evidence support the potential importance of FAO in GBM. A common characteristic of these tumors is the development of highly necrotic cores that contain substantial amounts of lipids and fatty acids[73]. This fact, along with the ability of fatty acids (FAs) to diffuse across the BBB, provide a readily available reservoir from which GBMs can access FA substrates required for beta-oxidation. In support of this, several studies using proton NMR (^{1}H NMR) have shown that GBMs do in fact have a large and distinct lipid signature. Additional studies have revealed that long-chain fatty acids (LCFAs), those that participate in beta-oxidation, are among the most prevalent FAs found in GBM[74, 75, 76].

The rate-limiting enzyme of FAO is carnitine palmitoyltransferase 1 (CPT1) which is located on the outer mitochondrial membrane[60]. This enzyme catalyzes the transfer of the acyl group of long-chain fatty acyl-CoA to L-carnitine, thereby allowing FAs to enter the mitochondria

for subsequent oxidation. There are three isoforms of CPT1 expressed in humans (CPT1A, CPT1B, and CPT1C). It has only recently been shown that expression of all three isoforms is common in GBM, but a rare occurrence elsewhere in the body[77]. Because of the rate-limiting properties of CPT1, it has been proposed as a promising target for FAO inhibition. To target CPT1, etomoxir (ETOM) has been implemented for both *in vitro* and *in vivo* studies[78]. ETOM is a potent, irreversible, CPT1-specific inhibitor that acts on all three CPT1 isoforms. A preclinical study published in 2010 demonstrated that SF188 glioblastoma cells oxidize fatty acids, and that inhibition of FAO with ETOM had widespread effects which include: a reduction in cellular ATP levels, decreased viability, and decreases in both NADPH and glutathione (GSH) levels[79]. The latter correspond with observed increases in reactive oxygen species (ROS), suggesting FAO may also play an important role in antioxidative defense.

It is of note that the high concentrations of ETOM (up to 1mM) typically used in such studies may have potential off-target effects. Recently, a group investigating the effects of ETOM in macrophages reported that excessive concentrations of ETOM (>3uM) caused depletion of free cellular coenzyme A (CoA) and inhibited adenine nucleotide translocase (ANT) and respiratory complex I[80]. ETOM has also been used in a clinical trial for congestive heart failure, but the study was discontinued due to the accumulation of certain enzymes associated with hepatotoxicity in ~5% of patients[81]. These results highlight the importance of FAO in GBM metabolism and suggest that targeting this pathway with more potent and specific inhibitors may offer benefits therapeutically.

Ketone Metabolism:

Another metabolic pathway that has drawn particular interest in cancer research lately is ketone metabolism. Because the majority of cancers rely extensively on glucose uptake and aerobic glycolysis, many researchers have theorized that the implementation of a ketogenic diet (KD) may serve as an effective adjuvant therapy[82, 83, 84]. The KD consists of a high fat, adequate protein, low carbohydrate diet. With traditional diets, carbohydrates are converted to glucose which then circulates throughout the body for fuel. The KD forces the body to primarily metabolize fats which are ultimately converted into ketone bodies (KBs) through a process called ketogenesis. KB production, of which ß-hydroxybutyrate (3-OHB) and acetoacetate are most prevalent, occurs primarily in the mitochondria of liver cells through the breakdown of fatty acids and ketogenic amino acids[85]. This process can be initiated by fasting, calorie restriction, strenuous exercise, or by dietary intervention such as with a KD. Circulating KBs are then taken up by tissues like the brain where they are converted back to acetyl-CoA for entry into the TCA cycle.

The ability of the brain to compensate for decreased glucose availability by shifting its metabolism away from glycolysis and towards ketolysis has been extensively documented[86, 87]. In fact, the KD has been implemented clinically and has shown promise in treating certain cases of epilepsy and diabetes that are refractory to standard therapy[88, 89, 90]. Studies investigating the effects of prolonged fasting estimate ketone body oxidation can account for ~30-40% of the human body's energy requirement and up to 60% of the brain[91]. This process has the added benefit of sparing what little glucose is available for cells that are unable to utilize KBs for energy production, such as erythrocytes and hepatocytes. The therapeutic premise of the KD for GBM, therefore, is reliant on the hypothesis that limiting glucose availability, combined with the inability of GBMs to fully

compensate with circulating KBs and FAs, will starve the tumor of necessary nutrients without harming healthy tissues.

The extent to which gliomas metabolize ketone bodies remains unclear. Several studies have suggested that gliomas may be unable to oxidize KBs for energy due to insufficient expression of the mitochondrial enzymes required to do so, such as acetyl-CoA acetyltransferase (ACAT), 3-oxoacid CoA transferase (OXCT1), and 3-hydroxybutyrate dehydrogenase 1 and 2 (BDH1 and 2)[92, 83, 93]. Contrarily, another report determined that both neuroblastoma and glioma cells express these three enzymes at comparable levels to the brain, while also providing evidence that KBs may be utilized more for lipid synthesis rather than as substrates for energy production[94]. Preclinical studies investigating the effectiveness of the KD in animal brain tumor models have yielded mixed results. A study investigating ketone metabolism in two separate rat glioma models concluded that the level of KB oxidation (3-OHB) taking place within the tumor was comparable to that of normal contralateral brain tissue[95]. This group also determined that expression of monocarboxylate transporter 1 (MCT1), one of the primary enzymes responsible for KB uptake, becomes upregulated within glioma tissue of tumor-bearing animals when placed on the KD. Another group using a U87 mouse xenograft model found that the KD (administered ad libitum) was not sufficient to decrease circulating blood glucose and had no inhibitory effects on tumor growth[96]. Only when a calorie-restricted KD was implemented were there observed increases in blood ketone levels and corresponding decreases in blood glucose and tumor size. This brings into question whether the KD, calorie-restriction, or a combination of the two offers the greatest therapeutic benefit, as previous work has also demonstrated the anti-tumor effects of calorie restriction irrespective of the KD[97, 98, 99].

While some of the above-mentioned studies may seem to contradict one another, it is likely that much of the disparity regarding KB metabolism in glioma arises from the heterogeneity of the disease. An assessment of ketolytic enzyme expression from 22 malignant glioma biopsies reinforces this point[93]. Mitochondrial expression of OXCT1 and BDH1 was found to be low (<20% positive cells relative to normal brain tissue) in most, but not all, of the tumors analyzed (14 of 17 GBMs, 1 of 5 anaplastic gliomas). However, most of the 22 tumors were also positive (>20%) for cytosolic BDH2 and mitochondrial ACAT1. Thus, it is reasonable to theorize that tumors with lower mitochondrial expression of these ketolytic enzymes may respond better to dietary intervention than those with greater expression. A more in-depth examination of the expression profiles of these critical ketolytic enzymes may be key to reconciling the true role of ketone metabolism in glioma and in directing future clinical approaches testing the effectiveness of KD therapy.

Pathway Interconnectivity and Redundancy

One of the largest hurdles to overcoming therapy-resistant cancers is the interconnectivity and redundancy of metabolic pathways and oncogenic signaling. The genetic and epigenetic alterations that occur in GBM drive metabolic reprogramming that favors the growth of rapidly dividing cells while simultaneously inhibiting signals previously programmed to keep cellular division in check. Oncogenic signaling pathways such as PI3K/Akt/mTOR that drive glycolysis and regulate several other anabolic and catabolic processes within the cell are frequently activated in GBM. However, due to redundancy, targeted therapies to inhibit this pathway have failed to elicit beneficial results. For example, this pathway can be stimulated by loss of PTEN or through activation of receptor tyrosine kinases (RTKs) such as EGFR, PDGFRa, and MET[100, 101]. Thus,

GBMs can circumvent direct inhibition of EGFR by signaling instead through other RTKs. Akt can also be activated independently of PI3K by a series of Ser/Thr/Tyr kinases such as Src, ACK1 (activated Cdc42-associated kinase), and PTK6 (Protein Tyrosine Kinase 6)[102]. To add to the complexity, mTOR can similarly be activated in a PI3K-independent manner through Wnt, Notch, and PDK1 (pyruvate dehydrogenase kinase 1) signaling[103, 104], thereby providing additional resistance mechanisms to overcome direct PI3K/Akt inhibition. The intricacy and redundancy of such signaling networks present a major challenge that researchers must overcome in order to develop more effective therapies for aggressive cancers such as GBM.

Another factor adding to the complexity of GBM physiology is the reality that metabolic pathways and the oncogene-directed modifications to these pathways do not occur in isolation. Breaking down cellular metabolism into individual pathways, as has been done here, can be highly useful for identifying targetable vulnerabilities. However, this approach often falsely oversimplifies the overall process. Substrates frequently participate in both catabolic and anabolic reactions that regulate one another. For example, AKT signaling promotes the catabolism of glucose through glycolysis for the purposes of generating ATP and lactate[105]. However, glucose catabolism also generates acetyl-CoA for anabolic biosynthesis of fatty acids in an Akt-dependent manner[32]. FAs can then be used to generate phospholipids for membrane production or can undergo FA beta-oxidation (FAO) to regenerate depleted stores of acetyl-CoA and NADH[59]. It has been shown that the acetyl-CoA and NADH produced during FAO can actually inhibit pyruvate dehydrogenase (PDH), which results in increased conversion of pyruvate to lactate[106, 107]. This process, often referred to as the Randle effect, demonstrates that FAO can actually promote the Warburg effect and represents just one example of the cross-regulation between metabolic pathways. Interestingly, FAs have also been shown to participate in "futile cycles", a process

during which cells run two opposing metabolic pathways in parallel[59]. Under certain conditions, cancer cells will simultaneously activate both FA synthesis and FA oxidation. This process acts as a safeguard for maintaining adequate production of both ATP and lipids for membrane synthesis, while also serving as a dynamic switch that is highly sensitive to changes in nutrient availability and enzymatic activity[108].

The fact that cancers commonly display altered metabolic phenotypes from that of healthy tissue has been known for the better part of a century, when in the 1920's Otto Warburg first reported that cancer cells utilize abnormally high rates of aerobic glycolysis[20]. However, despite decades of research and countless findings regarding this phenomenon, certain cancers such as GBM have continued to evade our grasp and our therapies. While GBM cells do metabolize glucose, it has become increasingly apparent in recent years that GBM is a complex metabolic disease, with the Warburg effect representing only a small chapter of a much larger story. The metabolic adaptations associated with oncogenic transformation bestow upon GBMs the increased flexibility to utilize multiple substrates (carbohydrates, lipids, ketones, and proteins) as energetic currency and as molecular building blocks to support their aggressive expansion. Understanding the interconnectivity and redundancy of oncogenic signaling networks, metabolic pathways, and cellular bioenergetics presents an enormous challenge to researchers. Yet, rapid technological advances and the ability to develop novel, target-specific drugs make targeting GBM metabolism one of the more promising approaches to establishing more effective therapies.

Metabolic characterization of isocitrate dehydrogenase (IDH) mutant and IDH wildtype gliomaspheres uncovers cell type-specific vulnerabilities

Abstract

There is considerable interest in defining the metabolic abnormalities of IDH mutant tumors to exploit for therapy. While most studies have attempted to discern function by using cell lines transduced with exogenous IDH mutant enzyme, in this study we perform unbiased metabolomics to discover metabolic differences between a cohort of patient-derived IDH1 mutant and IDH wildtype gliomaspheres. Using both our own microarray and the TCGA datasets, we performed KEGG analysis to define pathways differentially enriched in IDH1 mutant and IDH wildtype cells and tumors. Liquid chromatography coupled to mass spectrometry analysis with labeled glucose and deoxycytidine tracers was used to determine differences in overall cellular metabolism and nucleotide synthesis. Radiation-induced DNA damage and repair capacity was assessed using a comet assay. Differences between endogenous IDH1 mutant metabolism and that of IDH wildtype cells transduced with the IDH1 (R132H) mutation were also investigated. Our KEGG analysis revealed that IDH wildtype cells were enriched for pathways involved in *de novo* nucleotide synthesis, while IDH1 mutant cells were enriched for pathways involved in DNA repair. LC-MS analysis with fully-labeled ^{13}C-glucose revealed distinct labeling patterns between IDH1 mutant and wildtype cells. Additional LC-MS tracing experiments confirmed increased *de novo* nucleotide synthesis in IDH wildtype cells relative to IDH1 mutant cells. Endogenous IDH1 mutant cultures incurred less DNA damage than IDH wildtype cultures and sustained better overall

growth following X-ray radiation. Overexpression of mutant IDH1 in a wildtype line did not reproduce the range of metabolic differences observed in lines expressing endogenous mutations; but resulted in depletion of glutamine and TCA cycle intermediates, an increase in DNA damage following radiation, and a rise in intracellular ROS. These results demonstrate that IDH1 mutant and IDH wildtype cells are easily distinguishable metabolically by analyzing expression profiles and glucose consumption. Our results also highlight important differences in nucleotide synthesis utilization and DNA repair capacity that could be exploited for therapy. Altogether, this study demonstrates that IDH1 mutant gliomas are a distinct subclass of glioma with a less malignant, but also therapy resistant, metabolic profile that will likely require distinct modes of therapy.

Background

Alteration in cellular metabolism is a key pathway to the development of cancer. Most oncogenes and tumor suppressors influence cellular metabolism, and there are examples of mutations in metabolic genes that become tumorigenic[109]. Homologous mutations in the metabolic enzymes isocitrate dehydrogenase 1 and 2 (*IDH1* and *IDH2*) are found in acute myelogenous leukemia, colon cancer and glioma[51]. In glioma, these mutations generally co-occur with either 1p/19q co-deletion or with mutations in *TP53*, the former with more oligodendrocytic characteristics and the latter with more astrocytic characteristics[110]. In contrast to metabolic mutations that involve a loss of function, IDH mutations were found to bestow a new enzymatic function of reducing alpha-ketoglutarate (a-KG) to 2-hydroxyglutarate (2-HG)[44]. In the presence of IDH mutations, the 2-HG molecule, normally found at low levels, can increase to millimolar amounts. Understandably, there has been considerable interest in what role this potential "oncometabolite" might have on cells. Given the structural similarity of the 2-HG molecule to a-

KG it was suspected that 2-HG may be a competitive inhibitor that blocked access to a-KG dependent enzymes that regulate cell epigenetics[111, 112].

There has been considerable interest in defining what effects IDH mutations have on glioma cell biology, and what the discovery of an IDH mutation can tell us about a specific glioma. These questions are important for two reasons. The first reason comes from the rationale that if the IDH mutant enzyme changes the metabolic state of the cell, this may render the cell more or less vulnerable to certain types of therapy. For example, it has been reported that the IDH1 mutation makes cells more vulnerable to radiation[113] or NAD+ depletion[114]. This issue has become even more clinically relevant with the discovery that the presence of IDH mutations can be diagnosed via imaging even prior to surgery[115]. The second reason comes from the observation that glioblastoma patients with IDH mutant tumors have prolonged survival compared to patients with IDH wildtype tumors and that there are now pharmacological inhibitors of the IDH mutant enzymes available that block 2-HG formation[116]. If it is the case that the IDH mutation is actually a metabolic burden to the cell, then use of these inhibitors may actually aid the tumor cell and accelerate growth. Studies using mutant IDH inhibitors in *in vivo* xenograft models have led to mixed results with one showing slowed growth[117] and another showing accelerated growth[114].

Attempts to focus on isolating metabolic differences between IDH mutant and IDH wildtype glioblastomas have historically suffered from an unproven assumption that the metabolic differences between IDH mutant and IDH wildtype tumors can be largely attributed to the presence or absence of the IDH mutation itself[118, 119]. However, more recent evidence suggests that IDH mutation may be one of the initial mutations to occur in those gliomas[120, 52]. Large-scale bioinformatics analyses of mutational, expression and epigenetic datasets reveals that IDH mutant and IDH wildtype tumors are different on a very fundamental level[121] and may have different cells

of origin, and different paths of tumorigenesis. Unfortunately, attempts to study cells derived from endogenous IDH mutant tumors have been hampered by the difficulty involved in establishing and maintaining IDH mutant glioma cells in culture.

To address these issues, we have performed a metabolic analysis on a cohort of patient-derived IDH1 mutant and IDH wildtype tumor cells to determine differences between these groups that may potentially be exploitable for therapy. We demonstrate that when compared to IDH wildtype glioma cells and tumors, IDH1 mutant cells and tumors are enriched for gene sets associated with DNA repair, while wildtype cells have greater expression of gene sets associated with nucleotide biosynthesis. IDH1 mutant cells have metabolic profiles that are distinct from those of IDH wildtype cells and our findings indicate that at least some of these differences are not corrected by overexpression of mutant IDH1 in IDH wildtype cells. Functional studies surprisingly demonstrate that IDH1 mutant cells are better able to recover from radiation treatment and less prone to the effects of inhibition of *de novo* nucleotide biosynthesis. These findings indicate that IDH mutant and wildtype tumors may be responsive to different metabolically-directed therapies and that the previously held views that IDH mutant tumors are highly radiosensitive may not be correct for all subsets of IDH mutant tumors and needs further exploration.

Results

KEGG GSEA analysis- Expression data from fifty-nine gliomasphere lines (52 IDH WT GBM and 7 IDH1 mutant) was subjected to Gene Set Enrichment Analysis (GSEA) using KEGG gene modules[122, 123]. Microarray data (GSE98995) is from data described in Laks et al, 2016[124]. A similar comparative analysis was performed on IDH1 mutant and IDH WT tumor samples in the

TCGA dataset (183 IDH1WT, 19 IDH1mut). Each KEGG module was assigned a normalized enrichment score (NES) for each dataset and then plotted (Figure 1). We noted a positive correlation between the gliomasphere and TCGA datasets giving confidence that our *in vitro* cells are a good model for *in vivo* tumors.

There were fewer modules enriched in the IDH1 mutant group in both the TCGA (37/167 gene set modules) as well as our gliomasphere data set (50/186 gene set modules). To identify some potential target metabolic pathways, we used a cut-off enrichment value of 1.2. Even with this liberal cut-off we only identified four modules that were enriched in IDH1 mutant cells in both data sets. Of these four, the "Homologous Recombination" and "Nucleotide Base Excision Repair" modules were selected for further study due to the clinical relevance in terms of response to radiation. In contrast, there were 35 modules that were enriched in IDH WT cells (Figures 1 and 2). The "Pentose Phosphate Pathway" and "Amino Sugar and Nucleotide Sugar Metabolism" were selected for further study to determine if IDH1 WT cells are in fact more dependent on the *de novo* pathway of nucleotide synthesis.
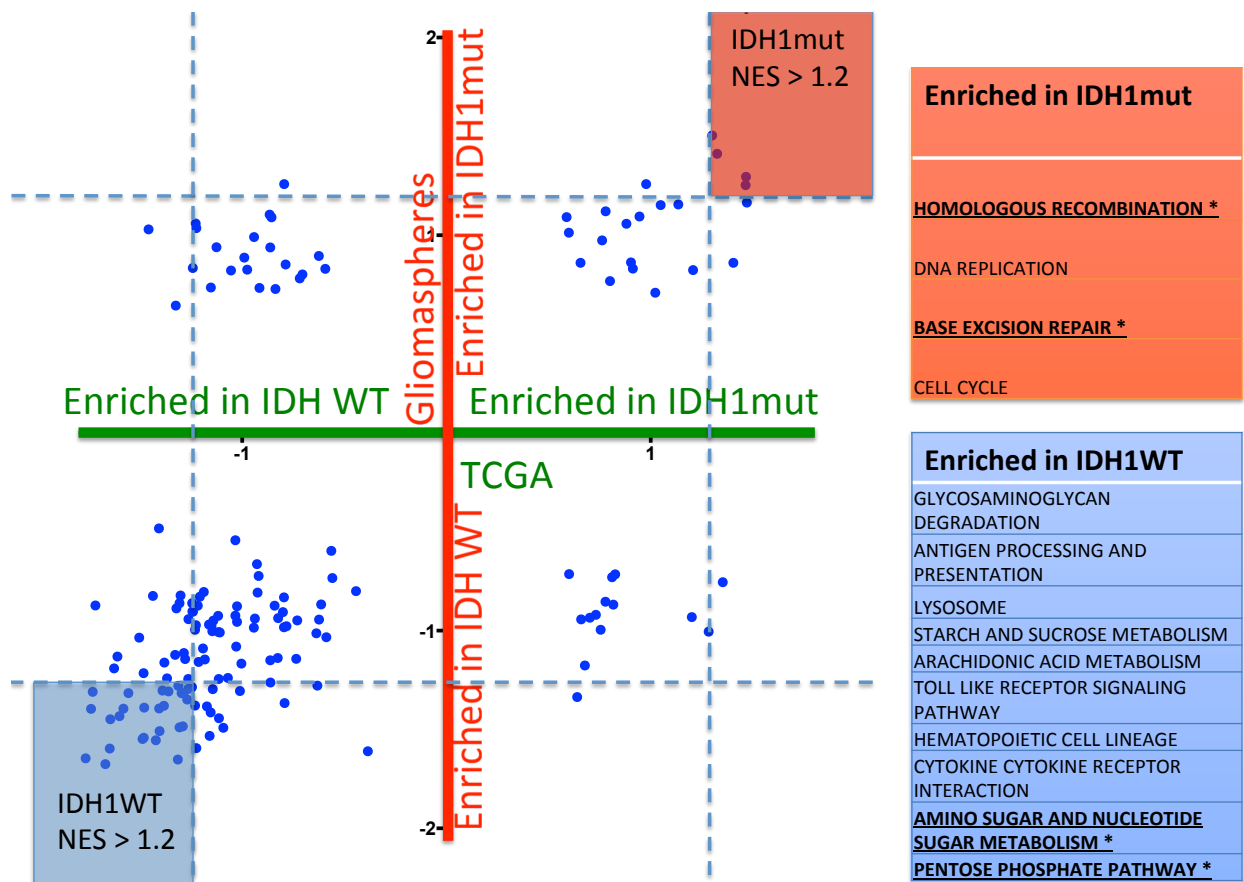
Figure 1. KEGG Gene Set Enrichment Analysis. Plot of expression data from TCGA (167 KEGG modules) and our gliomasphere dataset (186 KEGG modules). Each KEGG module was assigned a normalized enrichment score (NES) in either the IDH1 mutant or IDH1WT group. Each blue dot represents a different module. The enrichment score for a particular module in the TCGA data is plotted along the X-axis and that associated with the gliomasphere dataset for the same module is plotted on the Y-axis. Thus, a module that is highly enriched in IDH1 mutants compared to wildtype in both datasets would be in the upper right corner and modules highly enriched in IDH wildtype in both datasets would be in the lower left hand corner. Differentially enriched modules (NES > 1.2), listed on the right, were identified as potential candidates for further investigation.

Enriched in IDH1WT		Enriched in IDH1mut
GLYCOSAMINOGLYCAN DEGRADATION	APOPTOSIS	HOMOLOGOUS RECOMBINATION*
ANTIGEN PROCESSING AND PRESENTATION	NATURAL KILLER CELL MEDIATED CYTOTOXICITY	DNA REPLICATION
LYSOSOME	FOCAL ADHESION	BASE EXCISION REPAIR*
STARCH AND SUCROSE METABOLISM	B CELL RECEPTOR SIGNALING PATHWAY	CELL CYCLE
ARACHIDONIC ACID METABOLISM	NOD LIKE RECEPTOR SIGNALING PATHWAY	
TOLL LIKE RECEPTOR SIGNALING PATHWAY	CELL ADHESION MOLECULES CAMS	
HEMATOPOIETIC CELL LINEAGE	TYPE I DIABETES MELLITUS	
CYTOKINE CYTOKINE RECEPTOR INTERACTION	HYPERTROPHIC CARDIOMYOPATHY HCM	
AMINO SUGAR AND NUCLEOTIDE SUGAR METABOLISM*	GLUTATHIONE METABOLISM	
PENTOSE PHOSPHATE PATHWAY*	ARGININE AND PROLINE METABOLISM	
LEISHMANIA INFECTION	VIRAL MYOCARDITIS	
REGULATION OF ACTIN CYTOSKELETON	INSULIN SIGNALING PATHWAY	
COMPLEMENT AND COAGULATION CASCADES	MAPK SIGNALING PATHWAY	
LEUKOCYTE TRANSENDOTHELIAL MIGRATION	BLADDER CANCER	
ETHER LIPID METABOLISM	CHEMOKINE SIGNALING PATHWAY	
RIG I LIKE RECEPTOR SIGNALING PATHWAY	INTESTINAL IMMUNE NETWORK FOR IGA PRODUCTION	
JAK STAT SIGNALING PATHWAY	NICOTINATE AND NICOTINAMIDE METABOLISM	
ECM RECEPTOR INTERACTION		

Figure 2: KEGG gene set enrichment analysis of IDH1 mutant and wildtype gliomaspheres. Thirty-five modules were enriched in IDH wildtypes compared to 4 modules in IDH1 mutants.

Metabolic Profile- To assess the differences found in the expression analysis, and to investigate any further metabolic differences between groups, a cohort of IDH WT and IDH1 mutant lines were selected for further study. Key mutations and CNVs of the 5 IDH1 mutant cultures and 3 IDH WT cultures that were most intensively studied are listed in Figure 3. Of note, 4 of 5 of our IDH mutant cultures had pathogenic TP53 mutations and only one (BT142, obtained from ATCC) was 1p/19q co-deleted (Figure 3). Sample 322 was lost prior to detailed analysis, but clinical cytogenetics of the primary tumor demonstrated that it was not 1p/19q co-deleted, despite it being an oligodendroglioma.

Culture ID	Patient Age	Patient Sex	Diagnosis	Treatment	IDH1 Status	1p/19q co-deleted	EGFR	TP53	PTEN	ATRX	CDKN2A
HK211	41	F	Secondary GBM	N/A	p.R132H/ p.V178I	No	vIII	p.N235S/ p.Y234C			
HK213*	39	M	Secondary GBM	XRT, TMZ	p.R132H	No		p.P250L			
HK252*	40	M	Secondary GBM	XRT, TMZ	p.R132H	No		p.P250L			
HK322	37	F	Oligodendroglioma Grade II	N/A	p.R132H	No	CN Unknown	CN Unknown	CN Unknown	CN Unknown	CN Unknown
BT142**	38	M	Oligoastrocytoma Grade III	N/A	p.R132H	Yes		p.I50fs			
HK157	54	F	Primary GBM	N/A	WT	No		WT			
HK301	65	M	Primary GBM	N/A	WT	No	vIII	WT			
HK308	50	F	Recurrent GBM	XRT, TMZ, Avastin	WT	No	CN Unknown (vIII)	CN Unknown (p.A161T)	CN Unknown	CN Unknown	CN Unknown

*Different resections from same patient

**Obtained from ATCC

vIII- EGFR variant III mutant

Copy Number (CN)

CN Gain   CN Loss (-1)   CN Loss (-2)

Figure 3: Patient-derived gliomasphere culture characteristics. Relevant patient information and clinical characteristics for the primary, patient-derived gliomasphere cultures used in this study. Summary of selected copy-number alterations and mutations are also shown.

A cohort of 18 IDH WT and 5 IDH1 mutant cultures were subjected to a panel of metabolic measurements including glucose uptake, glutamine uptake, and lactate production rates. Glucose uptake rate was significantly higher in IDH WT cells although there was no significant difference in the lactate production to glucose uptake ratio, suggesting that both cohorts are highly glycolytic. The net glutamine uptake rate for all cells tested was near zero (Figure 4A-C). Consistent with these differences in glucose uptake, IDH wildtype cells grew faster than IDH1 mutant cells (Figure 5).
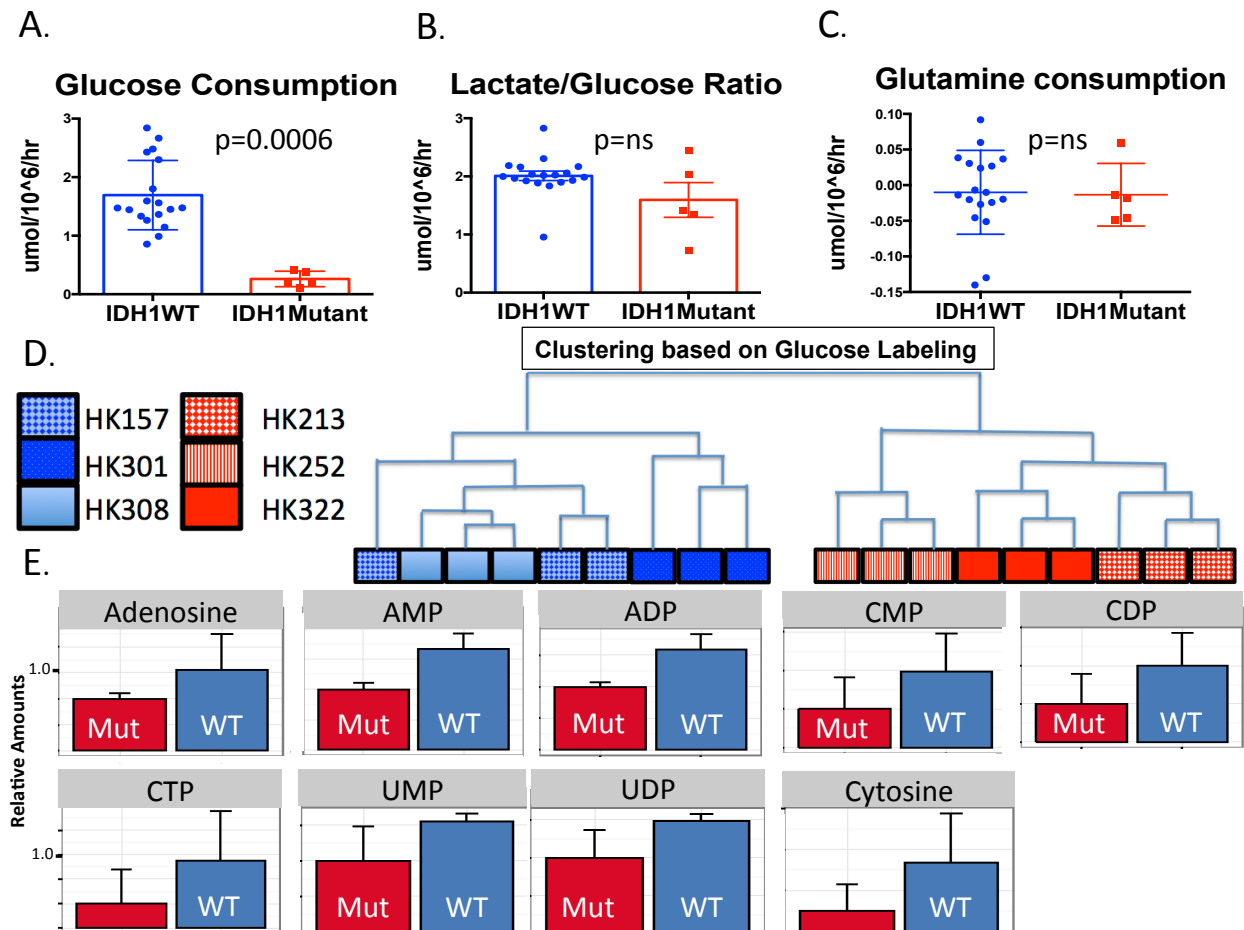
Figure 4

Figure 4. Metabolic profile of IDH1 mutant and wildtype cells. A-C. Quantification of glucose and glutamine consumption as well as the ratio of glucose consumed to lactate produced. Measurements were acquired using NOVA analysis (N= 18 IDH WT and 5 IDH1 mutant). Statistical significance was determined by Student's t-test. D. Clustering of three IDH1 mutant and three IDH wildtype lines according to LC-MS glucose labeling (IDHWTs: blue, IDH1 mutants: red). A glucose labeling index for each of the 159 metabolites analyzed was calculated for all 6 cell lines followed by non-hierarchical clustering analysis. Each line was run in triplicate and all samples are shown. E. Quantification of glucose labeling among nucleotide precursors by group. Relative amounts of metabolites were calculated by summing up all isotopologues of a given metabolite and normalized to the internal standard and cell number.

Figure 5: IDH wildtype cells show faster growth rate compared to IDH1 mutant cells. Six IDH wildtype and five IDH1 mutant gliomasphere cultures were assessed for proliferation rate by flow cytometry using carboxyfluorescein succinimidyl ester (CFSE). ($P<0.05$).
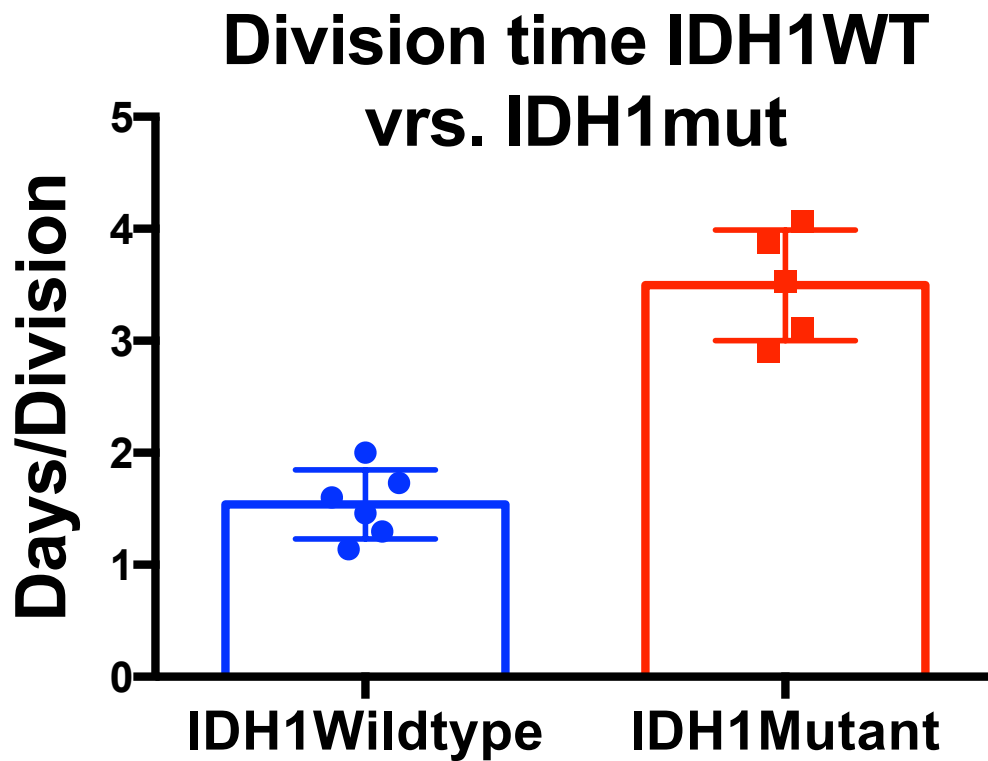
To further define the different utilization of these metabolites, we performed LC-MS on 3 IDH WT (HK157, HK301, and HK308) and 3 IDH1mutant (HK213, HK252, and HK322) lines with both fully labeled ^{13}C glucose and fully labeled ^{13}C glutamine. We then defined a single percent label for each metabolite and performed hierarchical clustering to identify if these six cell lines naturally partitioned into groups. Consistent with the observed differences in glucose uptake, IDH1 mutant and IDH WT samples partitioned into separate groups when assessed for glucose labeling (Figure 4D). Applying hierarchical clustering to the samples according to glutamine labeling or total metabolite amount did not distinguish the samples into distinct groups.

Since glucose labeling could distinguish between IDH1 mutant and IDH WT samples, we performed t-tests and compiled a list of all metabolites that had an uncorrected p-value<0.05. Thirty-two metabolites fulfilled this criterion of differential glucose labeling. Of these 32 metabolites, there was a significant over-representation of nucleotide precursors (9/32 chi-square p<0.007). Interestingly, all of the nucleotide precursors showed increased glucose labeling in the IDH WT group (Figure 4E, Figure 6).
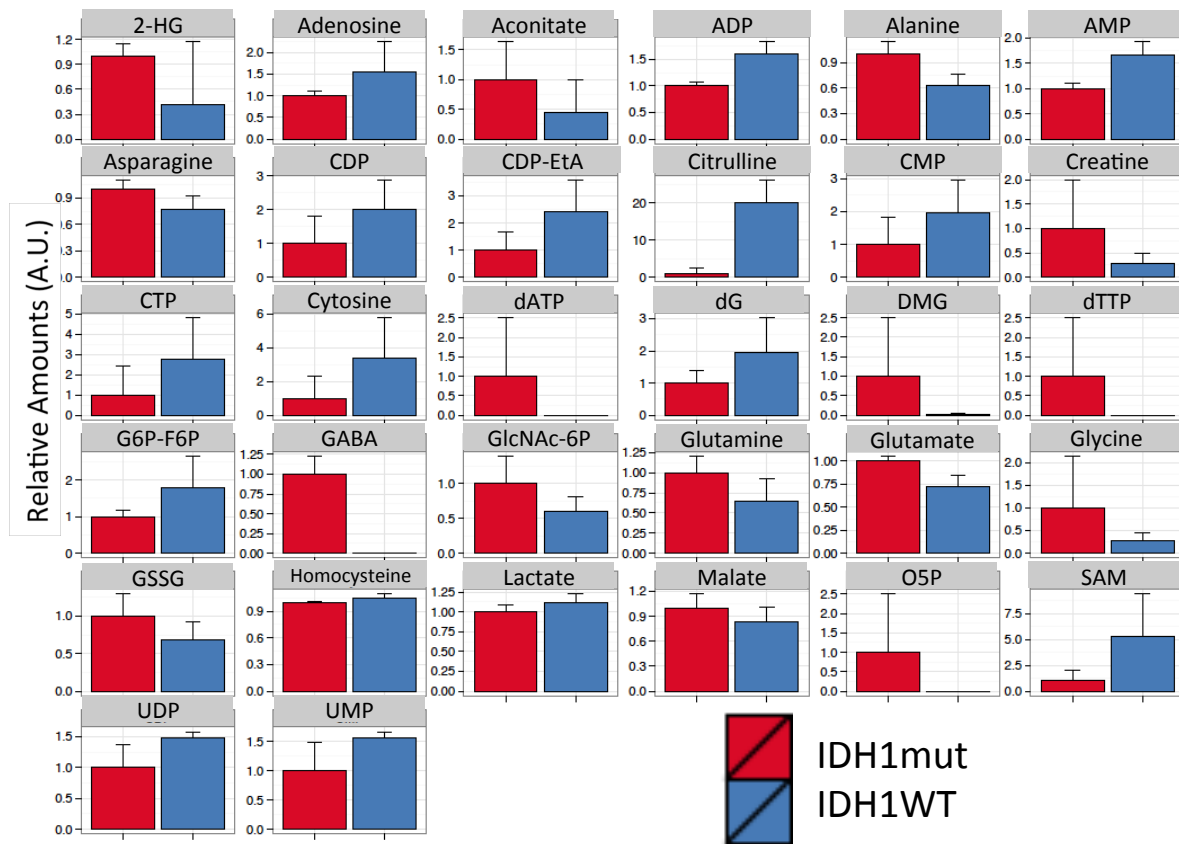
Figure 6: Glucose labeling of metabolites. Glucose fractional contribution was computed for all 159 metabolites. Metabolites that were significantly different between groups (uncorrected t-test p<0.05) are shown here.

De Novo versus Salvage Nucleotide Synthesis- Because our gene expression and metabolomics results are consistent with elevated nucleotide metabolism in IDH WT cells, we decided to investigate further whether IDH WT cells are more dependent on *de novo* nucleotide synthesis than IDH1 mutant cells. We profiled the de novo and salvage contribution to deoxycytidine triphosphate incorporation into newly replicated DNA using labeled ^{13}C glucose (to denote *de novo*) and labeled [$^{13}C9$,$^{15}N3$]dC (to denote salvage). Using the same set of three IDH WT lines and three IDH1 mutant lines we found that while all samples utilized both pathways, the IDH WT samples used primarily *de novo* synthesis while the IDH1 mutant samples used both pathways relatively equally (Figure 7A-B). To identify if this difference had functional relevance, we utilized high levels of deoxythymidine (dT), an inhibitor of the *de novo* pathway[125] to determine if there is any differential response between the two groups. Predicting that this inhibitor would have an effect on the ability of cells to pass through S-phase, we treated cells for four days (~1 doubling time) with dT and then performed cell cycle analysis using DAPI. All cell lines showed an increase in the number of cells in S phase; however, in the IDH1 mutant samples, cells were better able to pass through S phase and proceed with cell division. In contrast, at the end of the four-day treatment period almost all IDH wildtype cells were found in S phase (Figure 7C).
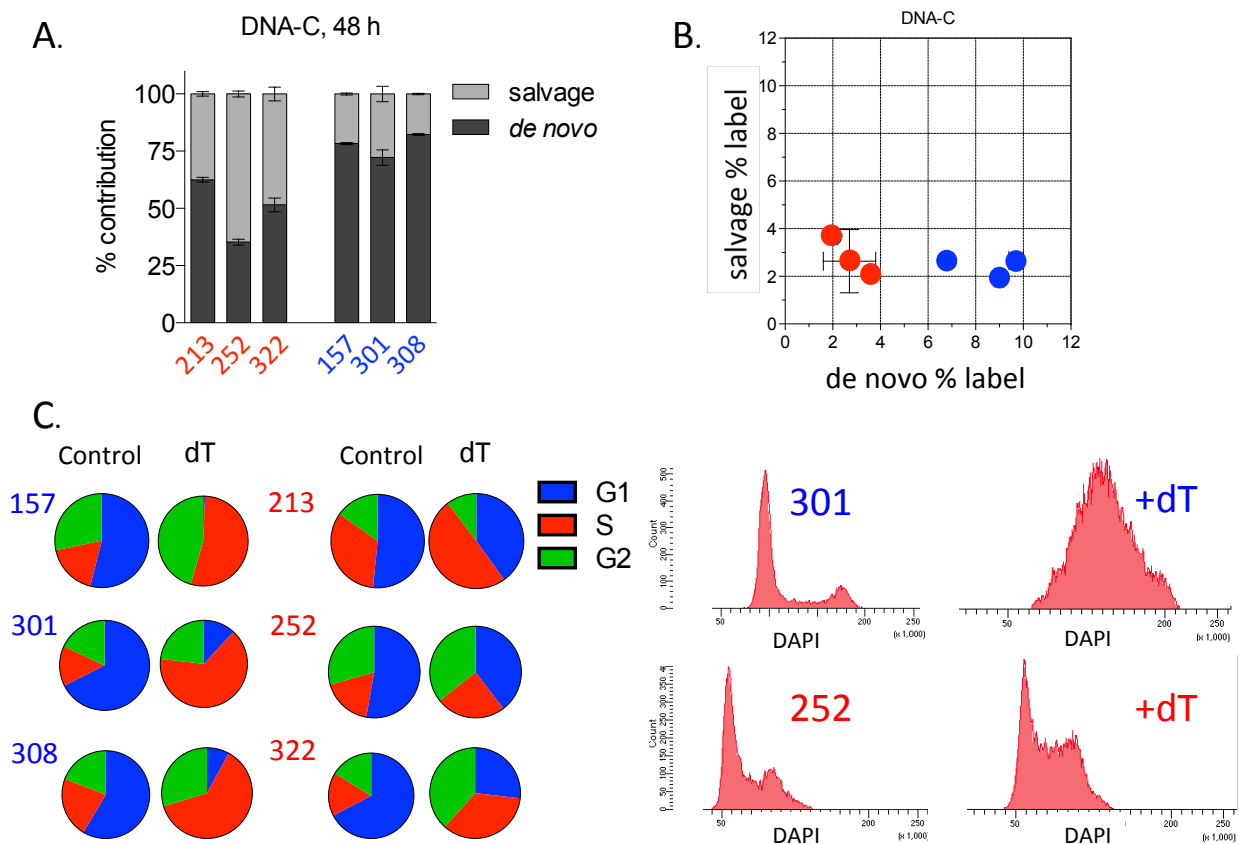
Figure 7. IDH1 mutant cells utilize *de novo* and salvage pathways for nucleotide biosynthesis. A-B. Quantification of *de novo* nucleotide synthesis and salvage pathway utilization by LC-MS with labeled glucose and nucleotides. A shows the relative contribution of each pathway plotted in bar graph format, while B shows the same data plotted 2 dimensionally. Error bars represent +/- STDEV. C. Cell cycle analysis by flow cytometry (DAPI) following four-day treatment with 1mM deoxythymidine (dT) or control (Left: distribution of cells in G1, S-phase, and G2; Right: representative histograms of cell cycle distribution for IDH1 mutant and WT cultures following dT treatment).

DNA repair in response to radiation- Having discovered that GSEA expression analysis accurately predicted that IDH1 mutant cells are less dependent on de novo nucleotide synthesis than are the IDH wildtype cells that we studied, we next turned to the modules that we found to be enriched in IDH1 mutant cells, namely modules involved with DNA repair and cellular response to radiation. Using a comet assay we first tested whether there was a difference in the amount of DNA damage incurred from a given dose of radiation and how quickly that DNA was repaired. For these experiments, we studied two of our IDH1/TP53 mutant lines as well as BT142, a highly studied IDH1 mutant that is 1p/19q-co-deleted but that also bears a TP53 mutation[126, 127]. At a dose of 10 Gy, significantly more IDH WT cells showed signs of DNA damage as compared to IDH1 mutant cells at all time points tested (Figure 8A-B). In IDH1 mutant cells, DNA damage peaked immediately after exposure to radiation, but that damage was largely repaired within four hours. Damage in IDH wildtype cells peaked after the first hour post-radiation and followed a similar trend with regard to repair. To examine repair dynamics, we next restricted our focus only to those cells with sustained measurable damage (comet tails) and then calculated tail moment length at different time points (0, 60, 120, and 240 minutes) to assess which group more efficiently repairs DNA. Again, the IDH1 mutant cultures showed significantly less initial damage following radiation and were able to resolve DNA breaks more quickly (Figure 8C). However, there was no significant difference in DNA damage between IDH1 mutant and wildtype cells by the final time point of the assay.
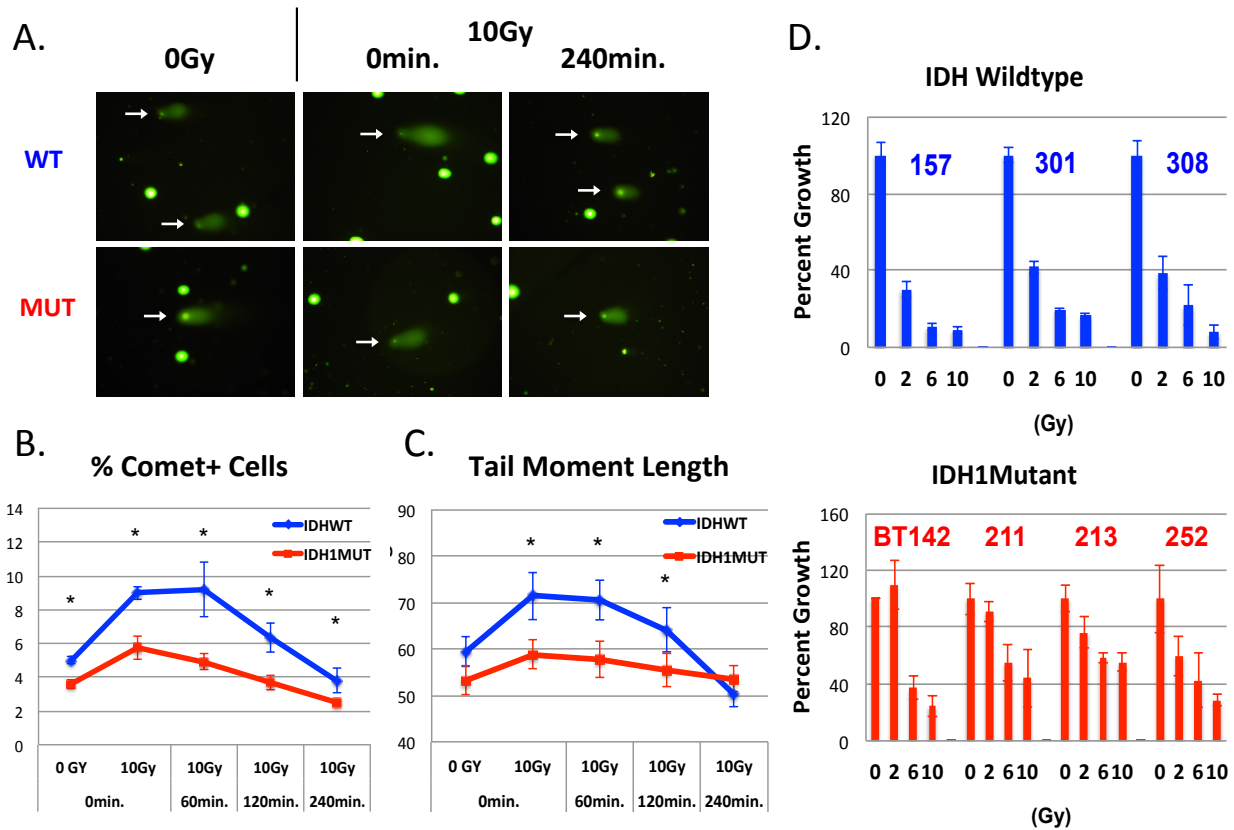
Figure 8. IDH1 mutant cells show diminished vulnerability to radiation. A-C.
Assessment of DNA damage and repair by comet analysis following irradiation (10Gy). A.
Representative images of cells following comet assay. White arrows indicate cells with comets. B.
Graph showing the percent of cells with comets. Comet number was calculated for each line
individually and then averaged by group. C. Tail moment length for each comet was calculated as
the length from the center of the comet head to the center of the tail. Tail moment length was
calculated for each line individually and then averaged by group. Significance levels were
calculated by ANOVA followed by posthoc t tests. Asterisks denote P<0.05, Error bars: +/- SEM.
D. Quantification of the effects of increasing doses of radiation (0, 2, 6, and 10Gy) on culture
growth as described in the Methods section. Graphs represent cell counts normalized to non-
irradiated controls.

We assessed the extent of apoptotic cell death using the TUNEL assay but saw relatively low levels of TUNEL staining and no significant difference between the two groups (Figure 9). However, when we examined the ability of cells to grow after radiation we again found that IDH1 mutant cells were better able to re-enter the cell cycle and divide as compared to IDH WT cells (Figure 8D).
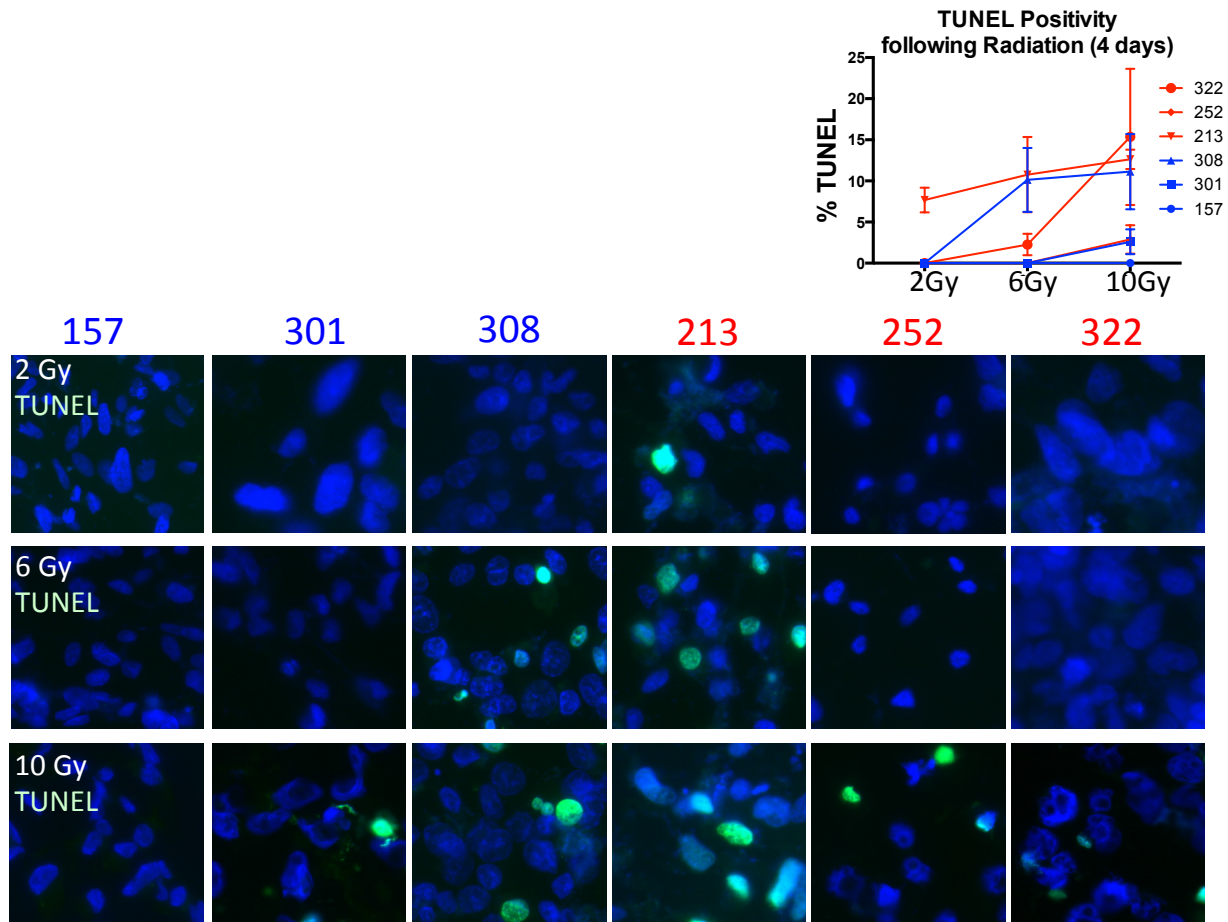
Figure 9: *Radiation leads to low levels of TUNEL staining in gliomaspheres.* Representative images and quantification of cells stained for TUNEL positivity four days after exposure to increasing doses of radiation. There is no significant difference between groups. Error bars represent +/- SEM.

IDH1 mutant overexpression as a model for IDH1 mutant glioma- IDH1 mutant over-expression in an IDH1WT background makes those cells more vulnerable to radiation[113]. With our new result that endogenous IDH1 mutant cells are less vulnerable to radiation than the IDH WT cells tested, it appeared that the IDH1mutation itself was not the sole determinant driving the difference between these two groups. To further test this hypothesis, we over-expressed the IDH1 mutant protein in an IDH WT background (HK308+IDH1mut) and pharmacologically inhibited the IDH1 mutant protein in an endogenous IDH1 mutant cell line (HK213+c227). We used LC-MS to confirm 2-HG production and inhibition respectively (Figure 10). Once we confirmed the appropriate effects on 2-HG production, we repeated the glucose-uptake clustering analysis to see if this artificial IDH1 mutant line (HK308+IDH1mut) clustered with the IDH WT or the IDH1 mutant groups (Figure 11A). We found that the HK308+IDH1mut samples clustered with the IDH WT group and the HK213+c227 clustered with the IDH1mut group. More specifically, neither IDH1 mutant over-expression nor the c227 inhibitor led to a change in glucose labeling of nucleotide precursors (Figure 12). This supports the hypothesis that the simple presence of IDH1 mutant protein or 2-HG was not driving the difference between these two groups over the time frames investigated.

2-hydroxyglutarate levels
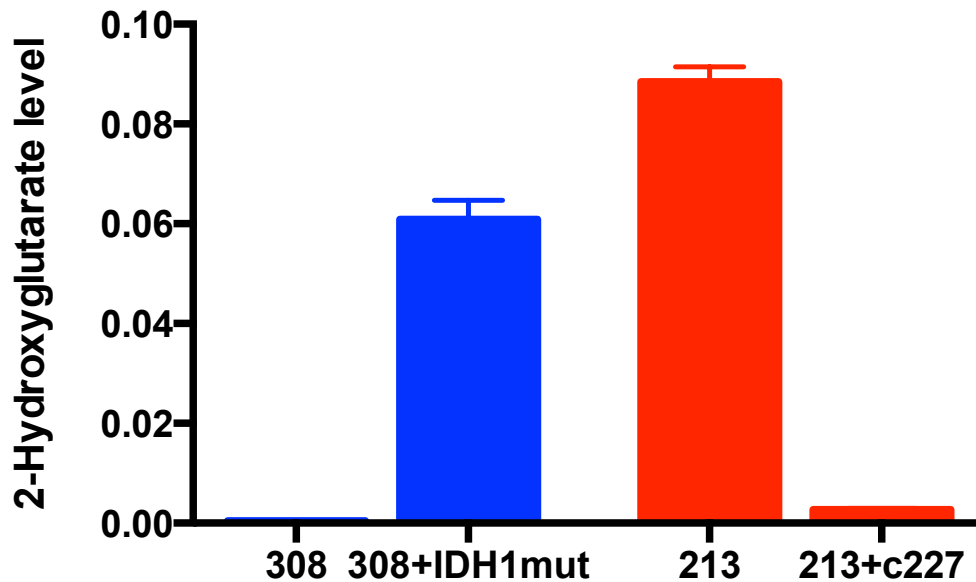
Figure 10: IDH1 mutant over-expression leads to high levels of 2-HG and the c227 inhibitor is an effective inhibitor of 2-HG formation. IDH wildtype gliomaspheres transduced with the IDH1 mutant enzyme (308+IDH1mut) and endogenous IDH1 mutant cells treated with 5 uM c227 inhibitor (213+c227) for 24 hours are compared to their respective controls (308 and 213) for 2-HG levels as determined by LC-MS. Data represent the means +/- SEM of three replicates per condition.
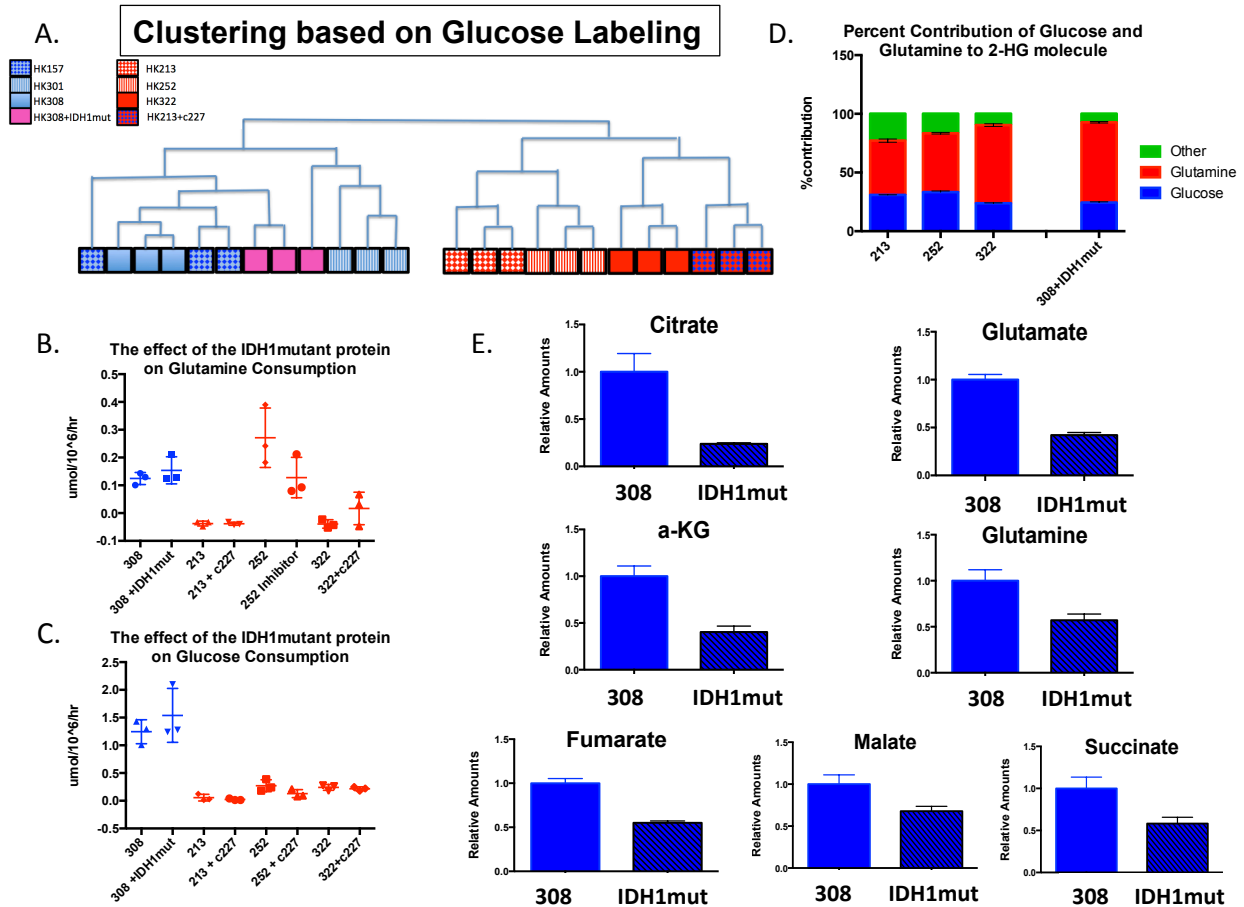
Figure 11. IDH1 mutant enzyme activity does not completely define the IDH1 mutant metabolic profile. A. Clustering of eight samples based on LC-MS glucose labeling as described in Figure 4. Analysis includes the same cohorts of IDH1 mutant and wildtype cultures with the addition of IDH1 mutant over-expression in an IDH WT line and inhibition of the endogenous mutant enzyme (308+IDH1mut and 213+c227 respectively). B, C. Quantification of glutamine and glucose consumption with IDH1 mutant overexpression and inhibition. D. Contribution of glucose and glutamine to 2-HG production in endogenous and transduced IDH1 mutants. E. Effects of IDH1 mutant over-expression on glutamine and TCA cycle intermediates quantified using LC-MS. P<0.05 for all 7 metabolites shown. Error bars denote +/- SEM.
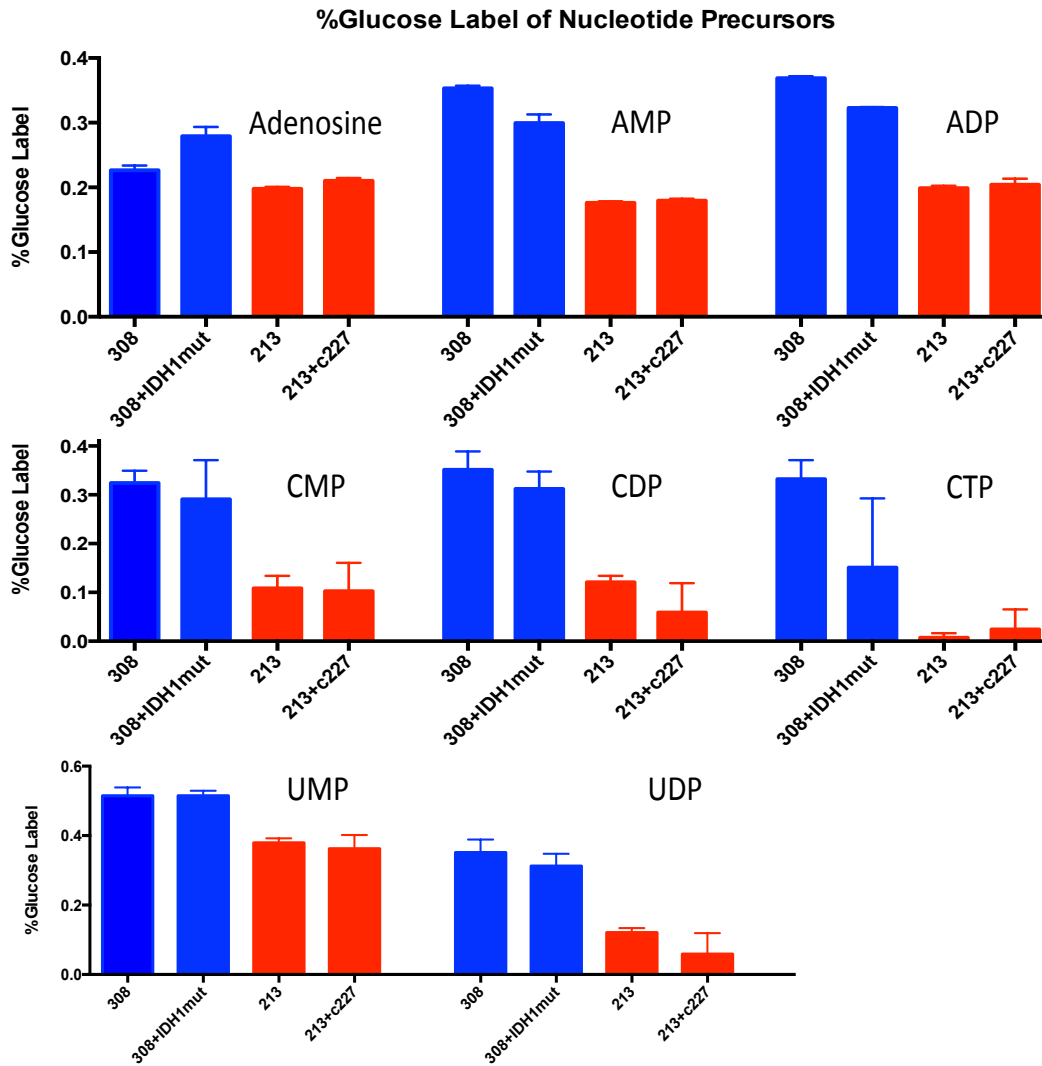
Figure 12: IDH1 mutant enzyme does not affect glucose labeling of nucleotide precursors. Cells were treated and analyzed as described for Figure 6 in order to determine the percent labeling of nucleotide precursors. There is no significant difference when comparing IDH1 mutant over-expression or endogenous mutant inhibition to their respective controls.

We next investigated what effect the presence of the IDH1 mutant protein had on cellular metabolism. We examined the effects on glutamine and glucose consumption and found that neither the addition nor inhibition of the endogenous IDH1 mutant enzyme influenced the consumption of either metabolite (Figure 11B-C). This was a surprising result given that the expression of the IDH1 mutant enzyme leads to production of high levels of 2-hydroxyglutarate and presumed consumption of alpha-ketoglutarate. To investigate this further, we used LC-MS tracing with labeled glucose and glutamine to determine how the cell makes 2-HG. Both endogenous IDH1 mutants as well as our over-expression model primarily used glutamine to make 2-HG (Figure 11D). However, given that we did not observe an increase in the amount of glutamine consumption with the addition of the IDH1 mutant gene, we hypothesized that the cells may be depleted of glutamine. Consistent with this prediction we saw significantly lower levels of glutamine as well as all TCA cycle intermediates when the IDH1 mutant gene was over-expressed (Figure 11E). In a recent study, Li et al. found that elevating 2-HG levels leads to a significant accumulation of succinate with corresponding decreases in fumarate and malate[128]. Interestingly, we observed decreased levels of succinate and increases in fumarate and malate with 2-HG inhibition (c227) in an endogenous IDH1 mutant line (HK213). However, this did not accurately reflect the differences between endogenous IDH1 mutant and IDH wildtype cells which had roughly comparable levels of glutamine and TCA cycle intermediates (Figure 13), suggesting that the IDH1 mutation is well-compensated for in the cells that carry it.
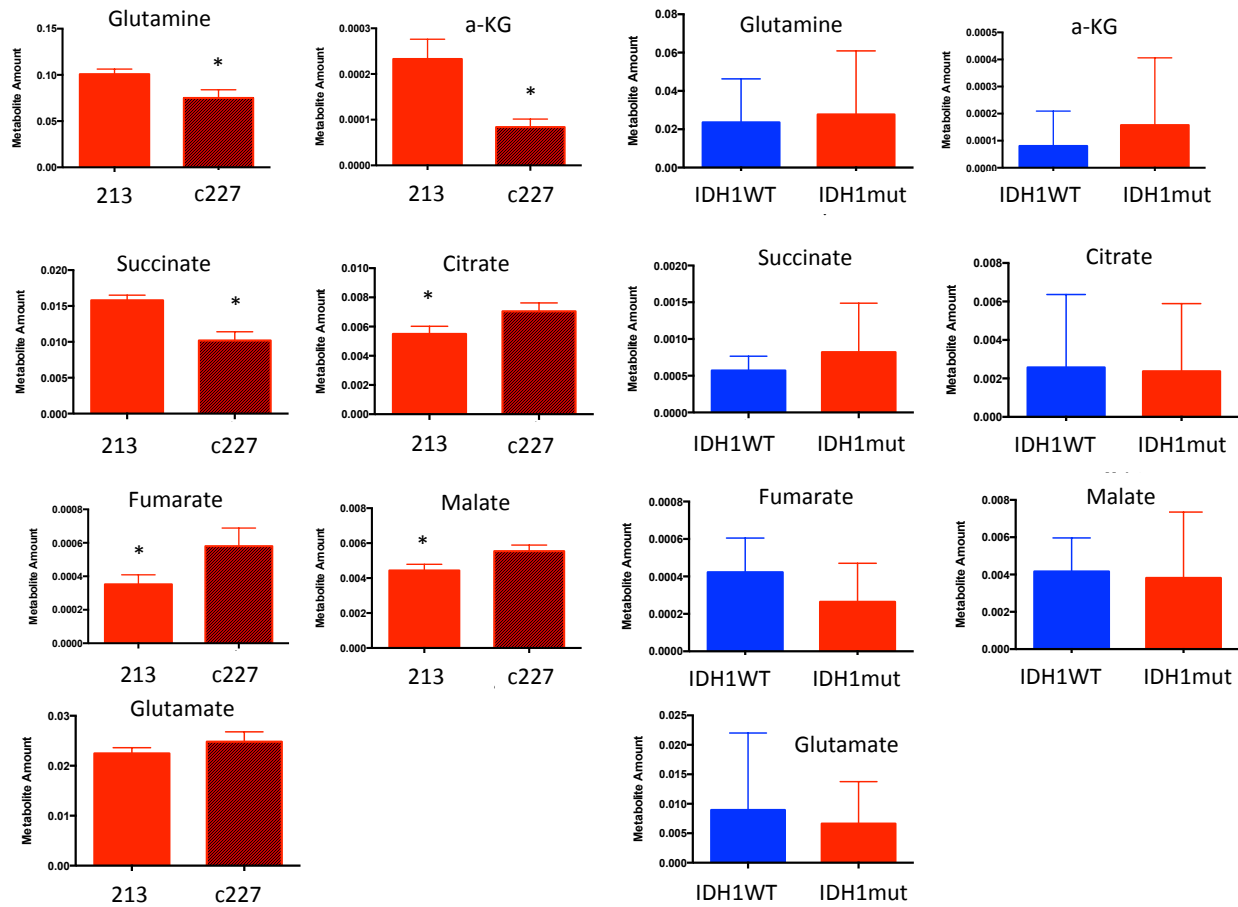
Figure 13: Effects of pharmacologic inhibition of the IDH1 mutant enzyme on TCA cycle intermediates. Cells were analyzed as described in Supporting Figure S5. Left: Metabolites with significantly different percent glucose labeling of metabolites in the endogenous IDH1 mutant line 213 treated with c227 inhibitor or control ($p < 0.05$). Right: Percent labeling from endogenous IDH1 mutant and IDH wildtype groups for metabolites that were not significantly different.

In order to further identify potential differences between the endogenous IDH1 mutant and overexpression models, as well as to help clarify differences between our observations of radiation sensitivity from previous reports[113], we repeated our radiation experiments on HK308 with and without over-expression of the IDH1 mutant enzyme. Over-expression of the mutation in this IDH wildtype line resulted in greater DNA damage and decreased repair immediately following radiation (Figure 14A-C). These results are contrary to what was observed when comparing endogenous IDH1 mutants to IDH wildtype cell lines (Figure 8). IDH1 mutant over-expression did, however, result in better growth following radiation (Figure 14D). One possible explanation for this is that exogenous expression of the IDH1 mutant enzyme in HK308 leads to significantly slower growth and this may give the cell more time to repair any DNA damage before re-entering the cell cycle.

Finally, we examined the effect of the IDH1 mutant enzyme on reactive oxygen species (ROS) levels. Interestingly, studies have reported mixed results regarding the effect of the IDH1 mutation on ROS with different results in different cell types[129, 130]. We found that the endogenous IDH1 mutant lines had significantly higher ROS levels than the IDH WT lines (Figure 15A). This appears to be due to the IDH1 mutation itself, because when we over-expressed the IDH1 mutant enzyme in HK308, the ROS levels increased significantly (Figure 15B).
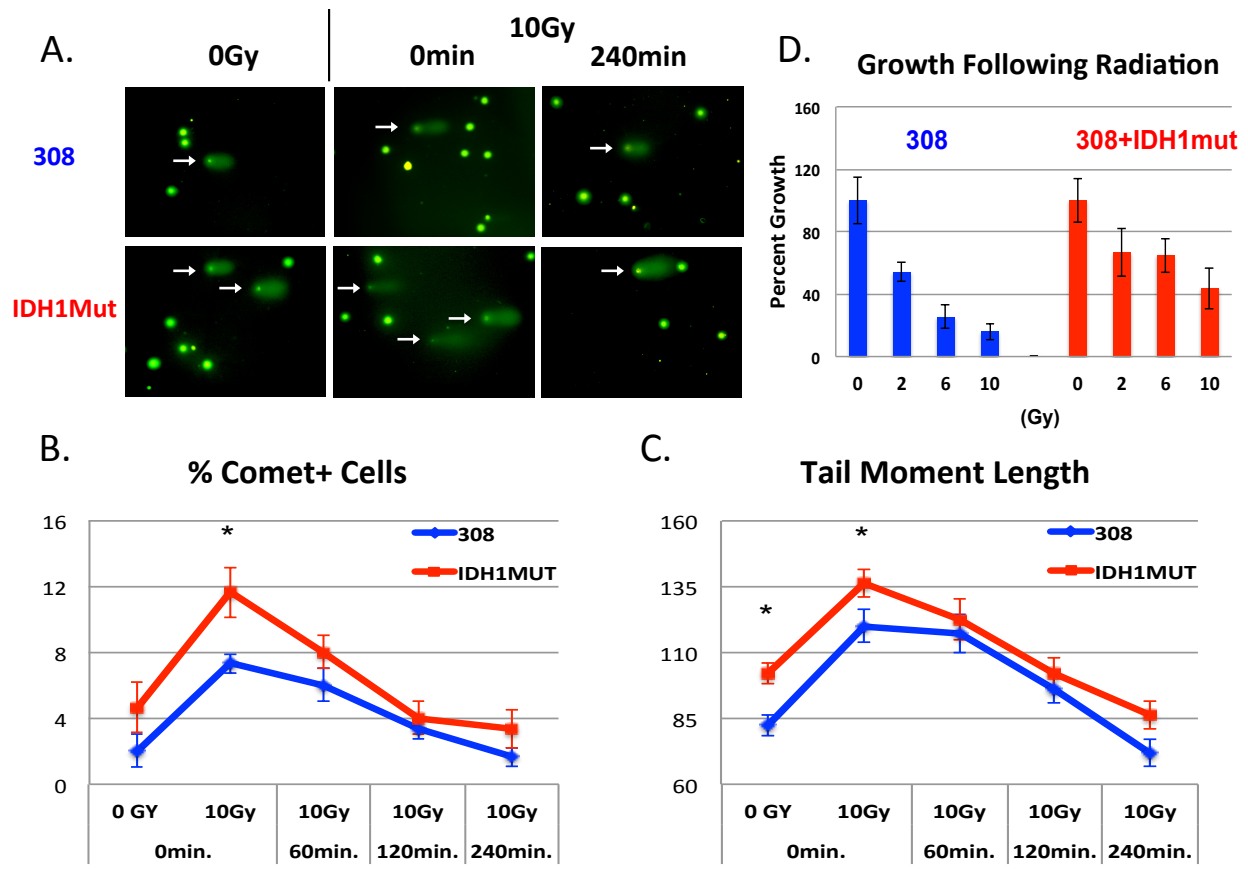
Figure 14. IDH1 mutant over-expression does not accurately mimic the DNA repair capacity of endogenous mutants. A-C. Assessment of DNA damage and repair by comet analysis following radiation (10Gy) A. Representative images of cells following comet assay. White arrows point to cells with comets. B. Graph shows the percent of cells with comets. Comet number was calculated for each line individually and then averaged by group. C. Tail moment length for each comet is calculated as the length from the center of the comet head to the center of the tail. Tail moment length was calculated for each line individually and then averaged by group. D. Quantification of the effects of increasing doses of radiation (0, 2, 6, and 10Gy) on culture growth as described in the Methods section. Graphs represent cell counts normalized to non-irradiated controls. Significance levels were calculated by ANOVA followed by posthoc t tests. Asterisks denote $P<0.05$, Error bars: +/- SEM.
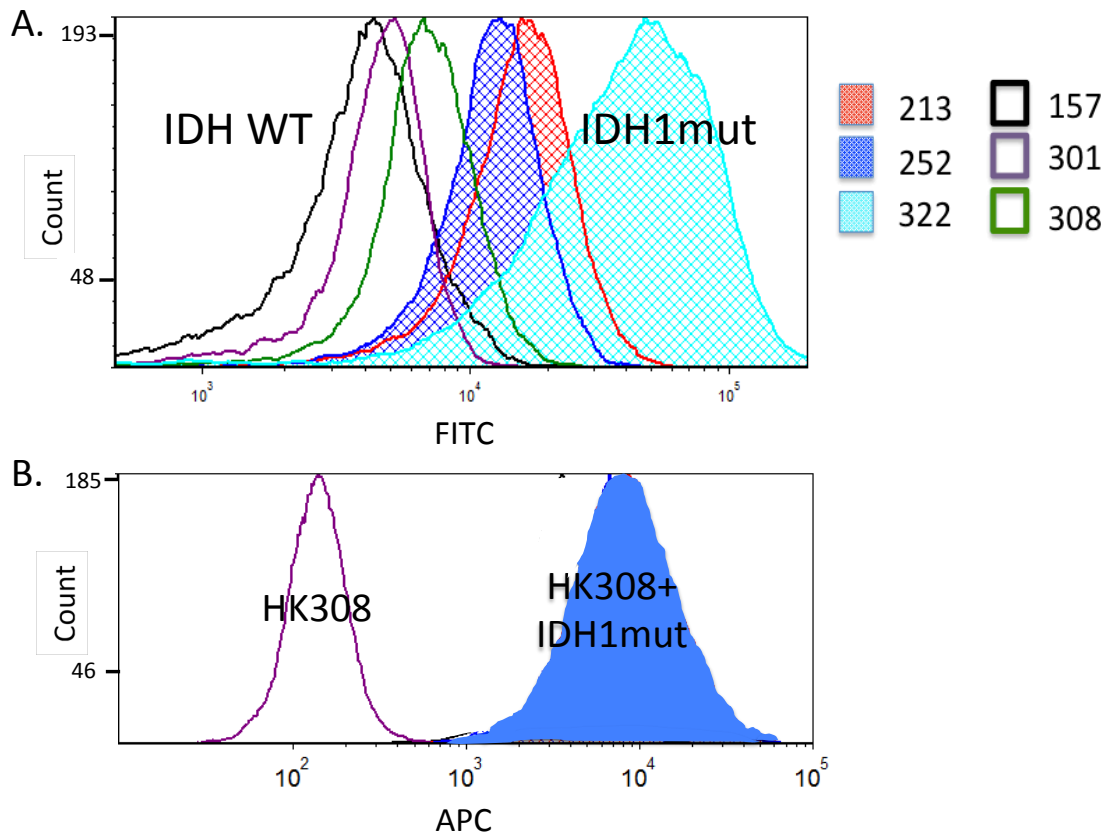
Figure 15. IDH1 mutant enzyme leads to higher ROS levels. A. Histogram displaying ROS levels of 3 IDH1 mutant and 3 IDH1wildtype gliomaspheres measured using flow cytometry (CellROX Green). B. Similar ROS analysis of an IDH WT line (HK308) with and without IDH1 mutant over-expression (CellROX Deep Red). Results shown are from individual experiments. Three replicates yielded identical findings.

Discussion

Many groups have attempted to determine the effect of the IDH1mutation on host cells as a way to discover metabolic vulnerabilities that may be exploited for therapy. Endogenous IDH1 mutant glioma cells are difficult to grow and maintain in culture—indeed, we lost one line during the process of these experiments--and thus the first experiments to determine the effect of the IDH1mutation on cells involved exogenous over-expression of the IDH1 mutant gene in an IDH WT background and performing mass spectroscopy to find differences in the levels of the various metabolites[119, 127, 131, 132, 133]. While many of these studies had overlapping findings (e.g. a decrease in glutamine and glutamate levels), other findings were more variable and seemed to depend on the cell model being used. Additionally, many of these *in vitro* differences did not translate to *ex vivo* patient tumor tissue[134].

Consistent with the aforementioned studies we also saw a decrease in glutamine and glutamate with exogenous IDH1 mutant over-expression. However, there was no difference in glutamine, glutamate, or any TCA cycle intermediates between IDH wildtype cells and endogenous IDH1 mutant cells. This suggests that endogenous IDH1 mutant cells may be able to compensate for many of the effects of the IDH1 mutant enzyme itself. One possible explanation for this is that IDH1 mutant glioma cells and IDH wildtype glioma cells are derived from different cell types with different properties. However, it is also possible that given enough time, the exogenous IDH1 mutant model would also be able to compensate for the IDH1 mutant enzyme and increase its glutamine and glutamate levels.

Another approach to determine the metabolic effect of the IDH1mutation on glioma cells is to inhibit the IDH1mutation in an endogenous IDH1 mutant line. Both the current study and the prior study of Tateishi et al[114] found a mixed effect of the IDH1 mutant inhibitor on TCA cycle

intermediates, with citrate being significantly increased in both studies. In our study, we used a relatively short incubation period (24hr) with the c227 inhibitor in order to isolate the differences in metabolic flux from the changes in gene expression that are associated with 2-HG and aberrant methylation. Although the Tateishi study did not find any significant changes in global methylation with prolonged c227 inhibitor treatment, they did find an increase in NADH levels likely due to increased Naprt1 expression and NAD synthesis. We did not see this change over our shorter time course and, in fact, we saw decreased NADH levels with c227 treatment.

A current challenge in IDH mutant research stems from the variability in methodological approaches used which can significantly alter findings. Identifying potential shortcomings of each will greatly improve the reliability of results. For example, by restricting comparisons to purely isogenic cell lines with or without IDH1 mutant enzyme over-expression or inhibition, the conclusions are limited to the effect of the IDH1 mutant enzyme itself and ignore differences between IDH1 mutant and IDH wildtype tumors that may be independent of the IDH1 mutation. Furthermore, metabolites do not act independently but function as parts of larger pathways. Using only the total cellular levels of various metabolites, it is difficult to draw any conclusions about particular pathways. In this study we utilized multiple methods to identify cell-type specific vulnerabilities. By using expression data and metabolic tracing studies we were readily able to distinguish several pathways as well as labeling patterns that clearly distinguished IDH1 mutant from IDH wildtype cells. This distinctive metabolic signature was intrinsic to the cell itself, was retained even with pharmacological inhibition of the IDH1 mutant enzyme, and was not seen in the exogenous over-expression model.

Further evidence of cell culture model variability between IDH mutant studies can be seen from two additional reports published during the preparation of this manuscript, Sulkowski et al.

and Lu et al.[135, 136], which demonstrated a diminished capacity for DNA damage repair in IDH1 mutant cells citing deficiencies in homologous recombination and compromised PARP-mediated DNA repair. We observed greater DNA damage and a similar decreased capacity for DNA repair only when using an IDH1 mutant over-expression model. In contrast, our results indicate greater DNA repair capacity in IDH1 mutant cells following radiation. One potential explanation could be that our cultures represent only a subset of IDH1 mutant tumors. Most, if not all, contain endogenous IDH1 R132H mutations and mutant TP53. Furthermore, the IDH wildtype GBM cultures that were selected as controls could influence the differences observed. While both of these prior studies utilize exogenously transduced IDH mutations, which may have different characteristics, one report did also utilize glioma cells with endogenous mutations for some of their key experiments[135]. However, it is not clear whether these mutant lines are similar to ours with respect to their other mutations. Furthermore, the endogenous mutant cultures from the prior report were propagated in serum, while ours are continuously maintained in serum-free conditions. The differences amongst these studies have important ramifications for therapy. If, as we propose, IDH1 mutants have a greater capacity for DNA repair following radiation, then radiation therapy may have diminished efficacy. Further study will be required to resolve these differences.

Many of the clinical trials that guide current treatment protocols for glioblastoma were conducted before the discovery of the IDH mutation and thus included a majority of IDH wildtype and a minority of IDH mutant patients. With evidence mounting that IDH mutant gliomas have very different cellular characteristics, it is unclear whether the results of these trials can be generalized to IDH mutant tumors. In particular, the results of this study show that IDH1 mutant gliomas are less vulnerable to radiation-induced DNA damage which draws into question the efficacy of radiation therapy for this subset of tumors. This result was surprising when combined

with the fact that exogenous IDH1 mutant over-expression makes cells more vulnerable to radiation[113], and that the IDH1 mutant enzyme significantly increases the amount of reactive oxygen species in the cell. While the cytotoxic and cytostatic mechanisms of radiation are multi-factorial, one of the main mechanisms is DNA damage through the indirect production of free radicals[137]. One possible explanation for the decreased DNA damage seen in IDH mutant cells following radiation is that in order to survive this mutation, IDH mutant cells must develop buffering mechanisms against high levels of reactive oxygen species. This adaptation in turn could make them more resistant to radiation induced DNA damage.

The clinical evidence for the efficacy of radiation in IDH1 mutant gliomas is mixed. In one study IDH1 mutant tumors seemed to show a better radiographic response following radiation[138]. However, another trial found that for supratentorial low grade gliomas (of which the majority are likely IDH-mutant) high dose radiation had worse survival than low dose radiation[139]. It is possible that both findings are correct and that radiographic response may not correlate with clinical survival. Conversely, it is possible that IDH mutant tumors are maximally sensitive to low dose radiation and higher doses do not provide any further benefit.

Our studies of nucleotide metabolism have potential implications for therapeutics. The availability of nucleotides for DNA synthesis can be a rate-limiting step in cellular proliferation[140]. Nucleotides are synthesized through either *de novo* or *salvage pathways*. Pharmacologically, the *de novo* pathway can be inhibited by high concentrations of dT and the salvage pathway can be inhibited by a novel class of compounds[125]. Our data suggest that IDH1 mutant tumors, in contrast to the majority of GBM, utilize this salvage pathway and would hence require both pathways to be inhibited in therapeutic strategies employing inhibition of nucleotide biosynthesis.

A limitation to the current study is that, while gene expression studies are performed using both cultured cells and data derived directly from IDH mutant tumors *in vivo*, our functional results are obtained from *in vitro* studies. Very few studies have investigated a spectrum of IDH mutant gliomas *in vivo*. This is undoubtedly due to the difficulty in propagating these cells in xenograft models. Although not shown, the cells we have utilized did not form xenografts in immunodeficient mice, either in the brain or subcutaneously. The reasons for this are unknown but suggest that the establishment of tumors from endogenous IDH1 mutants requires host-derived factors that are not present in our model systems. While our findings present novel hypotheses and avenues for future studies, some caution must be taken prior to applying our results directly to clinical trials.

With evidence mounting that IDH mutant gliomas constitute a distinct subclass that follows an independent path of tumorigenesis[141], we endeavored to characterize metabolic differences between IDH1 mutant and IDH wildtype gliomas. Our data are consistent with this concept and provide evidence that some of the distinctions may not be directly related to the IDH1 mutation itself. Furthermore, our data suggest that while IDH1 mutant gliomas may have a less malignant phenotype, they may also be relatively resistant to certain therapies, including radiation.

Methods

Collection of in vitro cultures- Samples were collected under institutional review board-approved protocols and graded by neuropathologists. We previously reported on gene expression analysis in these samples in all except one of the IDH mutants[124]. IDH wildtype samples were all from GBM. Of the 7 IDH1 mutant cultures, 5 were from GBM, one from a grade III oligoastrocytoma and one from a grade II oligodendroglioma. Cultures were prepared as described previously[124]. Briefly, on the day of resection, samples were digested with papain. Acellular debris was removed and remaining cells were incubated in gliomasphere media (DMEM/F12 supplemented with B27, penicillin/ampicillin, heparin, EGF and bFGF) for several days until spheres began to form. Frozen stocks were made at passage 5 to maintain cells at low passage. One IDH1 mutant line, BT142, was obtained through ATCC[126, 127]. Relevant information pertaining to the cultures used for *in vitro* experiments is summarized in Figure 3, which provides the characteristics of the patients and the tumor as reported by neuropathologists as well as data from comparative genomic hybridization and whole exome sequencing in the samples for which it was available. The majority of experiments were performed using the same 3 IDH WT lines (HK157, HK301, and HK308) and 3 IDH1 mutant lines (HK213, HK252, and HK322). Prior to the completion of data collection, the HK322 culture was lost. Therefore, two additional IDH1 mutant lines (BT142 and HK211) were included for the radiation experiments.

Whole exome sequencing and mutation analysis- Genomic DNA was extracted and fragmented by sonication using the Covaris acoustic disruptor (model E210, Covaris Inc.) to achieve an average fragment size of 200 base pairs. 200 ng of DNA from each sample were used for the construction of DNA libraries using Kapa Hyper DNA library prep kits and matched dual

index adapters (Integrated DNA Technologies). Exome capture was performed using the Nimblegen SeqCap EZ Exome enrichment kit. Sequencing was performed on an Illumina HiSeq 4000 following the manufacturer's instructions. 65-70 million 120-base, paired-end reads were obtained per sample on average, with a 50x average depth of coverage within the targeted exome. Raw image files were processed with the Illumina CASAVA 1.8 software (Illumina, San Diego, CA).

Whole exome sequencing was analyzed using the Genome Analysis Toolkit (GATK)[142] pipeline. Briefly, short reads were aligned using the Burrows-Wheeler Aligner (BWA)[143]. SAMtools was used to convert between SAM and BAM file format, and Picard tools to sort alignments and mark duplicates. Variants were called using the GATK HaplotypeCaller function with the following parameters: variant index parameter 128000; variant index type LINEAR; nda; maxAltAlleles 4; ERC GVCF; contamination 0.02. ANNOVAR[144] was used to annotate variants.

Copy number variation (CNV) analysis- DNA libraries were hybridized onto Affymetrix CytoScanHD arrays. We first processed the raw intensity CEL files using the R package affy2sv[145] to generate B-allele frequency (BAF) and log R ratio (LRR) values. Secondly, we used the PennCNV software (parameters: exome HMM model with gcmodel adjustment, filtered by 10 SNPs minimum 10 and with region length longer than 50k)[146], the R package GenoCN (parameters: cnv-only snpInfo$PFB>1; outputSNP 1; outputSeg TRUE)[147], and the R package Rawcopy (default parameters)[148] for CNV inference. CNV calls were obtained by integrating the output from all callers.

Gene set enrichment analysis- RNA was purified from 59 patient-derived gliomasphere

cultures and hybridized to Affymetrix U133 Plus 2.0 arrays. For KEGG-based analysis, we collapsed gene expression probes based on enzyme activity (Enzyme Commission numbers [EC]) rather than on gene identity to avoid unequal representation of equivalent enzymatic function within pathways, thus emphasizing potential flux through the network. The metric used for gene ranking was the signal to noise ratio (SNR) between the IDH1 mutant and IDH1WT samples. The metric was calculated for all candidate probesets of each gene or enzymatic activity and the probeset with maximum absolute metric value was retained. Probeset annotation was based on UniGene build #201 and UniGene identifiers were mapped to each EC using the gene names provided by KEGG. Pathways with fewer than three or greater than 500 nodes represented by the data were excluded from the analysis. This resulted in 167 KEGG modules in the TCGA dataset and 186 modules in the gliomasphere data set.

Glucose/Glutamine Uptake- 200,000 cells were plated in 3ml of gliomasphere media and allowed to grow for 24 hours. The cells were spun down and counted, and glucose and glutamine levels in the used media were measured using a NOVA Bioanalyzer and compared to blank control[149, 150, 151]. To evaluate the effects of IDH1 mutant inhibition on glucose/glutamine uptake, 5uM of c227 was added to the culture 24 hours before being harvested.

Cell proliferation studies (CFSE)- Cell proliferation of endogenous IDH1 mutant and IDH wildtype cultures was assessed using CFDA SE (CFSE; carboxyfluoresceindiacetate, succinimidyl ester) cell tracer kit (Invitrogen) as described previously[152]. Briefly, spheres were dissociated with Accumax (Innovative Cell Technologies), stained with CFSE according to manufacturer suggestions, and grown for 5 days under normal gliomasphere conditions at a density of 100,000

cells/mL. Preparation for FACS analysis was performed according to manufacturer guidelines using 4% paraformaldehyde as a fixative. Following FACS acquisition, Proliferation Wizard Basic Model was used to assess proliferative populations within each sample and to generate average division times.

Liquid chromatography–mass spectrometry (LC-MS)- Cells were cultured for 24 hours and rinsed with PBS, and either unlabeled media, 50% ^{13}C-glucose labeled media, or 50% ^{13}C-glutamine labeled media was added. After 24 hours, cells were rinsed with ice-cold 150mM NH_4AcO (pH 7.3), followed by addition of 400ul cold methanol and 400ul cold water. Cells were transferred to an Eppendorf tube, and 10 nmol norvaline (Sigma-Aldrich, N7502) as well as 400ul chloroform were added to each sample. For the metabolite extraction, samples were vortexed for 5 minutes on ice and spun down, and the aqueous layer was transferred into a glass vial and dried. Metabolites were resuspended in 70% ACN and 5 ul loaded onto a Phenomenex Luna 3u NH_2 100A (150 x 2.0 mm) column. The chromatographic separation was performed on an UltiMate 3000 RSLC (Thermo Scientific) with mobile phases A (5 mM NH_4AcO pH 9.9) and B (ACN) and a flow rate of 300 ul/min. The gradient ran from 15% A to 95% A over 18 min, 9 min isocratic at 95% A, and re-equilibration for 7 min. Metabolite detection was achieved with a Thermo Scientific Q Exactive mass spectrometer run in polarity switching mode (+3.0 kV/-2.25kV). TraceFinder 3.3 (Thermo Scientific) was used to quantify metabolites as the area under the curve using retention time and accurate mass measurements (< 3ppm). Relative amounts of metabolites were calculated by summing up all isotopologues of a given metabolite and normalized to the internal standard and cell number. Clustering analysis was done in R.

Metabolic Tracing using combined liquid chromatography and tandem mass spectrometry (LC-MS/MS)- Cell lines were grown in gliomasphere media supplemented with fully-labeled ^{13}C-glucose and ^{13}C9,^{15}N3-dC. The cells were allowed to grow for 48 hours at which point they were harvested and lysed. Genomic DNA was extracted using the Quick-gDNA MiniPrep kit (Zymo Research, D3021) and hydrolyzed to nucleosides using the DNA Degradase Plus kit (Zymo Research, E2021), following manufacturer-supplied instructions. In the final step of DNA extraction, 50 µL of water was used to elute the DNA into 1.5 mL Eppendorf tubes. A nuclease solution (5 µL; 10X buffer/DNA Degradase Plus™/water, 2.5/1/1.5, v/v/v) was added to 20 µL of the eluted genomic DNA in an HPLC injector vial. The samples were then incubated overnight at 37 ºC. Samples (20 µL) were injected onto a porous graphitic carbon column (Thermo Fisher Scientific Hypercarb, 100 x 2.1 mm, 5 µm particle size) equilibrated in solvent A (water/acetonitrile/formic acid, 95/5/0.2, v/v/v) and eluted (200 µL/min) with an increasing concentration of solvent B (acetonitrile/water/formic acid, 90/10/0.2, v/v/v) using min/%B/flow rates (µL/min) as follows: 0/0/200, 5/0/200, 10/15/200, 20/15/200, 21/40/200, 25/50/200, 26/100/700, 30/100/700, 31/0/700, 34/0/700, 35/0/200. The effluent from the column was directed to the Agilent Jet Stream ion source connected to the triple quadrupole mass spectrometer (Agilent 6460) operating in the multiple reaction monitoring mode using previously optimized settings. The peak areas for each nucleosides and nucleotides (precursor→fragment ion transitions) at predetermined retention times were recorded using the software supplied by the instrument manufacturer (Agilent MassHunter). To evaluate the effects of IDH1 mutant inhibition on glucose glutamine labeling 5uM of c227 was initially added to the culture and then re-added following PBS wash.

Deoxythymidine (dT) treatment- To evaluate the effects of nucleotide synthesis inhibition, a group of cells were grown in gliomasphere media and subjected to 1mM dT treatment and allowed to grow for four days. At this point the cells were harvested, stained with DAPI, and subjected to flow cytometry analysis to determine cell cycle distribution.

Radiation- To determine the extent of DNA damage following radiation, gliomaspheres were dissociated, plated at $1x10^5$ cells/mL, and subjected to a 10Gy dose of radiation using an X-ray irradiator (Gulmay Medical, Atlanta, GA) (5.519 Gy/min; 250 kV; a 4-mm Be, a 3-mm Al, and a 1.5-mm Cu filter). Neutral-buffered Oxiselect Comet Assay Kit (Cell Biolabs) was used to assess DNA damage according to manufacturer's instructions. Radiation-induced apoptosis was measured at four days after treatment using TUNEL staining. To determine effects of growth following radiation, cell lines were plated at $2x10^5$ cells in 3ml of gliomasphere media. They were then subjected to the indicated doses of radiation (0Gy, 2Gy, 6Gy, and 10Gy) and allowed to recover for a minimum of 4 days. When the control group of each cell line was ready to be passaged, all samples from that line were dissociated with Accumax (Innovated Cell Tech.), counted on a Countess Automated Cell Counter (Invitrogen, C10227) using 0.4% trypan blue, and compared to the non-irradiated control group. Each bar on the graph (dose of radiation) is the average percent of control based on a minimum of 3 independent replicates (Error bars= +/- SEM).

IDH1 mutant over-expression/ROS Measurement- cDNA for the IDH1 mutant gene (R132H) was cloned into a lentiviral vector and transfected into HK308 cell line. This vector encodes a murine orthologue and was found to maintain better and more consistent expression of the mutant protein and 2-HG than a human vector (data not shown). 500,000 IDH1WT cells were

dissociated and plated in 3ml of neurosphere mediated, infected with the lentivirus, and allowed to grow for 2 weeks. The cells were sorted for GFP and again allowed to grow and form spheres. All experiments were done within 6 weeks of infection. Over-expression of the IDH1 mutant protein was confirmed by western blot and 2-HG measurement. IDH1 mutant and IDH wildtype cells were allowed to grow in gliomasphere media. They were then collected, stained with CellROX reagents (Thermo Fisher), and analyzed by flow cytometry. The total ROS level was the integration of the area under the curve as previously described[153].

Statistical analysis- Statistical analyses were performed using the GraphPad Prism software. Sample comparisons and level of significance were determined using the ANOVA model and two-tailed Student's t-tests where appropriate. All quantitative data presented are the mean +/- standard error of the mean (SEM) unless otherwise noted. Experiments were performed in triplicate, with calculation of 95% confidence interval and P values in relevant comparisons.

Chapter 3

Metabolism of fatty acids and ketone bodies for growth by glioblastoma:

Implications for Ketogenic Diet Therapy

Abstract

Glioblastoma (GBM) metabolism has traditionally been characterized by a primary dependence on aerobic glycolysis, prompting the use of the ketogenic diet as a potential therapy. Recent preclinical evidence, however, suggests that alternative metabolic pathways may serve as important contributors. In this study we evaluated the effectiveness of the ketogenic diet in GBM and assessed the role of fatty acid oxidation (FAO) in promoting GBM propagation. *In vitro* assays with U87 glioma cells revealed growth-promoting effects of both ketone body and fatty acid (FA) supplementation under physiological glucose conditions. An *in vivo* assessment of the unrestricted ketogenic diet (administered *ad libitum*) surprisingly resulted in increased tumor growth and decreased animal survival. These effects on tumor growth and survival are abrogated by FAO inhibition using shRNAs or CRISPR-based knockdown of carnitine palmitoyltransferase 1 (CPT1), the rate limiting enzyme for fatty acid oxidation. Further *in vitro* assessment using primary GBM cultures revealed CPT1 functionality as well as decreased proliferation, increased apoptosis, and elevated mitochondrial ROS production with CPT1 inhibition with etomoxir. Liquid chromatography-mass spectrometry (LC-MS) metabolomic tracing with ^{13}C-labeled fatty acids showed significant FA utilization within the TCA cycle that also extended throughout the GBM metabolome, indicating that FAO could be used for both bioenergetics and the production of key intermediates. Finally, an assessment of both IDH1 mutant and wildtype gliomasphere cell lines

revealed differences in FAO utilization. Altogether, these data highlight important roles for FA and ketone body metabolism that could serve to improve targeted therapies in GBM.

Background

Glioblastoma (GBM), the most aggressive and therapy resistant form of brain tumor, is traditionally characterized by its reliance on the Warburg effect. Under normal physiological conditions the healthy adult brain meets most of its energy demand by complete oxidation of glucose. This produces pyruvate which is then converted into acetyl-CoA for entrance into the TCA cycle to support the electron transport chain[101]. Thus, glycolysis and respiration remain tightly connected and result in more efficient ATP production with little lactic acid production. In contrast, the Warburg effect dramatically increases the rate of aerobic glycolysis and lactic acid production in the cytosol. While the benefits of this phenomenon are not completely understood, it has been posited that its main advantages are increased biomass production and facilitated invasion due to acidification of the microenvironment[22].

GBMs have been identified as highly reliant on aerobic glycolysis to the point that they are sometimes referred to as being "glucose addicted". Several common signaling pathways found to be altered in GBM, such as PI3K-Akt-mTOR and Myc pathways, promote this phenotype by increasing expression of genes that allow cells to take up large amounts of glucose for increased glycolysis and lactate production[101, 154, 155, 156]. Alterations to these pathways are often associated with mutations common to GBM such as EGFR and PTEN. EGFR, an activator of PI3K, is amplified in ~40% of GBMs with approximately half of those tumors expressing the constitutively active EGFRviii variant[16]. The tumor suppressor protein PTEN, a potent PI3K antagonist, is also altered in 30-40% of GBMs[19]. Similar to EGFR amplification, loss of PTEN function by either

mutation or deletion results in hyperactivation of the PI3K/Akt signaling network. Despite these findings, little progress has been made therapeutically in targeting enzymes reported to regulate glucose metabolism in GBM.

The interconnection between oncogenic signaling networks and metabolic pathways is complex in GBM. For example, while EGFR and PTEN mutations affect PI3K/Akt/mTOR activation, a major contributor to "glucose addiction", this signaling node also acts as a master regulator for switching between metabolic utilization of glucose, glutamine, fatty acids, and ketones[59,157,158,159]. Mutations in isocitrate dehydrogenases (IDH) 1 and 2 are also commonly found in gliomas. Wildtype metabolic function of these enzymes is primarily restricted to the TCA cycle where they produce alpha-ketoglutarate through the oxidative decarboxylation of isocitrate. However, these enzymes often incur neomorphic gain-of-function mutations that result in the production of 2-hydroxyglutarate (2-HG)[44], a proposed oncometabolite, along with widespread changes that extend far beyond the TCA cycle. The effects of IDH mutations have been attributed to altered glucose and nucleotide metabolism, DNA repair capacity, and reactive oxygen species (ROS) regulation, to name a few[1,160,161]. Thus, the mutations present in any given tumor (such as EGFR, PTEN, and IDH1) may determine the extent to which it can adjust to declining substrate availability, pathway inhibition, or therapeutic insult. Reconciling mutational status with metabolic flexibility represents a critical step to establishing more effective metabolic therapies for GBM.

The ketogenic diet (KD), which is a high fat, low carbohydrate, adequate protein diet has been proposed as a potential adjuvant therapy for a number of cancers including GBM[162,83]. With traditional diets, carbohydrates are plentiful and converted to glucose which then circulates to the brain as a major source of fuel. The KD limits carbohydrate availability and forces the production

of ketone bodies such as ß-hydroxybutyrate and acetoacetate in the liver. Once in the brain these ketone bodies are converted to acetyl-CoA for entrance into the TCA cycle. The ability of the brain to oxidize ketone bodies is well-established, with one report estimating that up to 60% of the human brain energy requirement can be matched by ketone body oxidation[91]. The therapeutic premise of the KD is therefore dependent on the hypothesis that reducing glucose availability will starve cancer cells of necessary nutrients without causing harm to healthy brain tissue. The degree to which GBM cells can oxidize ketone bodies, however, is not completely understood, with several preclinical studies using the KD in animal brain tumor models showing varying levels of success[82, 163, 96].

FAs participate in a number of cellular processes including signal-transduction, membrane synthesis, and energy storage. FAs are typically synthesized from excess glucose and stored within the body as triglycerides in adipose tissue; however, they are also generated and stored endogenously by highly proliferative tissues like cancers through *de novo* FA synthesis. The elevated production of fatty acids in cancer is often driven by oncogenic mutations themselves[164]. Increased PI3K/Akt signaling, which can occur through mutations to EGFR or PTEN, results in upregulation of SREBP-1-mediated fatty acid synthesis and cholesterol uptake[165, 166, 167]. Similarly, oncogenic KRAS upregulates FA synthesis through mTORC1 and SREBP-mediated activation of fatty acid synthase (FASN)[168]. These FAs can then be used for membrane biosynthesis or as bioenergetic molecules. When cells require additional energy, FAs can undergo fatty acid beta-oxidation (FAO) within the mitochondria to generate acetyl-CoA to feed the TCA cycle and electron transport chain. In addition to ATP production, FAO also supports the production of a number of important cellular building blocks. For example, FA-derived citrate and malate can exit the TCA cycle to participate in the generation of both amino acid and lipid precursors[79]. FAO was

largely overlooked in the brain until recently, likely due to long-standing misconceptions that fatty acids (FAs) do not cross the blood brain barrier (BBB) and FAO does not take place. These misconceptions have since been dispelled and suggest that FAs play a large role in overall brain metabolism[169, 66, 170, 67].

In this study we investigate the ability of GBM cells to utilize both ketone bodies and FAs to support tumor growth and survival, especially because of the mounting interest in the ketogenic diet as an adjuvant therapy. We determined that implementation of the KD (administered *ad libitum*) can actually promote GBM tumor growth, but that this can be overcome by inhibition of CPT1A-mediated FAO. Functional studies show that both fatty acids and ketone bodies are used to a greater extent when compensating for decreased levels of glucose. We also identify that FAs in particular participate as metabolic substrates to support a number of critical metabolic pathways throughout the GBM metabolome, as opposed to functioning solely in the production of ATP. This study suggests that GBM metabolism is more adaptable than previously thought whereby they utilize pathways other than aerobic glycolysis to promote cell viability and proliferation.

Results

Fatty acid and ketone oxidation in U87

In order to determine whether GBMs are capable of oxidizing fatty acids we first examined expression levels of CPT1, the rate-limiting enzyme required for FAO. Analysis of the TCGA dataset from primary GBM tumors reveals that of the three CPT1 isoforms found in humans, CPT1A and CPT1C are most highly expressed in GBM (Figure 16A). Inhibition of these enzymes with the CPT1-specific inhibitor etomoxir (ETOM) significantly diminished U87 cell growth (cell number) *in vitro* (Figure 16B).
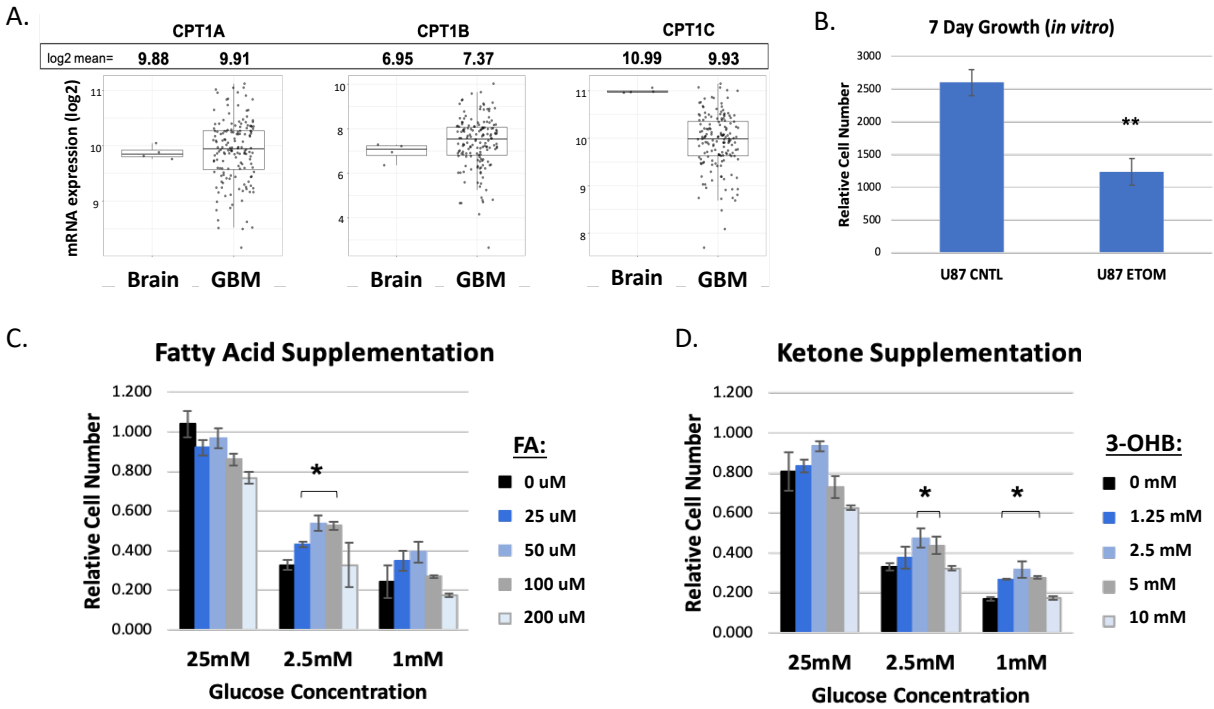
Figure 16. U87 GBM cells oxidize fatty acids and ketone bodies to support growth. A. Relative mRNA expression of the 3 CPT1 isoforms in GBM based on analysis of the TCGA dataset from primary human GBM tumors. B. Quantification of the effects of 100 uM ETOM treatment on U87 cell growth. Culture growth was assessed following a 7 day treatment with ETOM administered twice per week. C-D. Effects of FA and ketone supplementation under variable concentrations of glucose following a 7 day growth period in U87 cells. Error bars denote +/- SD. (* = p<0.05)

Because gliomasphere media used for *in vitro* studies contains high levels of glucose (25 mM) not found naturally in the human brain or in brain tumors, a glucose-limiting assay was performed to assess both fatty acid and ketone body utilization under more physiologically relevant glucose levels, with 2.5 mM glucose representing extracellular levels commonly found in the brain and 1 mM glucose serving as a low glucose condition to more closely mimic levels found in tissue that do not have adequate access to vascular supplies of glucose[171]. Palmitic acid supplementation (25-100 mM) partially rescued U87 cell growth under 2.5 mM low glucose conditions (Figure 16C), whereas ketone supplementation with 2.5-5 mM 3-hydroxybutyrate (3-OHB) promoted cell growth in both 2.5 mM and 1 mM glucose (Figure 16D). Neither FA nor ketone supplementation had growth-promoting effects under non-physiological conditions of high glucose (25 mM).

To further determine how and where FAs are utilized within U87 cells, untreated CNTL cells, cells treated with ETOM, and cells with CPT1A knockdown were subjected to LC-MS metabolomic analysis using fully-labeled ^{13}C palmitic acid in physiological glucose conditions (2.5 mM). Analyzing fractional contribution (or the percent of labeled carbons for each metabolite) within these samples revealed labeling throughout the TCA cycle as well as in the ubiquitously important currency metabolite ATP. Treatment with ETOM or CPT1A knockdown dramatically diminished this labeling (Figure 17A). Similar effects were observed when analyzing the relative amounts of these metabolites, wherein ETOM treatment and CPT1A knockdown significantly decrease levels of TCA-associated metabolites, acetyl-CoA, and ATP (Figure 17B). Taken together these data confirm FAO utilization while also suggesting that of the 3 CPT1 isoforms, CPT1A appeared to be the primary isoform regulating this process in GBM.
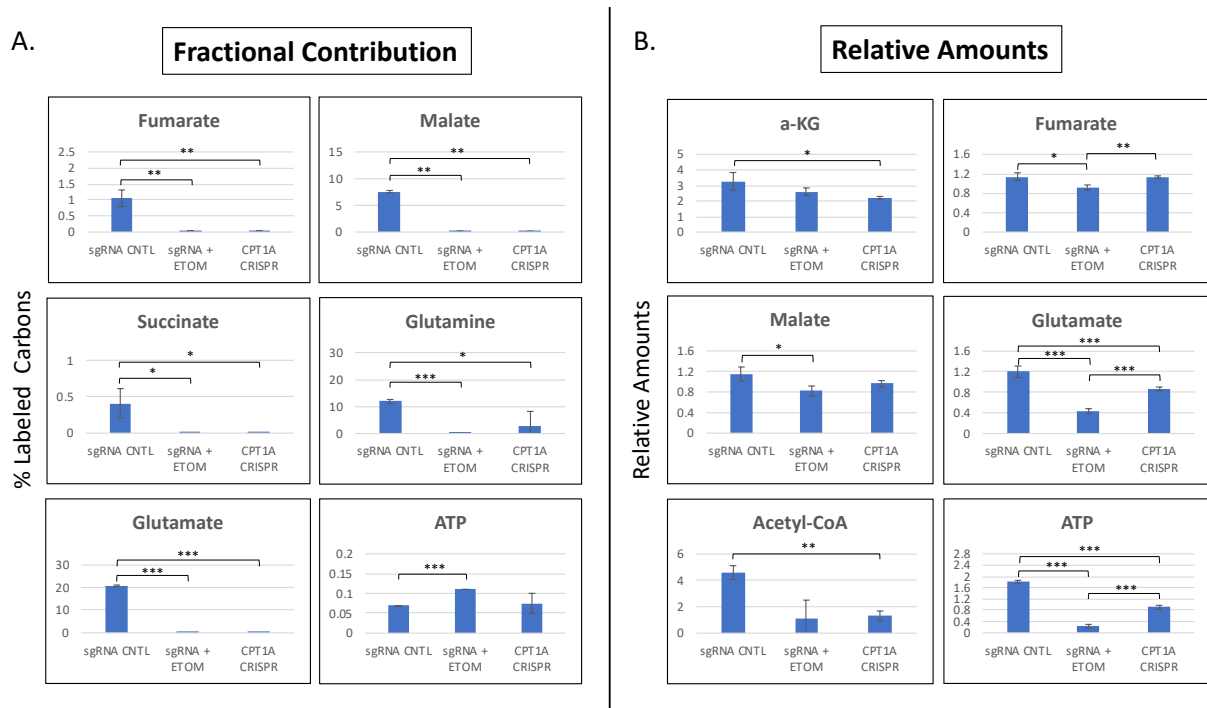
Figure 17. U87 GBM cells oxidize fatty acids to generate TCA cycle intermediates and currency metabolites. A-B. Effects of ETOM and CPT1A knockdown in U87 cells on fractional contribution (the percent of labeled carbons for each metabolite) and relative amounts of relevant TCA cycle intermediates and currency metabolites using ^{13}C-palmitate LC-MS analysis. Glucose concentration = 2.5 mM) Error bars = +/- SD. (*=p<0.05, **=p<0.01, ***=p<0.001).

CPT1A knockdown and the ketogenic diet

Based on these initial results and previous studies[172, 173] that have indicated that many brain tumors may lack the ability to oxidize ketones as an energy substrate, we sought to determine if inhibiting FAO while concurrently implementing a ketogenic diet using an orthotopic xenograft model in mice might serve as an effective therapeutic strategy. It is thought that this strategy would reduce the availability of glucose as an energy substrate and make the GBM cells more vulnerable to cell death (starvation) by also inhibiting FAO as an alternative energy source. Because expression data indicated that CPT1A is most highly expressed in GBM, lentiviral shRNAs were used to knockdown CPT1A in U87 cells expressing firefly luciferase-GFP (Fluc-GFP). While this did not result in complete knockdown, the degree of knockdown was sufficient to significantly inhibit *in vitro* cell growth by ~40% to levels near what was observed with ETOM alone (Figure 18A), once again suggesting that CPT1A is the primary isoform regulating FAO in these cells. This also demonstrates the importance of endogenous fatty acid oxidation to the maintenance of normal *in vitro* cell growth in these GBM cells despite U87s having a PTEN mutation which increases PI3K/AKT/mTOR signaling, which has been previously thought to inhibit FAO in GBM. To assess these results *in vivo* as well as to determine the effectiveness of the KD on tumor growth, U87 cells (shCNTL and shCPT1A) were injected into the striatum of adult NSG mice. On day 4, half of each group was switched to a calorie-unrestricted KD followed by weekly bioluminescent imaging with luciferin as shown in Figure 18B. At 21 days post-injection, animal weights, blood glucose levels, and blood ketone levels were evaluated. Both of the ketogenic diet cohorts (shCNTL and shCPT1A) exhibited decreased total body weight, decreased blood glucose levels, and increased blood 3-hydroxybutyrate levels, confirming ketosis was achieved in these animals (Figure 18C-E).
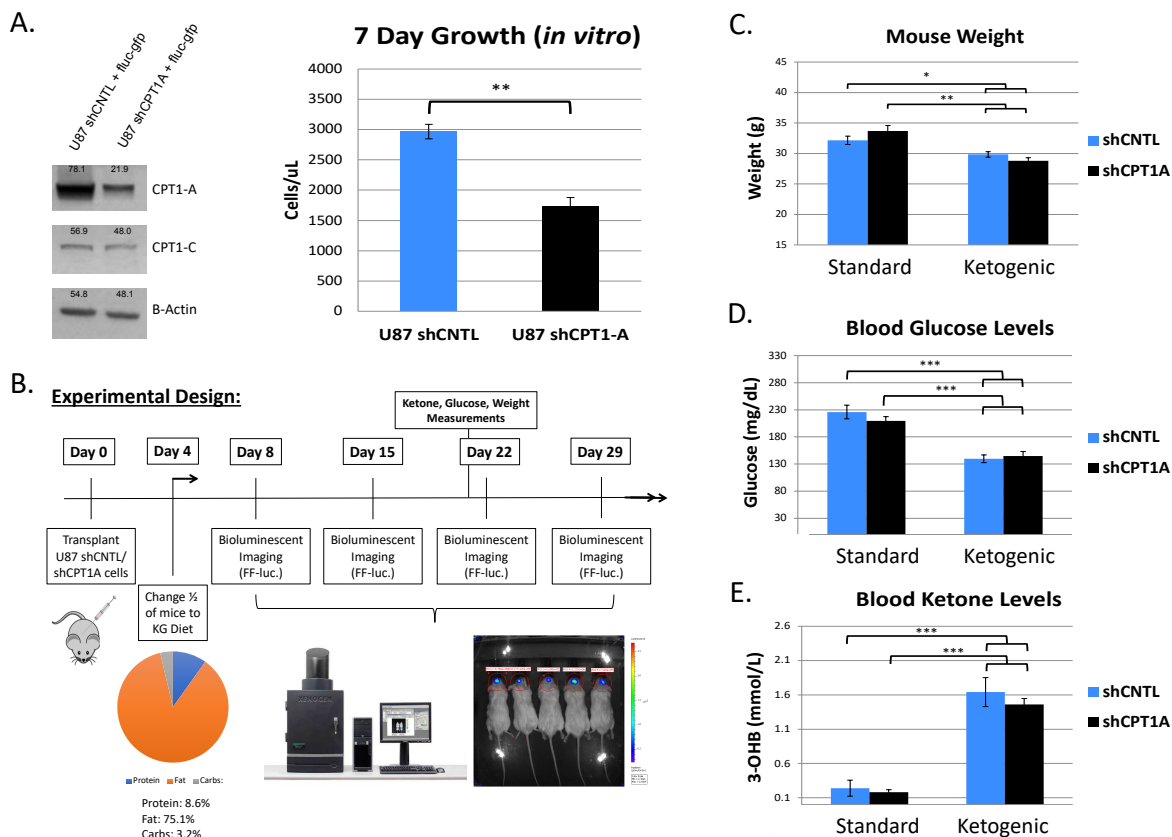
Figure 18. The unrestricted ketogenic diet causes ketosis in mice transplanted with U87 cells. A. Western blot of fluc-GFP expressing U87 cells infected with either shCNTL or shCPT1A lentivirus. Quantification of 7 day growth in U87 shCNTL and U87 shCPT1A (Error bars = +/- SD). B. Basic schematic of the experimental design for the U87 shCPT1A ketogenic diet xenotransplant experiment. Cells were injected on Day 0. Mice were kept on standard chow for 4 days to allow appropriate recovery, after which half of each group was placed on the ketogenic diet. On Day 8, weekly bioluminescent imaging was initiated. On Day 21 mouse weight, blood glucose and ketone measurements were taken. C-E. Assessment of mouse weight, blood glucose, and blood ketone levels on Day 21. Error bars denote +/- SEM.

Contrary to our initial hypothesis, analysis from weekly bioluminescent imaging shows that the shCNTL cohort receiving the KD had the greatest percent increase in tumor size, but that this increased growth was abrogated by CPT1A knockdown (Figure 19A). A similar experiment using a CPT1A CRISPR/Cas9 system corroborated the finding that the KD promoted U87 tumor growth, but that this could be overcome by CPT1A-mediated FAO inhibition (Figure 20). These findings were mirrored by analysis of mouse survival. The poorest survival was observed in the shCNTL group receiving the KD and the greatest in the shCPT1A group receiving standard chow. (Figure 19B). Immunohistochemisty of sectioned post-mortem tissue confirmed that CPT1A knockdown was maintained throughout the length of the experiment (Figure 19C). Knockdown of CPT1C in U87 had inhibitory growth effects *in vitro*, albeit not to the degree of CPT1A knockdown, but there were no observable differences in tumor growth *in vivo* when compared to shCNTL cells. The findings using our model, while surprising, may indicate a previously unknown ability of GBM cells to thrive under ketosis while also highlighting an important role of CPT1A-mediated FAO in regulating this process.
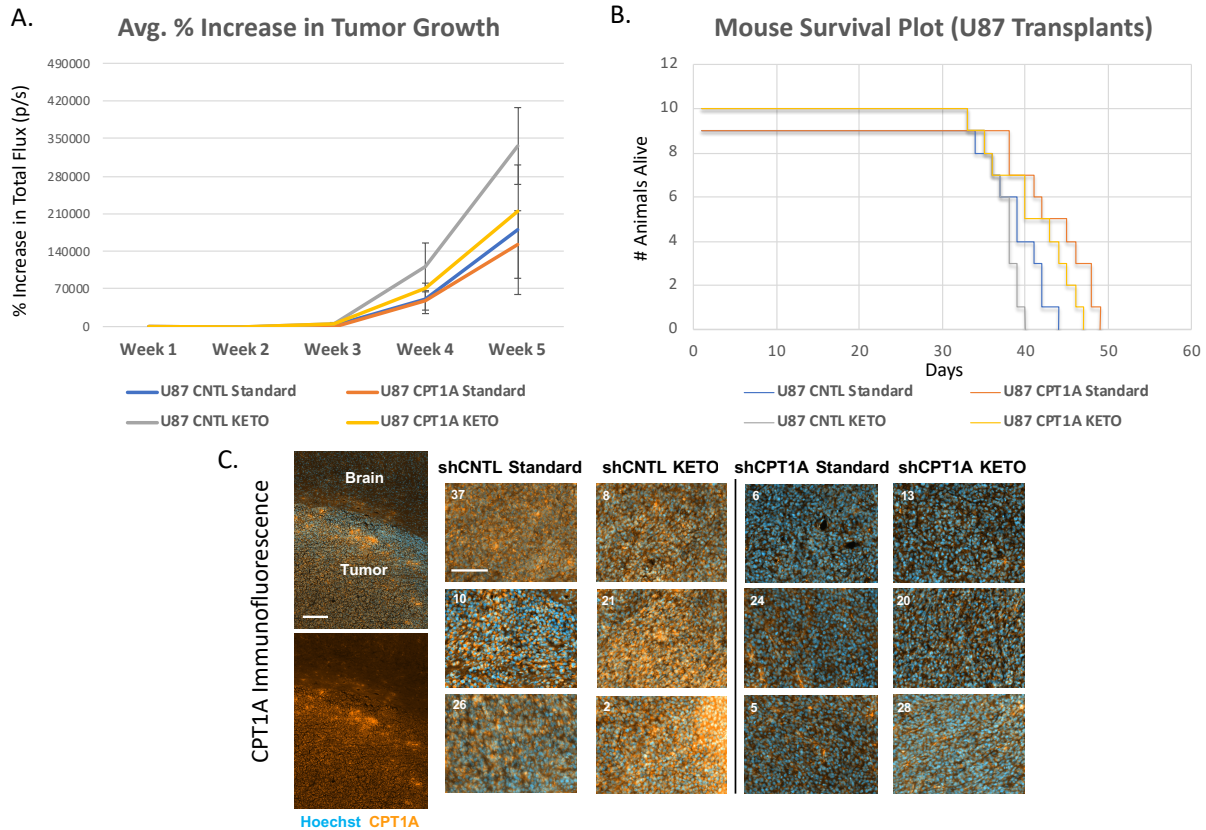
Figure 19. The ketogenic diet increases U87 tumor growth but this is overcome by CPT1A knockdown. A. Evaluation of tumor growth based on percent increase in total flux [p/s] from Week 1 measurements. Tumor growth was quantified for each individual animal and then averaged by group (Error Bars = +/- SD). B. Assessment of mouse survival over the course of the experiment. Survival was tracked for individual animals until either death or progression to a moribund state. C. Immunohistochemistry of CPT1A in sectioned tissue following brain perfusion. Tissue was sectioned at a thickness of 20 uM.
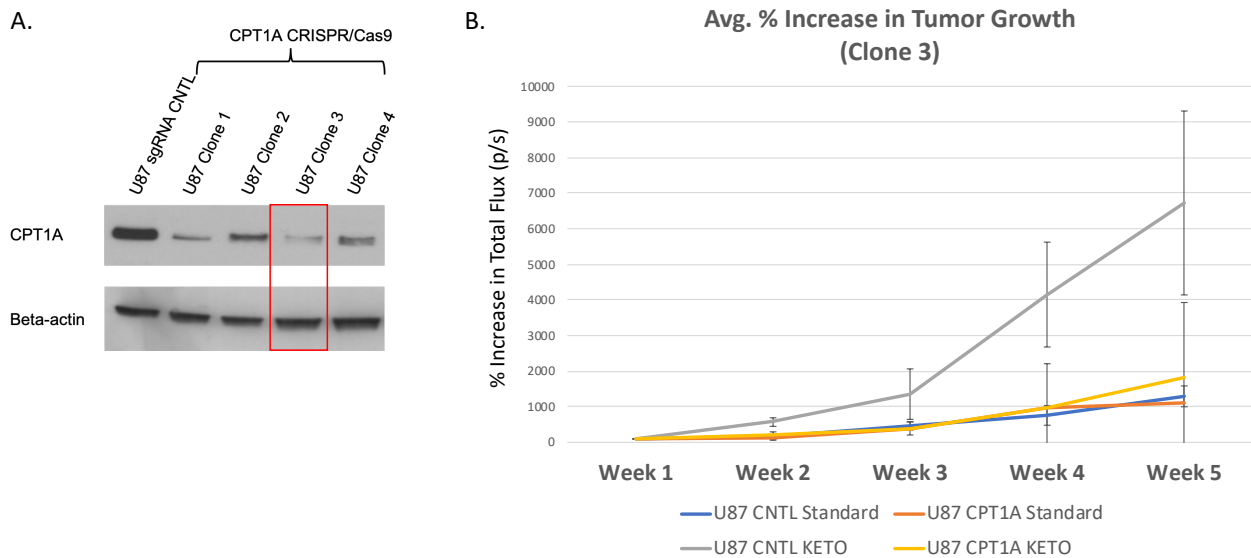
Figure 20. CRISPR/Cas9 model validates the effects of the ketogenic diet and shCPT1A knockdown on U87 tumor growth. A. Western blot showing expression of CPT1A relative to beta-actin for cells infected with either CNTL or CPT1A CRISPR guideRNA/Cas9. B. Evaluation of tumor growth based on percent increase in total flux [p/s] from Week 1 measurements. Tumor growth was quantified for each individual animal and then averaged by group (Error Bars = +/- SD). The experimental design for these transplants can be found in Figure 18B.

While U87 cells are a reasonable model to test biochemical hypotheses in GBM, the cells bear significant differences from primary GBM cells. In order to confirm the potential importance of fatty acid oxidation in GBM we examined the potential of primary gliomasphere cultures to oxidize FAs and ketone bodies to support growth and cell survival. Analysis of our gliomasphere microarray dataset[124] was performed to determine whether our primary cultures express the CPT1 isoforms, similar to that of tumors (Figure 16A). This analysis revealed once again that CPT1A and CPT1C were more highly expressed than CPT1B (Figure 21A). Protein expression of these isoforms was confirmed using Western blot and immunocytochemistry. Respiration using palmitoyl-CoA as a substrate in primary GBM lines confirmed that CPT1-mediated FAO occurred in these cells (Figure 21B).

While other studies have utilized ETOM up to millimolar concentrations, more recent research indicates that 3 μM ETOM is sufficient to fully inhibit CPT1 activity in macrophages, with excessive concentrations resulting in off-target effects[80]. The concentration of ETOM required to fully saturate CPT1 activity in GBM has not yet been established, however, so we sought to address this issue by analyzing differences between 3 μM and 100 μM ETOM on basal oxygen consumption rates. The higher dose slightly decreased oxygen consumption in two of the cell lines, suggesting a potential off-target effect of 100 μM ETOM (Figure 21C). However, further analysis using palmitic acid and ETOM clearly demonstrated that GBM cells are able to actively oxidize both endogenous and exogenous FAs (Figure 21D). We also assessed the ability of a primary GBM (HK157) to utilize exogenously supplied FA and 3-OHB as an energy substrate to support cellular growth in both physiological and high glucose conditions (Figures 21E-F). Similar to what was observed in U87 cells, both exogenously supplemented FA and 3-OHB had growth-

promoting effects under lower and more physiologically relevant glucose levels (2.5 mM), demonstrating the ability of the primary GBM to utilize alternative substrates.
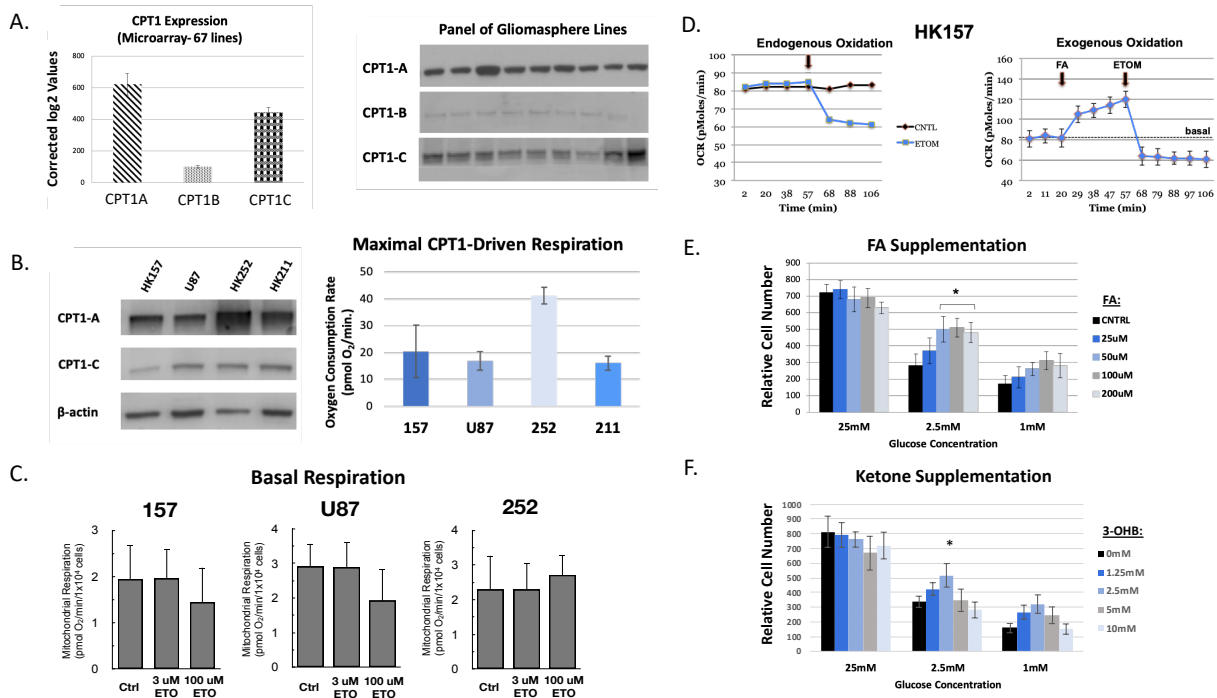
Figure 21. Primary GBM cells oxidize fatty acids and ketone bodies to support growth. A. Relative CPT1 isoform expression (mRNA) based on our microarray dataset from 67 primary gliomasphere cell lines and relative protein expression (Western blot) of CPT1 isoforms across a panel of gliomasphere cell lines. B. Western blot showing expression of CPT1A and CPT1C relative to beta-actin for the 4 lines used for Seahorse analysis. Quantification of maximal CPT1-driven respiration in lysed cells treated with palmitoyl-CoA using Seahorse analysis. C. Quantification of basal respiration (OCR) in cell lines incubated with either 0 uM, 3 uM, or 100 uM ETOM to test for potential off-target effects using Seahorse. D. Seahorse analysis to assess both endogenous and exogenous FAO. Endogenous oxidation was measured by adding 100 uM ETOM (indicated by arrow). Exogenous oxidation was measured by adding palmitic acid (FA arrow) followed by 100uM ETOM (ETOM arrow). E-F. Effects of FA and ketone supplementation

in a primary GBM cell line (HK157) under variable concentrations of glucose following a 7 day

growth period. Error bars denote +/- SD.

To further assess inhibition of endogenous FAO on GBM cell growth and survival we tested the effects of ETOM in a panel of primary GBM cultures. These experiments were initially done under high glucose, non-FA supplemented conditions. A 7-day treatment with ETOM resulted in diminished overall culture growth for all gliomasphere lines tested (Figure 22A). This analysis yielded no significant differences with regard to IDH1 mutant status, PTEN deficiency, EGFR amplification, or the presence of the EGFRviii mutation (data not shown). Interestingly, ETOM treatment did not inhibit the growth of cultured human fetal neurospheres or SVZ-derived mouse neurospheres. This may indicate that FAO is GBM-specific, irrespective of mutational status, and less important to healthy tissue making it a potentially attractive therapeutic target. Following a 4-day treatment with ETOM we found a significant decrease in actively dividing cells as assessed using bromodeoxyuridine (Brdu) incorporation (Figure 22B), demonstrating the importance of endogenous FAO to the maintenance of cell proliferation even in GBMs (HK301) with a mutation that enhances AKT pathway signaling. In addition to these effects on proliferation we also observed an increase in cell death as measured by annexin V/propidium iodide staining (FACS) following treatment with ETOM (Figure 22C). Analysis of ETOM treatment on intracellular reactive oxygen species (ROS) levels revealed no change in total intracellular ROS. Treatment did increase mitochondrial superoxide levels across all lines tested (Figure 22D) suggesting that etomoxir, which binds to CPT1 on the outer mitochondrial membrane, specifically alters ongoing FA mitochondrial oxidative metabolism. A 7-day growth assay in a number of primary GBM lines of varying mutational status was performed in 2.5 mM glucose, representative of physiological levels. This showed a slight increase in sensitivity to ETOM inhibition of endogenous FAO than what was observed in 25 mM glucose (Figure 22E). We also assessed the ability of the primary GBMs to utilize exogenously supplied FA and 3-OHB as an energy substrate

to support cellular growth at 2.5 mM glucose (Figure 22E). Our results indicate that there is increased variability in the ability of the cells to promote cell growth from what was observed in the U87 glioma cell line (Figure 16C-D), likely representing a heterogeneity among GBMs to utilize these alternative substrates in place of glucose. Taken together, these data support our hypothesis that FAO is a significant contributor to overall GBM metabolism and growth, which is not prevented by PI3K/AKT/mTOR pathway-promoting mutations in our lines as has been observed in previous studies on GBM glucose dependency and fatty acid utilization[174, 175, 176].
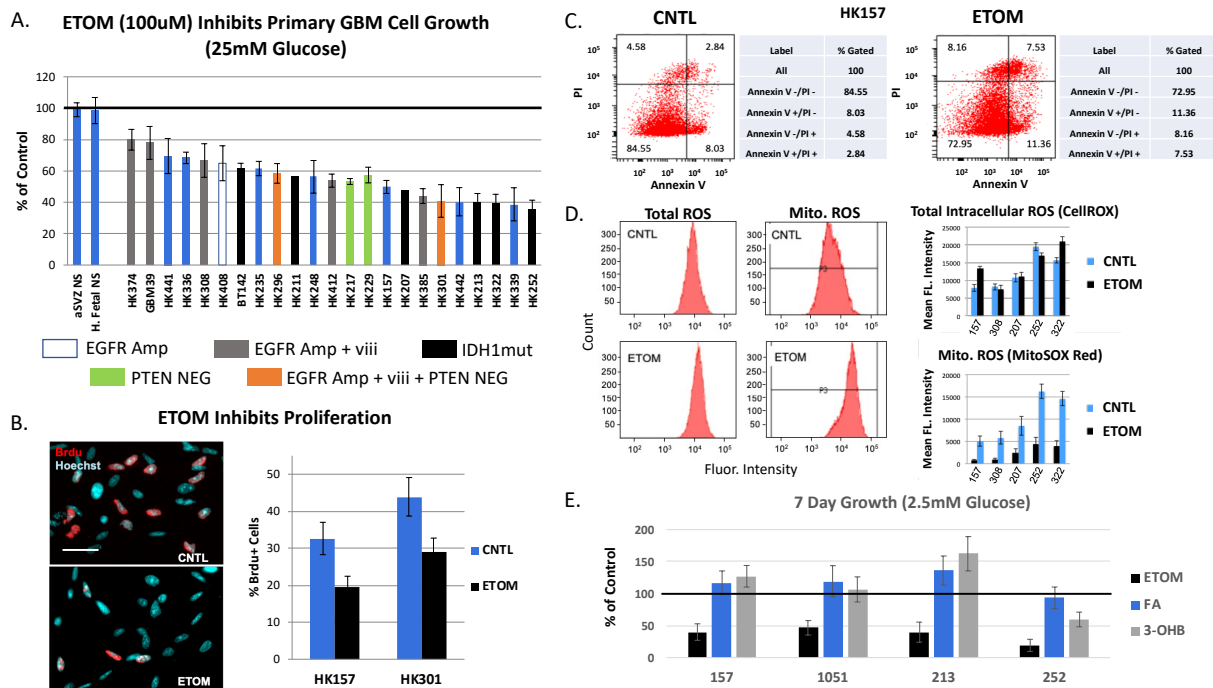
Figure 22

Figure 22. Etomoxir inhibits primary GBM cell proliferation and promotes cell death while increasing mitochondrial ROS levels. A. Quantification of the effects of 7 day 100 uM ETOM treatment (administered twice per week) across a panel of primary GBM cell lines and two non-GBM controls (adult mouse-derived neurospheres and human fetal-derived neurospheres). Cell growth was calculated based on actual cell counts. Error bars = +/- SEM. Cultures that are EGFR amplified, EGFR ampified + EGFRviii mutant, IDH1 mutant, and PTEN deficient are indicated. B. Assessment of actively dividing cells by Brdu immunocytochemisty in two primary GBM lines grown for 4 days in the presence of 100 uM ETOM. C. FACS analysis of cell death using dual Annexin V/PI staining in HK157 cells following 4 day treatment with 100 uM ETOM. D. Evaluation of total ROS levels (CellROX Deep Red) and mitochondrial superoxide levels (with MitoSOX Red Reagent) by flow cytometry. Left: histogram showing actual fluorescent readout of one cell line. Right: Graph quantifying mean fluorescent intensities for each line. E. 7 day growth assessment (cell counts) with 100 uM ETOM, 50 mM palmitate (FA), and 1.25 mM 3-OHB in 2.5 mM glucose. All other experiments were performed in 25 mM glucose. Error bars = +/- SD.

LC-MS with fully-labeled palmitic acid

We utilized LC-MS analysis with fully-labeled ^{13}C palmitic acid to characterize the contribution of FAO to the metabolome of primary GBM cells. Fractional contribution studies revealed that ETOM treatment caused widespread changes in carbon labeling across the metabolome (Figure 23A). Importantly, ETOM resulted in diminished labeling of acetyl-CoA, the end product of FAO, along with an increase in the amount of labeled palmitate within the cell (Figure 23B). Both results confirmed that labeled FAs were taken up and oxidized within the cell. In addition to acetyl-CoA, ETOM treatment also resulted in diminished labeling within the TCA cycle and among metabolites that commonly feed into the TCA cycle such as glutamine, glutamate, and lactate (Figure 23B). Analysis of the relative amounts of metabolites with ETOM treatment did not result in changes to overall acetyl-CoA or palmitate levels. However, ETOM treatment did result in lower relative levels of TCA-associated metabolites which include alpha-ketoglutarate, citrate, fumarate, glutamine, and glutamate (Figure 23C). A full list of significantly altered metabolites resulting from FAO inhibition with ETOM (Table 1) demonstrates that GBM cells utilize FAO to support a number of critical metabolic pathways throughout the GBM metabolome.
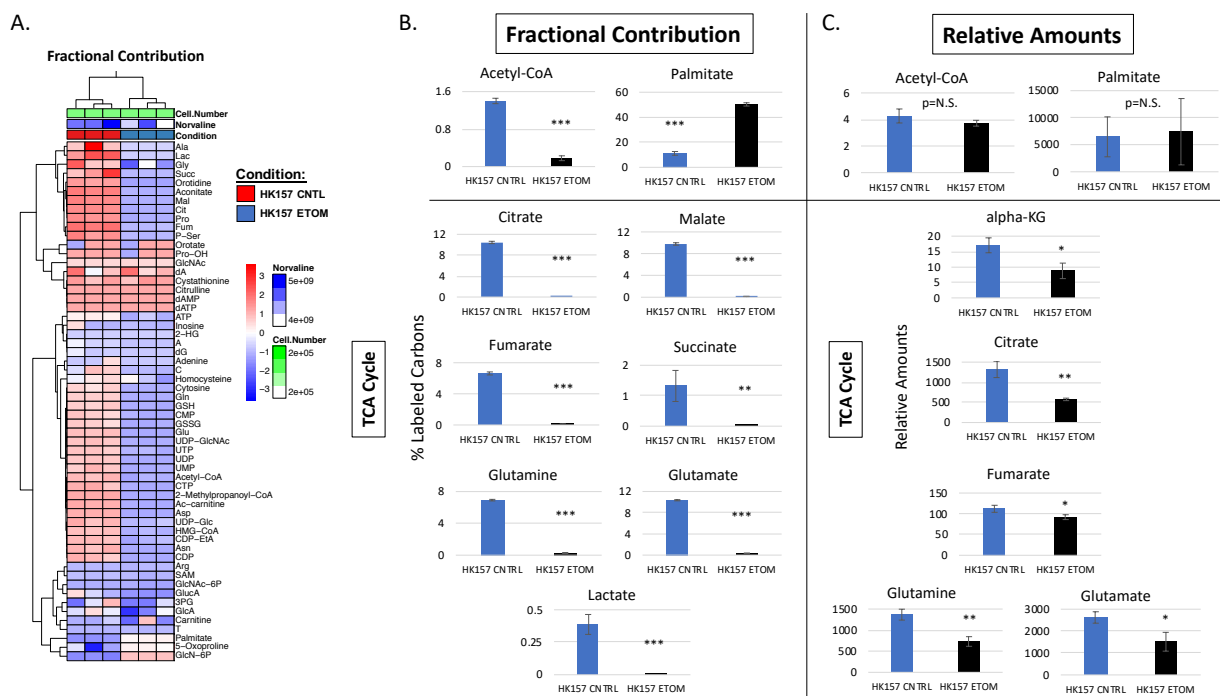
Figure 23. GBM cells oxidize FAs to generate acetyl-CoA for use within the TCA cycle. A-B. LC-MS analysis of ^{13}C-palmitic acid fractional contribution following treatment with 100 uM ETOM. A. Heat map showing effects of ETOM on fractional contribution across metabolites. B. Quantification of the effects of ETOM on intracellular carbon labeling of acetyl-CoA, palmitic acid, and other relevant metabolites associated with the TCA cycle. C. Effects of ETOM on relative amounts of relevant metabolites as in B. ETOM concentration used: 100 uM. Error bars = +/- SD. (* = p<0.05, ** = p<0.01, *** = p<0.001).

Significantly different Metabolites (p<0.05): (* indicates increased levels with ETOM)

	TCA Cycle	Pentose Phosphate	Nucleotide Metabolism	Amino Acid Metabolism	Fatty Acid/Lipid Metabolism	Currency	Other
Fractional Contribution	Aconitate	SAM	5M-adenosine	Asn	Ac-carnitine	Acetyl-CoA	GlcN-6P*
	Cit		ATP	Asp	CDP	ATP	HMG-CoA
	Fum		C	Pro	CDP-EtA	GSH	
	Lac		CMP	P-Ser	Palmitate*	GSSG	
	Mal		CTP				
	Succ		Cytosine				
			Hypoxanthine				
	Gln		Orotidine				
	Glu		UDP				
			UDP-Glc				
			UDP-GlcNAc				
			UMP				
			UTP				
Relative Amounts	a-KG	Cystathionine	ATP	Ala	Ac-carnitine	ATP	GlcN-6P
	Cit	G6P-F6P	dATP	Pro	P-Choline	Creatine	4-OH-PheLac
	Fum	IMP*	CDP	Ser	P-EtA	NADH	Inositol
	Aconitate	R5P*	CTP	Thr		AMP/ATP Ratio*	Vit-C
			GTP	Citrulline			
			UTP	2-Methylpropanoyl-CoA			
	Gln		Orotidine				
	Glu		C*				
			Cytosine*				
			G*				

Table 1. GBM cells utilize fatty acids to support other metabolic pathways in addition to the TCA cycle. List of all metabolites significantly altered by ETOM (100 uM) treatment with regard to fractional contribution and relative amounts of labeled ^{13}C-palmitic acid using LC-MS analysis. Cell line: HK157. (p<0.05 for all metabolites listed).

Fatty acid oxidation in IDH1 mutant GBM

Recent studies, including one from our own group[1], have demonstrated that GBMs harboring an isocitrate dehydrogenase 1 (IDH1) mutation represent a metabolically distinct subset of glioma. Because of this, we sought to identify potential differences in FAO utilization between our IDH1 mutant and IDH WT gliomasphere cultures. Analysis of microarray data from 67 gliomasphere lines, 7 of which are IDH1 mutant, revealed elevated mRNA expression of CPT1A in IDH1 mutant lines (Figure 24A) compared to IDH wildtype cultures. Western blot analysis confirmed elevated CPT1A protein expression (Figure 24B). Similar to IDH WT cells, LC-MS analysis with fully-labeled palmitic acid in an IDH1 mutant cell line showed diminished labeling of acetyl-CoA and several TCA-associated metabolites when treated with ETOM (Figure 24C). Interestingly, 2-hydroxyglutarate (2-HG), a proposed oncometabolite and the resulting product of the IDH1 mutant enzyme itself, was among the most heavily labeled metabolites in this particular IDH1 mutant line. Treatment with ETOM significantly diminished both the fractional contribution and relative amount of intracellular 2-HG, suggesting that FAO may serve as a major contributor to 2-HG production in IDH1 mutant GBMs (Figure 24C-D). FAO inhibition with ETOM in IDH1 mutant cells did not result in a decrease in the relative amounts of TCA cycle intermediates as was observed in IDH WT cells (Figure 24D, Figure 25), perhaps indicating a greater reliance on FAO to feed the TCA cycle in IDH WT GBM. Analysis of the full list of significantly different metabolites revealed fewer overall metabolites altered by ETOM treatment in IDH1 mutant cells (Table 2). These data confirm FAO utilization in both IDH1 mutant and wildtype cells while highlighting several potentially important metabolic differences between the two. Further investigation with a greater number of IDH mutant and wildtype lines will be needed to fully elucidate these differences.
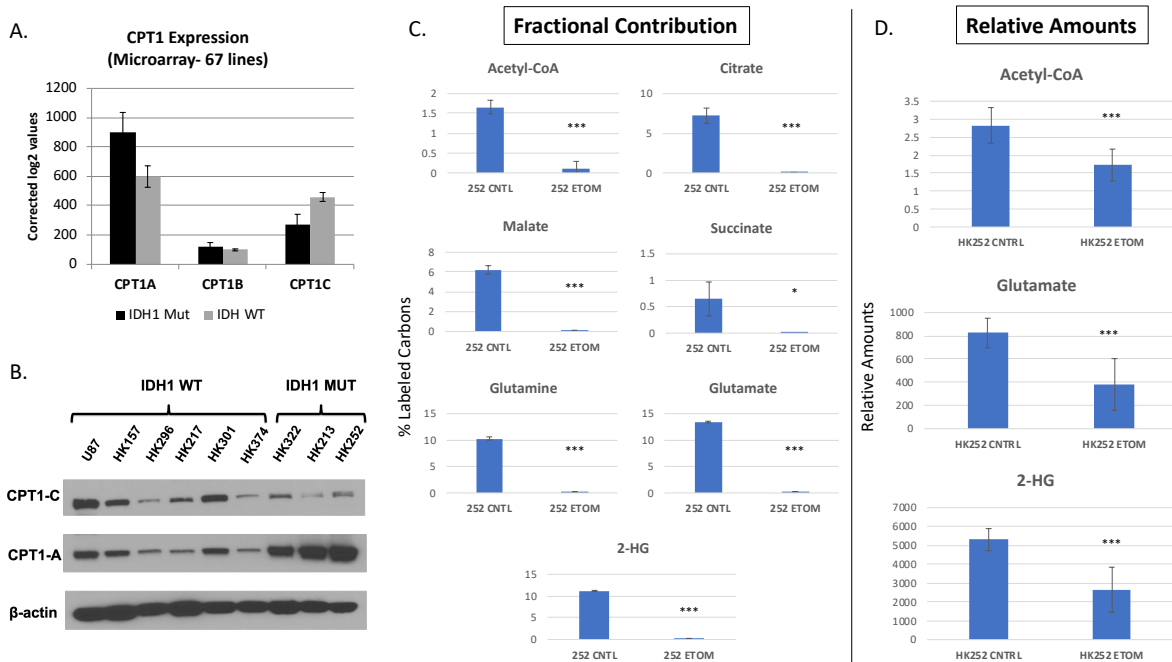
Figure 24. IDH1 mutant GBM cells express higher levels of CPT1A and utilize fatty acids to produce 2-HG. A. mRNA expression of CPT1 isoforms in IDH1 mutant and wildtype primary GBM cultures based on analysis of microarray data as in Figure 21A. B. Protein expression (Western blot) of CPT1A and CPT1C across a panel of IDH wildtype and IDH1 mutant lines. C-D. Analysis of the effects of ETOM (100 uM) in an IDH1 mutant cell line on fractional contribution and relative amounts of relevant metabolites using ^{13}C-palmitic acid LC-MS. Error bars = +/- SD. (* = p<0.05, ** = p<0.01, *** = p<0.001).
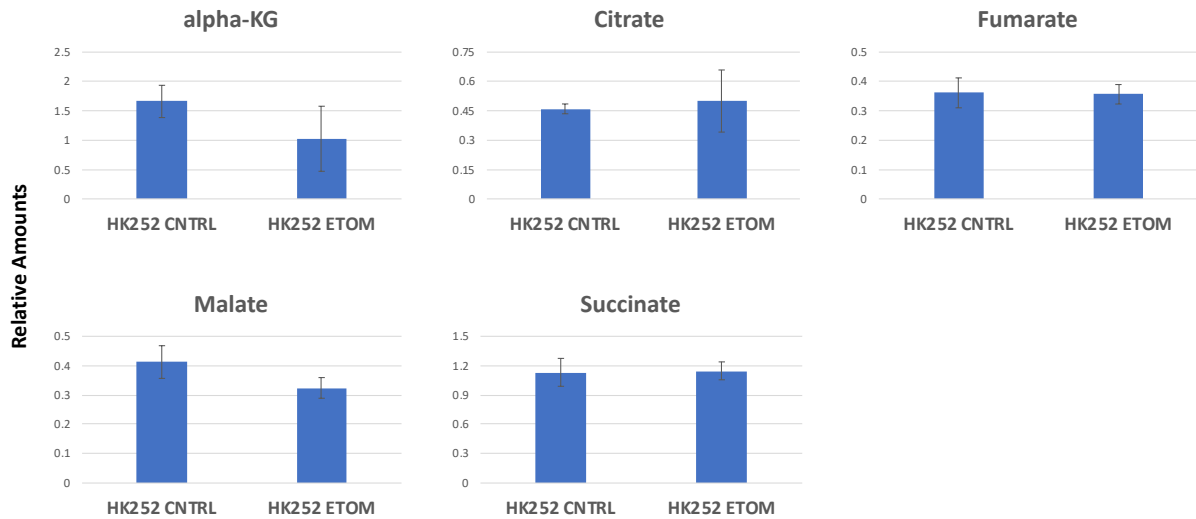
Figure 25. CPT1 inhibition with ETOM does not alter relative amounts of TCA metabolites in IDH1 mutant cells. Analysis of the effects of 100 uM ETOM on relative amounts of TCA metabolites in an IDH1 mutant line using ^{13}C-palmitic acid (LC-MS). Error bars = +/- SD. p-value = >0.5 (N.S.) for all metabolites shown.

Significantly different Metabolites (p<0.05): (* indicates increased levels with ETOM)

	TCA Cycle	Nucleotide Metabolism	Amino Acid Metabolism	Fatty Acid/Lipid Metabolism	Currency	Other
Fractional Contribution	Aconitate	A	Asn	Ac-carnitine	Acetyl-CoA	GlcNAc-6P
	Cit	Adenine	Asp	CDP	ATP	
	Mal	ATP	Arg*	CDP-EtA	GSH	
	Succ	C	Homocysteine		GSSG	
	2-HG	CMP	Pro			
	Gln	CTP				
	Glu	Cytosine				
		dG				
		Inosine				
		Orotidine				
		UDP				
		UDP-Glc				
		UDP-GlcNAc				
		UMP				
		UTP				
Relative Amounts	**2-HG**	Adenine*	2-Methylpropanoyl-CoA		Acetyl-CoA	F16BP
	Glu	dA*	Gly		Creatine	G6P-F6P
		GMP			NADH	GlcN-6P
		Inosine*				GlcNAc-6P
		Orotate*				Pantothenate
						Sorbitol

Table 2. IDH1 mutant GBM cells may utilize FAs differently than IDH wildtype. Identical analysis to that of Table 1 showing all metabolites that are significantly altered by ETOM (100 uM) treatment in an IDH1 mutant line (HK252). The metabolites listed in Table 1 are from analysis of an IDH wildtype line. (p<0.05 for all metabolites listed).

Discussion

Identifying metabolic vulnerabilities in cancer for use in targeted therapies has been a topic of interest for decades. While glucose metabolism has drawn the most attention in the scientific community, the ability of brain tumor cells to use other substrates for cellular maintenance and to meet bioenergetic demands has become increasingly evident[23, 159, 177, 97]. In the current study we sought to investigate the ability of brain tumors to oxidize two such metabolic substrates to support growth: fatty acids and ketone bodies. We demonstrated that GBM cells are able to oxidize both FAs and ketones, particularly under physiologically relevant glucose conditions. We also found that the ketogenic diet (KD) administered *ad libitum* was sufficient to induce ketosis and, contrary to expectations, this diet resulted in long-term increases in GBM tumor growth using an animal orthotopic xenograft model. This increased tumor growth could be abrogated, however, by inhibition of FAO through CPT1A knockdown. A more in-depth *in vitro* assessment using primary GBM cultures demonstrated CPT1 functionality in these cells. Inhibition of CPT1-mediated FAO either through CPT1 knockdown using lentiviral shRNAs or pharmacologically with the CPT1-specific inhibitor etomoxir resulted in decreased proliferation, increased cell death, and elevated ROS production. LC-MS tracing experiments with fully-labeled FAs showed significant FA utilization within the TCA cycle that extended throughout the GBM metabolome, highlighting a potential reliance on FAO to support GBM's aggressive phenotype.

Several lines of evidence exist for the use of a KD to treat brain tumors. The first lies with the innate ability of the human body to efficiently adapt to ketosis[178]. For example, the KD has been successfully implemented to treat certain diseases such as refractory pediatric epilepsy with no clear sustained adverse health effects[179, 180, 181]. Additionally, several previous studies have indicated that many brain tumors may lack the ability to oxidize ketones due to decreased

expression of several mitochondrial genes required to do so[172, 173], although there is also evidence suggesting gliomas oxidize ketone bodies at comparable levels to the brain when exposed to a KD[95]. Our study shows that as glucose levels are diminished, GBM cells can adapt by at least partially shifting their metabolism to accommodate ketone body oxidation. Prior animal studies investigating the therapeutic potential of the KD have yielded mixed results, usually depending on the manner of administration and ability to achieve ketosis[82, 96, 182, 183]. One study using U87 cells in a mouse tumor model found that an *ad libitu*m KD resulted in increased blood ketone levels without affecting blood glucose or tumor growth[96]. Only with a calorie-restricted KD were glucose levels and tumor growth diminished. This is consistent with other studies demonstrating anti-tumor effects of calorie restriction irrespective of the KD[97, 98, 99]. Here we report that the *ad libitum* KD, albeit of a slightly different formulation and longer period of administration, significantly elevated blood ketone levels, decreased blood glucose, but resulted in increased tumor growth. While it is possible that the KD can have some therapeutic utility depending on its implementation, our data suggest that clinical trials investigating such treatments need to proceed with a great deal of caution[163, 184, 185, 186].

In addition to ketone body metabolism, this study also focused on the ability of GBMs to oxidize FAs. Similar to other previous studies, we report that GBM cells express the necessary enzymes involved in FAO, utilize FAs to support overall metabolism, and that inhibition of this process has anti-proliferative effects[79, 78, 77]. Our results also suggest that the ability to oxidize FAs may be intrinsic to GBM and is not directly counteracted by EGFR amplification, constitutive activation (EGFRviii mutation), or PTEN mutations, as U87 cells themselves, are deficient in PTEN, as are a number of our primary gliomasphere lines. Activation of the PI3K/Akt/mTOR pathway have been implicated in glucose addiction, a dependence on aerobic glycolysis and

inability to efficiently utilize alternative substrates that leaves malignant cells particularly vulnerable to glucose starvation[105, 187], and can produce metabolic shifts towards FA synthesis[165]. However, our current study suggests that under physiologically relevant glucose conditions (2.5 mM), FAs play a central role in the overall GBM metabolome regardless of mutational status. Our findings of a mutation-independent use of FAO in GBMs may be due to methodological differences with previous studies such as our use of physiological glucose levels or lower ETOM concentrations to limit off-target effects. Furthermore, our surprising *in vivo* findings that show an increase in U87 tumor growth with a ketogenic diet support our *in vitro* findings that AKT-enhancing mutations don't make GBMs "glucose addicted" under physiological conditions. The ketogenic diet limits the availability of glucose to the tumor *in vivo,* so the enhanced tumor growth we observed must have been supported by the use of alternative energy substrates despite U87s having PTEN mutations.

FAO by these tumors may at first glance seem counterintuitive since the brain receives an ample supply of glucose, the most highly utilized substrate in GBM. ATP generation by FAO also demands more oxygen, is a slower overall process, and generates more superoxide than glycolysis[71]. While the idea of simultaneous FA synthesis and oxidation seems counterproductive, studies such as this make it increasingly clear that the ability to oxidize FAs make malignant cells more resilient and adaptable to conditions of metabolic stress, which highly proliferative and migratory cells like GBMs experience during tumor formation. FAs represent a readily available and easily stored substrate that can be utilized to support both bioenergetic demands and as a raw material for the production of other cellular components. In malignant glioma tumors, lipid levels have been reported to be higher compared with normal brain tissues[188, 189, 190]. Gliomas can both produce free fatty acids and lipid stores endogenously via *de novo* synthesis from excess glucose

and via uptake of exogenously produced free fatty acids from blood. Our experiments suggest that both endogenous and exogenous sources of fatty acids can be used as an energy substrate to support cell growth in GBMs. Perhaps the most notable aspect of FAO is that it results in the production of acetyl-CoA, an important metabolite that regulates a number of cellular processes including the TCA cycle. Recent evidence demonstrates that much of the acetyl-CoA produced by malignant gliomas is derived from sources other than glucose[191], highlighting FAO as a potentially critical contributor to overall brain tumor metabolism. Our ^{13}C-labeled FA tracing experiments support this finding and demonstrate that in addition to feeding into the TCA cycle, FAO contributes extensively throughout the GBM metabolome.

While investigating FA metabolism in GBM as a whole, we also sought to characterize potential differences in FAO utilization between IDH1 mutant and wildtype GBM cells. Recent evidence suggests that GBMs harboring IDH mutations represent a distinct subclass of glioma[141]. Our group previously demonstrated that IDH1 mutant gliomaspheres are metabolically distinguishable from their WT counterparts based on expression profiles, glucose consumption, and nucleotide synthesis utilization[1]. The results of this study suggest further metabolic differences in IDH mutant GBM cells with regard to FAO. Analysis of CPT1-isoform expression revealed increased expression of CPT1A in IDH1 mutant cultures relative to IDH wildtype cells. LC-MS tracing experiments with ^{13}C-palmitic acid revealed extensive FA utilization throughout the metabolomes of both IDH mutant and WT cells. However, the effects of FAO inhibition with ETOM was more pronounced within the TCA cycle of IDH WT cells. Importantly, 2-HG was among the most heavily labeled metabolites in IDH mutant cells. Treatment with ETOM significantly decreased both the fractional contribution and relative amount of 2-HG, indicating FAs may serve as a vital component for the production of this proposed oncometabolite. While

these effects were only tested in a single IDH1 mutant cell line, and thus require further investigation, these results suggest FAO represents an additional mechanism contributing to the unique metabolic phenotype of IDH mutant gliomas.

In this study we also report that inhibition of CPT1A-mediated FAO results in decreased tumor growth and improved survival using a murine orthotopic xenograft model. Of note, we identified that CPT1A knockdown was sufficient to nullify the observed increases in tumor growth resulting from administration of a ketogenic diet. While the KD leads to increased production of ketone bodies such as beta-hydroxybutyrate, it also results in increased FA availability with the potential to be taken up and utilized by the tumor[192, 193]. Our results suggest that GBMs are able to compensate for decreased glucose availability by shifting their metabolism toward FAO. This hypothesis is supported by a study in which FAO inhibition through administration of etomoxir prolonged survival in a syngeneic mouse model of malignant glioma[78]. Similarly, our orthotopic xenograft experiments resulted in prolonged survival for those cohorts bearing tumors with CPT1A knockdown, irrespective of the ketogenic diet. These results provide strong evidence that FAO is a significant pathway in GBM and may serve as a valuable therapeutic target either alone or in combination with other currently investigated treatments.

Although our findings emphasize the complex and highly adaptable nature of brain tumor metabolism, important aspects of these studies require further investigation. *In vivo* tumor studies were conducted in immunosuppressed mice using the U87 malignant glioma cell line. This cell line was used because of its experimental consistency, similar FAO profile to primary GBM lines, and its ability to establish tumors quickly. The speed of tumor formation was important, not simply for convenience, but it allowed us to take into account concerns regarding significant weight loss and the overall health of animals receiving a long-term ketogenic diet. Utilizing multiple primary

cell lines or adapting an *in vivo* model in immunocompetent animals to better mimic brain tumor physiology and the tumor microenvironment could further our understanding of these intricate metabolic processes. The preponderance of evidence reported in this study support the conclusion that GBMs oxidize FAs. Inhibition of FAO with ETOM resulted in overall deficits in cellular growth and FA-mediated mitochondrial respiration. Meanwhile, FA supplementation under physiologically relevant glucose concentrations demonstrated inverse effects to that of ETOM. Our LC-MS studies also clearly show that FAs are taken up, oxidized, and utilized throughout the GBM metabolome. Finally, many of the effects of FAO inhibition achieved with ETOM were validated using multiple methods of CPT1A knockdown. The fact that etomoxir has been shown to exhibit off-target effects in certain cells at high doses cannot be overlooked, however. Developing more potent and specific FAO inhibitors, perhaps even for individual CPT1 isoforms, could prove essential for targeting brain tumors in patients. Due to the grim prognosis associated with glioma and the currently inadequate treatment options available, this study highlights several important aspects of brain tumor metabolism that have direct application to improving current standard of care therapy.

Methods

Collection and Maintenance of In Vitro Cultures:

Tumor samples were collected under institutional review board-approved protocols and graded by neuropathologists. Primary gliomasphere cultures were prepared as follows. Immediately after receiving resected tissue, samples were digested with papain and acellular debris was removed. Those cells which remained were incubated in gliomasphere defined media containing DMEM/F12 supplemented with B27, heparin, EGF, bFGF, and penicillin/streptomycin

until sphere formation was achieved. Gliomasphere stocks were frozen down at approximately passage 5 to maintain cells at low passage throughout the study. All cell lines used in this study, including U87, were continuously grown in serum-free gliomasphere media.

Expression Analysis:

Relevant expression, mutational status (such as EGFR and IDH1), and patient characteristics for the majority of cell lines used in this study have been previously reported[124,1]. The following cultures are known to be PTEN deficient (U87, HK217, HK229, HK296, HK301) but there may be other cultures that are PTEN mutated/deleted as well. Also of note, while BT142 is IDH1 mutant (R132H), it does not produce 2-HG. HK211 is both IDH1 (R132H) and EGFRviii mutant. Known status of EGFR, PTEN, and IDH1 are indicated in Figure 22A for primary GBM cultures. Analysis of CPT1-isoform expression is based on the microarray dataset (GSE98995) previously described by Laks et al. 2016 and available in the Gene Expression Omnibus (GEO) repository.

Variable Glucose Media and Substrate Supplementation:

All media described contain B27, heparin, EGF, bFGF, and penicillin/streptomycin. For 25 mM glucose the base media used is Neurobasal-A Medium ([-] Glutamine) (Gibco #10888-022) supplemented with GlutaMax Supplement (Gibco #35050061). 2.5 mM and 1 mM glucose media was made by combining the Neurobasal-A Medium ([-] Glutamine) above with Neurobasal-A Medium ([-] D-glucose, [-] Sodium Pyruvate) (Gibco #A24775-01) to achieve the desired glucose concentration. Glutamax Supplement and sodium pyruvate (Gibco #11360-070) were then added to reach a final concentration of 1X. Palmitic acid was purchased from Sigma-Aldrich

(#P0500) and conjugated with fatty acid free, low endotoxin bovine serum albumin (BSA, Sigma Aldrich, #A1595). Carnitine (Sigma Aldrich, #C0283) was included in fatty acid-supplemented conditions. 3-hydroxybutyrate (3-OHB) was also purchased from Sigma (#166898).

shRNA and CRISPR/Cas9 Lentiviral Knockdown:

Plasmids with shCPT1A (RHS4531-EG1374 glycerol set), shCPT1-C (RHS4531-EG126129 glycerol set), and the non-silencing shCNTL (RHS4346) cloned into pGIPZ expression vectors were purchased from Dharmacon. The firefly luciferase-GFP virus Fluc-GFP (backbone= pRRL-sinCMV-iresGFP) was produced by UCLA Vectorcore and supported by Molecular Technologies Core (IMTC) CURE/P30 DK41301-26. These plasmids were transfected into 293T cells along with 1st generation viral ΔR8.74 package and VSV-g envelope for production of lentivirus. For CRISPR experiments the following plasmids were used: CPT1A-validated CRISPR guideRNA (Edigene SG00441287A), LentiCas9-EGFP (Addgene 63592), and pgRNA-humanized plasmid, (Addgene 44248). Each plasmid was used to generate three separate lentiviruses as described above. For CPT1A-CRISPR knockdown experiments cells were then infected sequentially: first with either the CPT1A guideRNA or pgRNA-humanized (CNTL) virus, and then with the LentiCas9-EGFP virus. Cells expressing both fluorophores for the guideRNA and Cas9 were selected for by fluorescence. Those selected cells were then plated at clonal density and expanded to achieve a more uniform population expressing both the guideRNA and Cas9 vectors.

U87 In Vivo Orthotopic Xenotransplants:

All animal experimentation was performed with institutional approval following NIH guidelines using adult NSG mice. Intracranial xenotransplants were performed similarly to previous descriptions with minor changes[194].

-CPT1A /Ketogenic Diet:

One hundred thousand U87 cells expressing firefly luciferase-GFP (Fluc-GFP) along with either shCNTL or shCPT1A plasmids were stereotactically injected into the striatum of non-obsese diabetic gamma null (NSG) mice under isoflurane anesthesia over 5 minutes using the following coordinates: 1.5 mm lateral to and -0.5 mm anterior to Bregma, and 3.0 mm below the pial surface. N= 10 mice per group. As shown in Figure 18B, mice were kept on standard chow for 4 days to allow appropriate recovery, after which half of each group was placed on the ketogenic diet (BioServ, S3666). On Day 8, weekly bioluminescence imaging was initiated as described below. On Day 21 mouse weight, blood glucose and ketone measurements were taken. Tumor growth was measured until each animal either died or became morbid. Mouse survival was tracked for all groups. This experimental design was also implemented for CPT1A CRISPR/Cas9 transplants.

-CPT1-C Transplants:

Transplants for this experiment were carried out as described above with the exception that the ketogenic diet was not implemented and therefore only 20 total mice were used (10 per group).

Bioluminescent Imaging:

Optical imaging was performed at the Preclinical Imaging Technology Center at the Crump Institute for Molecular Imaging at UCLA. 100 μl of D-luciferin (GoldBio) dissolved in phosphate buffer saline without Ca2+ or Mg2+ (30 mg/ml) was introduced to each animal by intraperitoneal (IP) injection. After 7 minutes of conscious uptake, mice were anesthetized by inhalation of 2.6%

isoflurane in oxygen and placed in dedicated imaging chambers. The IVIS Lumina 2 imaging system (Caliper Life Sciences) was utilized for *in vivo* bioluminescent imaging. A corresponding photograph of the mice was taken and co-registered with the luminescent image for signal localization. Images were analyzed by drawing regions of interest and quantified as total flux (photons/second) with the Living Image software package (Perkin Elmer).

Western Blot and Immunohistochemistry:

Western blots were performed using the following antibodies: mouse anti CPT1A (abcam, 128568), rabbit anti CPT1B (abclonal, A6796), rabbit anti CPT1C (LsBio, LS-C167010), rabbit and mouse anti beta-actin (Abcam). To prepare samples for immunohistochemical analysis, Mouse brains from U87 transplant experiments were perfused using 4% paraformaldehyde (PFA) and incubated overnight in PFA at 4°C for 24 hours. Tissue was washed with PBS and incubated in 20% sucrose at 4°C for a minimum of 24 hours in preparation for sectioning on a cryostat. Sections (20 μM thick) were post-fixed for 15 minutes with cold 4% paraformaldehyde followed by 3x washes with TBS prior to performing immunohistochemistry for CPT1A.

Seahorse Respirometry Methods:

All respirometry studies were conducted in a Seahorse XFe96 Analyzer. All experiments were conducted at 37°C, and at pH 7.4 (intact cells) or 7.2 (permeabilized cells). On the day of the assay, glioblastoma cells were acutely spun onto Seahorse XF96 plates (600g for 5 min) coated with Cell-Tak (Corning C354240) according to manufacturer's instructions at 4.3×10^4 cells/well. Respiratory parameters were calculated according to standard protocols[195], and all rates were

corrected for non-mitochondrial respiration/background signal by subtracting the oxygen consumption rate insensitive to rotenone and antimycin A.

-Intact Cells:

Potential off-target effects of etomoxir in intact glioblastoma cells was assessed by measuring respiration in response to both 3 μM and 100 μM etomoxir[80]. Prior to conducting the assay, cell culture medium was replaced with DMEM (Sigma D5030) supplemented with 8 mM glucose, 2 mM pyruvate, 2 mM glutamine and 5 mM HEPES. Respiration was measured in the basal state as well as in response to 2 μM oligomycin, FCCP (two sequential pulses of 800 nM), and 0.2 μM rotenone with 1 μM antimycin A. Etomoxir (3 μM or 100 μM) was added to the assay medium 30 min prior to measurements.

-Permeabilized Cells:

The plasma membrane of cells was selectively permeabilized with recombinant, mutant perfringolysin O[196] and experiments were conducted as previously described[80]. Immediately prior to the assay, cell culture medium was replaced with MAS buffer containing 3 nM rPFO, 40 μM palmitoyl CoA, 1 mM malate, 0.5 mM carnitine, and 4 mM ADP. Maximal CPT-1-driven respiration rates are given as the rate stimulated by 2 μM FCCP corrected for background with 0.2 μM rotenone with 1 μM antimycin A.

Acute etomoxir treatment and fatty acid and ketone supplementation:

Dissociated cultures were plated at a density of 50k cells/ml in triplicate in gliomasphere defined media containing 25 mM glucose unless otherwise indicated. Cells were incubated for 24 hours after which point 100 μM etomoxir was added to each sample and again on day 4. [(+)-Etomoxir sodium salt hydrate, Sigma Aldrich, #E1905]. For FA and ketone supplementation,

4,000 cells were plated per well (96-well plates) and incubated for 24 hours after which either FAs or ketones were added to yield the following final concentrations of each. For FA: 25-200 µM palmitate (Sigma Aldrich, #P0500) bound to fatty-acid free BSA (5g/50mL in 10% PBS) (Sigma Aldrich, #A1595) and 500 µM carnitine (Sigma Aldrich, # C0283). For 3-OHB (Sigma Aldrich, #166898): final concentrations were 1.25-10 mM. Blood plasma concentrations of these substrates in healthy adults range from 111-260 µM palmitate and 67 µM carnitine[197, 198, 199]. Cells were allowed to grow for the indicated period of time prior to analysis using the Dojindo Cell Counting Kit 8 (#CK04-20) according to manufacturer instructions.

Cell growth analysis:

Single-cell suspensions were made from bulk cultures of the U87 and primary glioma cell lines and counted using a Countess automated cell counter. Cells were plated at 50k cells/mL in 6-well plates and grown as gliomaspheres in control or experimental conditions. For ETOM experiments, cells were treated 24 hours after initial plating and treatment was re-administered on Day 4. After 7 days the gliomaspheres in each well were fully dissociated and re-counted to assess changes in cell number during treatment. This analysis of cell number examines both cell survival and proliferation in response to treatment.

Proliferation analysis with bromodeoxyuridine (BrdU):

Single cell suspensions were plated as a monolayer on laminin-coated glass coverslips (Sigma, L2020) in 24-well plates followed by a 4 day ETOM treatment. Two BrdU pulses were given 2 hours apart and cells were fixed for 15 minutes with 4% paraformaldehyde. Coverslips

were washed with PBS and immunocytochemistry was performed to assess the % of BrdU-positive cells by visual microscopic cell counts.

Annexin V/PI FACS Analysis:

Single cell samples were treated with 100uM ETOM for 4 days after which spheres were re-dissociated with 200 µl accumax, centrifuged, and washed 1x with PBS. Annexin V/propidium iodide (PI) staining was carried out according to manufacturer protocol using the Annexin V APC flow cytometry kit (Thermo Fisher) while including a 1µl/ml final concentration of PI. Samples were gently mixed and incubated with Annexin V/PI binding buffer and incubated for 15 minutes at room temperature protected from light. Samples were kept on ice and analyzed within 1 hour by flow cytometry.

Reactive Oxygen Species Analysis:

Mitochondrial superoxide and total intracellular ROS levels were assessed according to manufacturer instructions following a 3 hour incubation with ETOM (100 µM) by FACS analysis. Mitochondrial ROS was detected using MitoSOX™ Red Mitochondrial Superoxide Indicator (Thermo Fisher, M36008). Total intracellular ROS was measured using CellROX™ Deep Red Reagent, for oxidative stress detection (Thermo Fisher, C10422).

LC-MS with fully labeled ^{13}C palmitate:

Gliomaspheres were dissociated into single cells with Accumax™ and 200k cells were cultured for 48 hours in 2.5 mM glucose media in triplicate for each sample. Cells were then rinsed with PBS and re-plated in 2.5 mM glucose media, either unlabeled or containing 200 µM fully-

labeled ^{13}C-palmitic acid for an additional 48 hours. Cells were then centrifuged and rinsed with 1ml ice-cold 150 mM ammonium acetate (pH 7.3). Centrifugation was performed again and 1ml of ice-cold 80% methanol was added. Cells were transferred to an Eppendorf tube, and 10 nmol norvaline (Sigma-Aldrich, N7502) was added to each sample. Samples were centrifuged for 5 min. at top speed and the supernatant was transferred into a glass vial. Samples were resuspended in 200 μl cold 80% methanol, followed again by centrifugation, after which the supernatant was added to the glass vial. Samples were dried in an EZ-2Elite evaporator. The remaining pellet was resuspended in RIPA buffer and a Bradford assay was performed to quantify protein levels for sample normalization. Dried metabolites were resuspended in 50% ACN and 5 μl loaded onto a Luna 3 μm NH2 100 A (150 × 2.0 mm) column (Phenomenex). The chromatographic separation was performed on an UltiMate 3000 RSLC (Thermo Scientific) with mobile phases A (5 mM NH4AcO pH 9.9) and B (ACN) and a flow rate of 200 μl/min. The gradient from 15% A to 95% A over 18 min. was followed by 9 min. isocratic flow at 95% A and re-equilibration. Metabolite detection was achieved with a Thermo Scientific Q Exactive mass spectrometer run in polarity switching mode (+3.5 kV/− 3.5 kV). TraceFinder 4.1 (Thermo Scientific) was used to quantify the area under the curve for metabolites by using accurate mass measurements (< 3 ppm) and the retention time of purchased reference standards. Relative amounts of metabolites were calculated by summing up all isotopologues of a given metabolite and normalized to cell number. Correction for naturally occurring ^{13}C as well as calculation of fractional contributions and clustering analyses were done in R.

Statistical Analysis:

Statistical analysis was performed using either Microsoft Excel or GraphPad Prism software. The statistical significance of comparative samples was determined using an ANOVA model and two-tailed Student's t tests where appropriate. All quantitative data and associated error bars represent the mean ± either the standard deviation or standard error of the mean (SEM) as indicated for each figure. Experiments were performed in triplicate at a minimum, with 95% confidence intervals and p values calculated for relevant comparison. For all figures, p values are represented as follows: $* = p<0.05$, $** = p<0.01$, $*** = p<0.001$.

Chapter 4

Summary and Perspectives

Glioblastoma (GBM) is one of the most lethal cancers and new therapeutic strategies are desperately needed. Although there has been considerable progress in defining the molecular characteristics that drive gliomagenesis, the complexities of the metabolic signaling networks responsible for GBM's aggressive phenotype remain unsolved. Despite underwhelming results from previous attempts to establish metabolic therapies for GBM, targeting GBM metabolism remains an attractive approach for several reasons. While oncogenic mutations bestow added flexibility and adaptability, those same mutations also make GBM cells reliant on metabolic pathways that are not overtly essential to surrounding healthy tissue. Obtaining maximal efficacy with minimal side effects epitomizes the ideal outcome for any cancer regimen. Furthermore, because of the significant overlap between oncogenic and metabolic signaling, current oncogene-directed therapies can be easily adapted to include additional targets based on metabolic dynamics. Combinatorial therapy likely represents the most effective way to overcome the interconnected, often redundant, signaling cascades activated during oncogenesis and metastasis. Finally, technological advances in drug development have made targeting metabolic enzymes an easier process in recent years. These advancements allow for the production of novel compounds and small-molecule inhibitors with increased specificity and uptake, promoting more personalized anti-cancer therapeutic approaches. More than ever, we are equipped with both the knowledge and technology to establish more effective therapies for GBM.

In this study we have added to the framework of past reports demonstrating the high plasticity of GBM cells to adapt to changes in nutrient availability and to establish a unique

phenotype that drives tumorigenesis. To this end, the work presented here has elucidated several important factors that should be taken into account when designing future treatments for GBM. Our results with IDH mutant cultures demonstrate that IDH mutant GBMs represent a distinct class of glioma with unique characteristics that differentiate them from their IDH wildtype counterparts. Our experiments reveal that IDH mutant cells display clear differences in expression patterns, glucose utilization, ROS production, nucleotide biosynthesis, and DNA repair capacity with the potential to be exploited for therapy. Furthermore, our assessment of fatty acid (FA) and ketone metabolism highlight that while glycolysis is a major pathway activated in GBM, alternative metabolic substrates may serve equally important physiological roles. We discovered extensive utilization of FAs throughout the GBM metabolome under physiological glucose conditions, identified CPT1-mediated fatty acid oxidation (FAO) as a potential therapeutic target, and determined that dietary intervention should be approached with caution, as our results indicate that the ketogenic diet (KD) can have adverse effects on tumor growth.

Informing Therapeutic Strategies for GBM:

IDH mutations:

IDH mutations represent attractive therapeutic targets for several reasons. Recent studies offer compelling evidence that IDH mutations occur very early in gliomagenesis and are therefore present in the majority of gliomas. IDH1 mutations are found in approximately 80% of low grade gliomas[45, 46, 47] and are present in GBM, albeit within a smaller percentage of these more aggressive tumors[48, 49]. This would seem to provide a certain degree of homogeneity in an otherwise highly heterogenous disease. Our clustering analysis of both expression (KEGG) and metabolic (LC-MS)

profiles support this idea by demonstrating that IDH mutant and wildtype gliomaspheres have clear and distinguishing characteristics. In particular, our experiments that show increased DNA repair capacity following radiation and a greater dependence on the nucleotide salvage pathway in IDH1 mutants have direct therapeutic application. If, as we propose, endogenous IDH1 mutants have a greater capacity for DNA repair following radiation, it brings into question the efficacy of radiation therapy for this subset of tumors. We also demonstrated that IDH1 mutant cells maintain elevated levels of ROS, a potential buffering adaptation that makes them more resistant to radiation-induced production of free radicals. There are a number of cellular pathways activated upon exposure to radiation that can disrupt mitochondrial function and lead to both immediate and persistent changes to nucleic acid, protein, and lipid metabolism[200]. IDH1 mutant cell utilization of both the *de novo* and salvage pathways for nucleotide synthesis may thus represent an additional mechanism that contributes to resistance.

Standard of care for GBM, which includes radiation and treatment with the alkylating agent temozolomide (TMZ), offers little benefit to long-term patient survival[11]. Our data suggest that, contrary to IDH WT cells which rely primarily on *de novo* nucleotide synthesis, inhibition of both *de novo* and salvage pathways may be required to overcome resistance to current therapy. The development of IDH mutant-specific inhibitors has shown some promise in certain cancers both *in vitro* and *in vivo*. Enasidenib is currently approved for treatment of IDH2-mutated acute myeloid leukemia (AML) and ivosidenib, an IDH1-mutant inhibitor, has entered clinical trials[160]. The literature surrounding whether the IDH phenotype is a result of the IDH mutation itself, the resulting 2-HG production, disruption of wildtype IDH function, or a combination the three, has yet to be fully established. However, the effects of IDH mutant-specific inhibitors in a clinical setting offers a promising new outlook in the field. The results presented here and in Chapter 2 of

this dissertation suggest new avenues for implementing combinatorial therapies that directly target the unique metabolic phenotype of IDH mutant tumors.

Fatty Acids and Ketone Bodies:

Over the past several decades, the role of glucose metabolism in brain tumors has been extensively documented. Oncogenic signaling networks commonly activated in GBM, such as PI3K/Akt/mTOR, promote the use of aerobic glycolysis and have led some to propose a state of "glucose addiction". This has led researchers to theorize that metabolic targeting or dietary intervention, such as the KD, may serve as effective adjuvant therapies. However, results of targeting glucose metabolism have fallen short of expectation. Recent studies, including the one presented in Chapter 3, reveal a high plasticity of glioblastoma cells to change metabolic dynamics based on nutritional supply. Here we report that while glucose is a necessary component of GBM metabolism, utilization of FAs and ketone bodies (KBs) represent two additional substrates that require consideration for improving therapy.

One of the more unexpected findings of this study was the observation that the KD resulted in increased U87 tumor growth in our mouse xenotransplant models. Numerous groups have investigated dietary manipulation, such as the KD or calorie restriction, with reports ranging from no effect to varying levels of success[82, 96, 182, 183]. One of the potential reasons for the observed increase in tumor growth may be due to the length of KD implementation. Our study utilized a long-term KD that far exceeds the typical length of previous dietary experimental designs. While unexpected, our results investigating ketone metabolism highlight the ability of GBM cells to oxidize KBs while also suggesting that future clinical trials investigating such treatments proceed with a great deal of caution.

The current study also suggests that under physiologically relevant glucose conditions, GBMs can oxidize FAs to support bioenergetic demands and cellular maintenance regardless of Akt-activating mutations, such as EGFR and PTEN, that have been implicated in glucose addiction. Inhibitors of EGFR (such as erlotinib, gefitinib, and lapatinib) have been investigated clinically, but none exhibited efficacy either alone or in combination with the other drugs or small molecule inhibitors tested[37, 38, 39, 40]. Early clinical trials with PI3K inhibitors yielded a similar result[42]. One reason for therapy resistance may be due to the ability of GBMs to oxidize FAs. Based on our observations with CPT1 inhibition, it is reasonable to hypothesize that combining inhibitors of EGFR/PI3K/Akt and of FAO would elicit a more potent response. Simultaneous inhibition of oncogene-driven glycolysis (EGFR/PI3K/Akt) and CPT1A-driven FAO would preferentially target the tumors' metabolic adaptability over healthy surrounding tissue, as both enzyme expression and activity of these pathways are significantly elevated in GBM. The orthotopic xenograft model used in Figures 19 -20 could serve as a useful platform to test this theory, as U87 cells are PTEN deficient and thus have inherent Akt activation. Utilizing a primary GBM cell line would be the preferred route of investigation for physiologic relevance. As with any treatment approach, monitoring the subjects' health will be paramount. Etomoxir itself may not be an ideal compound for CPT1 inhibition as it has shown off-target effects *in vitro*[80] and toxicity *in vivo*[201]. However, there are other inhibitors of both pathways currently available or in development that offer exciting new therapeutic opportunities[43, 202].

Due to the poor prognosis of GBM and the currently insufficient treatment options available, the work presented here emphasizes several important characteristics of glioma metabolism with the potential for direct therapeutic application. GBM represents a unique, complex, and formidable metabolic disease. While the intricacies of oncogenic signaling and

metabolic networks make targeting GBM an immense challenge, studies such as this bring us one step closer to understanding the underlying mechanisms of pathogenesis and to developing more effective precision-guided therapies.

References

1. Garrett, M. *et al.* Metabolic characterization of isocitrate dehydrogenase (IDH) mutant and IDH wildtype gliomaspheres uncovers cell type-specific vulnerabilities. *Cancer Metab* **6**, 4 (2018).

2. Siegel, R. L., Miller, K. D. & Jemal, A. Cancer statistics, 2018. *CA Cancer J Clin* **68**, 7–30 (2018).

3. Hanahan, D. & Weinberg, R. A. The hallmarks of cancer. *Cell* **100**, 57–70 (2000).

4. Hanahan, D. & Weinberg, R. A. Hallmarks of cancer: the next generation. *Cell* **144**, 646–674 (2011).

5. Dolecek, T. A., Propp, J. M., Stroup, N. E. & Kruchko, C. CBTRUS statistical report: primary brain and central nervous system tumors diagnosed in the United States in 2005-2009. *Neuro-oncology* **14 Suppl 5**, v1-49 (2012).

6. Ostrom, Q. T. *et al.* CBTRUS Statistical Report: Primary Brain and Other Central Nervous System Tumors Diagnosed in the United States in 2011-2015. *Neuro-oncology* **20**, iv1–iv86 (2018).

7. Wesseling, P. & Capper, D. WHO 2016 Classification of gliomas. *Neuropathol. Appl. Neurobiol.* **44**, 139–150 (2018).

8. Louis, D. N. *et al.* The 2007 WHO classification of tumours of the central nervous system. *Acta Neuropathol.* **114**, 97–109 (2007).

9. Claus, E. B. *et al.* Survival and low-grade glioma: the emergence of genetic information. *Neurosurg Focus* **38**, E6 (2015).

10. Omuro, A. & DeAngelis, L. M. Glioblastoma and other malignant gliomas: a clinical review. *JAMA* **310**, 1842–1850 (2013).

11. Koshy, M. *et al.* Improved survival time trends for glioblastoma using the SEER 17 population-based registries. *J. Neurooncol.* **107**, 207–212 (2012).

12. Egeblad, M., Nakasone, E. S. & Werb, Z. Tumors as organs: complex tissues that interface with the entire organism. *Dev. Cell* **18**, 884–901 (2010).

13. Langhans, J. *et al.* The effects of PI3K-mediated signalling on glioblastoma cell behaviour. *Oncogenesis* **6**, 398 (2017).

14. Wang, G. *et al.* Inhibition of glycolytic metabolism in glioblastoma cells by Pt3glc combinated with PI3K inhibitor via SIRT3-mediated mitochondrial and PI3K/Akt-MAPK pathway. *J. Cell. Physiol.* **234**, 5888–5903 (2019).

15. Downward, J. *et al.* Close similarity of epidermal growth factor receptor and v-erb-B oncogene protein sequences. *Nature* **307**, 521–527 (1984).

16. Felsberg, J. *et al.* Epidermal Growth Factor Receptor Variant III (EGFRvIII) Positivity in EGFR-Amplified Glioblastomas: Prognostic Role and Comparison between Primary and Recurrent Tumors. *Clin. Cancer Res.* **23**, 6846–6855 (2017).

17. Libermann, T. A. *et al.* Amplification, enhanced expression and possible rearrangement of EGF receptor gene in primary human brain tumours of glial origin. *Nature* **313**, 144–147 (1985).

18. Maire, C. L. & Ligon, K. L. Molecular pathologic diagnosis of epidermal growth factor receptor. *Neuro-oncology* **16 Suppl 8**, viii1-6 (2014).

19. Benitez, J. A. *et al.* PTEN regulates glioblastoma oncogenesis through chromatin-associated complexes of DAXX and histone H3.3. *Nat Commun* **8**, 15223 (2017).

20. Warburg, O., Wind, F. & Negelein, E. THE METABOLISM OF TUMORS IN THE BODY. *J. Gen. Physiol.* **8**, 519–530 (1927).

21. Warburg, O. On the origin of cancer cells. *Science* **123**, 309–314 (1956).

22. Vander Heiden, M. G., Cantley, L. C. & Thompson, C. B. Understanding the Warburg effect: the metabolic requirements of cell proliferation. *Science* **324**, 1029–1033 (2009).

23. Marie, S. K. N. & Shinjo, S. M. O. Metabolism and brain cancer. *Clinics (Sao Paulo)* **66 Suppl 1**, 33–43 (2011).

24. Barthel, A. *et al.* Regulation of GLUT1 gene transcription by the serine/threonine kinase Akt1. *J. Biol. Chem.* **274**, 20281–20286 (1999).

25. Pedersen, P. L. Warburg, me and Hexokinase 2: Multiple discoveries of key molecular events underlying one of cancers' most common phenotypes, the 'Warburg Effect', i.e., elevated glycolysis in the presence of oxygen. *J. Bioenerg. Biomembr.* **39**, 211–222 (2007).

26. Lee, J.-H. *et al.* Stabilization of phosphofructokinase 1 platelet isoform by AKT promotes tumorigenesis. *Nat Commun* **8**, 949 (2017).

27. Kim, Y., Roh, S., Lawler, S. & Friedman, A. miR451 and AMPK mutual antagonism in glioma cell migration and proliferation: a mathematical model. *PLoS ONE* **6**, e28293 (2011).

28. Liberti, M. V. & Locasale, J. W. The Warburg Effect: How Does it Benefit Cancer Cells? *Trends Biochem. Sci.* **41**, 211–218 (2016).

29. Levine, A. J. & Puzio-Kuter, A. M. The control of the metabolic switch in cancers by oncogenes and tumor suppressor genes. *Science* **330**, 1340–1344 (2010).

30. DeBerardinis, R. J., Lum, J. J., Hatzivassiliou, G. & Thompson, C. B. The biology of cancer: metabolic reprogramming fuels cell growth and proliferation. *Cell Metab.* **7**, 11–20 (2008).

31. Cairns, R. A., Harris, I. S. & Mak, T. W. Regulation of cancer cell metabolism. *Nat. Rev. Cancer* **11**, 85–95 (2011).

32. Ward, P. S. & Thompson, C. B. Metabolic reprogramming: a cancer hallmark even warburg did not anticipate. *Cancer Cell* **21**, 297–308 (2012).

33. Estrella, V. *et al.* Acidity generated by the tumor microenvironment drives local invasion. *Cancer Res.* **73**, 1524–1535 (2013).

34. Colegio, O. R. *et al.* Functional polarization of tumour-associated macrophages by tumour-derived lactic acid. *Nature* **513**, 559–563 (2014).

35. Kahlon, A. S., Alexander, M., Kahlon, A. & Wright, J. Lactate levels with glioblastoma multiforme. *Proc (Bayl Univ Med Cent)* **29**, 313–314 (2016).

36. Sena, L. A. & Chandel, N. S. Physiological roles of mitochondrial reactive oxygen species. *Mol. Cell* **48**, 158–167 (2012).

37. Peereboom, D. M. *et al.* Phase II trial of erlotinib with temozolomide and radiation in patients with newly diagnosed glioblastoma multiforme. *J. Neurooncol.* **98**, 93–99 (2010).

38. Uhm, J. H. *et al.* Phase II evaluation of gefitinib in patients with newly diagnosed Grade 4 astrocytoma: Mayo/North Central Cancer Treatment Group Study N0074. *Int. J. Radiat. Oncol. Biol. Phys.* **80**, 347–353 (2011).

39. Reardon, D. A. *et al.* Phase I/randomized phase II study of afatinib, an irreversible ErbB family blocker, with or without protracted temozolomide in adults with recurrent glioblastoma. *Neuro-oncology* **17**, 430–439 (2015).

40. Reardon, D. A. *et al.* A phase I/II trial of pazopanib in combination with lapatinib in adult patients with relapsed malignant glioma. *Clin. Cancer Res.* **19**, 900–908 (2013).

41. Westphal, M., Maire, C. L. & Lamszus, K. EGFR as a Target for Glioblastoma Treatment: An Unfulfilled Promise. *CNS Drugs* **31**, 723–735 (2017).

42. Rodon, J., Dienstmann, R., Serra, V. & Tabernero, J. Development of PI3K inhibitors: lessons learned from early clinical trials. *Nat Rev Clin Oncol* **10**, 143–153 (2013).

43. Zhao, H.-F. *et al.* Recent advances in the use of PI3K inhibitors for glioblastoma multiforme: current preclinical and clinical development. *Mol. Cancer* **16**, 100 (2017).

44. Dang, L. *et al.* Cancer-associated IDH1 mutations produce 2-hydroxyglutarate. *Nature* **462**, 739–744 (2009).

45. Balss, J. *et al.* Analysis of the IDH1 codon 132 mutation in brain tumors. *Acta Neuropathol.* **116**, 597–602 (2008).

46. Sanson, M. *et al.* Isocitrate dehydrogenase 1 codon 132 mutation is an important prognostic biomarker in gliomas. *J. Clin. Oncol.* **27**, 4150–4154 (2009).

47. Hartmann, C. *et al.* Type and frequency of IDH1 and IDH2 mutations are related to astrocytic and oligodendroglial differentiation and age: a study of 1,010 diffuse gliomas. *Acta Neuropathol.* **118**, 469–474 (2009).

48. Bleeker, F. E. *et al.* IDH1 mutations at residue p.R132 (IDH1(R132)) occur frequently in high-grade gliomas but not in other solid tumors. *Hum. Mutat.* **30**, 7–11 (2009).

49. Kang, M. R. *et al.* Mutational analysis of IDH1 codon 132 in glioblastomas and other common cancers. *Int. J. Cancer* **125**, 353–355 (2009).

50. Yan, H. *et al.* IDH1 and IDH2 mutations in gliomas. *N. Engl. J. Med.* **360**, 765–773 (2009).

51. Parsons, D. W. *et al.* An integrated genomic analysis of human glioblastoma multiforme. *Science* **321**, 1807–1812 (2008).

52. Watanabe, T., Nobusawa, S., Kleihues, P. & Ohgaki, H. IDH1 mutations are early events in the development of astrocytomas and oligodendrogliomas. *Am. J. Pathol.* **174**, 1149–1153 (2009).

53. Noushmehr, H. *et al.* Identification of a CpG island methylator phenotype that defines a distinct subgroup of glioma. *Cancer Cell* **17**, 510–522 (2010).

54. Christensen, B. C. *et al.* DNA methylation, isocitrate dehydrogenase mutation, and survival in glioma. *J. Natl. Cancer Inst.* **103**, 143–153 (2011).

55. Pollard, P. J. & Ratcliffe, P. J. Cancer. Puzzling patterns of predisposition. *Science* **324**, 192–194 (2009).

56. Rush, G. F. *et al.* Organic hydroperoxide-induced lipid peroxidation and cell death in isolated hepatocytes. *Toxicol. Appl. Pharmacol.* **78**, 473–483 (1985).

57. Lee, S. M. *et al.* Cytosolic NADP(+)-dependent isocitrate dehydrogenase status modulates oxidative damage to cells. *Free Radic. Biol. Med.* **32**, 1185–1196 (2002).

58. Foster, D. W. Malonyl-CoA: the regulator of fatty acid synthesis and oxidation. *J. Clin. Invest.* **122**, 1958–1959 (2012).

59. Strickland, M. & Stoll, E. A. Metabolic Reprogramming in Glioma. *Front Cell Dev Biol* **5**, 43 (2017).

60. Currie, E., Schulze, A., Zechner, R., Walther, T. C. & Farese, R. V. Cellular fatty acid metabolism and cancer. *Cell Metab.* **18**, 153–161 (2013).

61. Tao, B.-B. *et al.* Up-regulation of USP2a and FASN in gliomas correlates strongly with glioma grade. *J Clin Neurosci* **20**, 717–720 (2013).

62. Lewis, C. A. *et al.* SREBP maintains lipid biosynthesis and viability of cancer cells under lipid- and oxygen-deprived conditions and defines a gene signature associated with poor survival in glioblastoma multiforme. *Oncogene* **34**, 5128–5140 (2015).

63. Furuta, E. *et al.* Fatty acid synthase gene is up-regulated by hypoxia via activation of Akt and sterol regulatory element binding protein-1. *Cancer Res.* **68**, 1003–1011 (2008).

64. Bensaad, K. *et al.* Fatty acid uptake and lipid storage induced by HIF-1α contribute to cell growth and survival after hypoxia-reoxygenation. *Cell Rep* **9**, 349–365 (2014).

65. Geng, F. & Guo, D. Lipid droplets, potential biomarker and metabolic target in glioblastoma. *Intern Med Rev (Wash D C)* **3**, (2017).

66. Williams, W. M., Chang, M. C., Hayakawa, T., Grange, E. & Rapoport, S. I. In vivo incorporation from plasma of radiolabeled palmitate and arachidonate into rat brain microvessels. *Microvasc. Res.* **53**, 163–166 (1997).

67. Lam, T. K. T. *et al.* Hypothalamic sensing of circulating fatty acids is required for glucose homeostasis. *Nat. Med.* **11**, 320–327 (2005).

68. Erecińska, M. & Silver, I. A. ATP and brain function. *J. Cereb. Blood Flow Metab.* **9**, 2–19 (1989).

69. Erecińska, M. & Silver, I. A. Tissue oxygen tension and brain sensitivity to hypoxia. *Respir Physiol* **128**, 263–276 (2001).

70. Galea, E. *et al.* Oxidative stress underlying axonal degeneration in adrenoleukodystrophy: a paradigm for multifactorial neurodegenerative diseases? *Biochim. Biophys. Acta* **1822**, 1475–1488 (2012).

71. Schönfeld, P. & Reiser, G. Why does brain metabolism not favor burning of fatty acids to provide energy? Reflections on disadvantages of the use of free fatty acids as fuel for brain. *J. Cereb. Blood Flow Metab.* **33**, 1493–1499 (2013).

72. Panov, A., Orynbayeva, Z., Vavilin, V. & Lyakhovich, V. Fatty acids in energy metabolism of the central nervous system. *Biomed Res Int* **2014**, 472459 (2014).

73. Hambardzumyan, D. & Bergers, G. Glioblastoma: Defining Tumor Niches. *Trends Cancer* **1**, 252–265 (2015).

74. Kuesel, A. C., Sutherland, G. R., Halliday, W. & Smith, I. C. 1H MRS of high grade astrocytomas: mobile lipid accumulation in necrotic tissue. *NMR Biomed* **7**, 149–155 (1994).

75. Howe, F. A. *et al.* Metabolic profiles of human brain tumors using quantitative in vivo 1H magnetic resonance spectroscopy. *Magn Reson Med* **49**, 223–232 (2003).

76. Horská, A. & Barker, P. B. Imaging of brain tumors: MR spectroscopy and metabolic imaging. *Neuroimaging Clin. N. Am.* **20**, 293–310 (2010).

77. Cirillo, A. *et al.* High grade glioblastoma is associated with aberrant expression of ZFP57, a protein involved in gene imprinting, and of CPT1A and CPT1C that regulate fatty acid metabolism. *Cancer Biol. Ther.* **15**, 735–741 (2014).

78. Lin, H. *et al.* Fatty acid oxidation is required for the respiration and proliferation of malignant glioma cells. *Neuro-oncology* **19**, 43–54 (2017).

79. Pike, L. S., Smift, A. L., Croteau, N. J., Ferrick, D. A. & Wu, M. Inhibition of fatty acid oxidation by etomoxir impairs NADPH production and increases reactive oxygen species resulting in ATP depletion and cell death in human glioblastoma cells. *Biochim. Biophys. Acta* **1807**, 726–734 (2011).

80. Divakaruni, A. S. *et al.* Etomoxir Inhibits Macrophage Polarization by Disrupting CoA Homeostasis. *Cell Metab.* **28**, 490-503.e7 (2018).

81. Holubarsch, C. J. F. *et al.* A double-blind randomized multicentre clinical trial to evaluate the efficacy and safety of two doses of etomoxir in comparison with placebo in patients with moderate congestive heart failure: the ERGO (etomoxir for the recovery of glucose oxidation) study. *Clin. Sci.* **113**, 205–212 (2007).

82. Stafford, P. *et al.* The ketogenic diet reverses gene expression patterns and reduces reactive oxygen species levels when used as an adjuvant therapy for glioma. *Nutr Metab (Lond)* **7**, 74 (2010).

83. Maurer, G. D. *et al.* Differential utilization of ketone bodies by neurons and glioma cell lines: a rationale for ketogenic diet as experimental glioma therapy. *BMC Cancer* **11**, 315 (2011).

84. Abdelwahab, M. G. *et al.* The ketogenic diet is an effective adjuvant to radiation therapy for the treatment of malignant glioma. *PLoS ONE* **7**, e36197 (2012).

85. Laffel, L. Ketone bodies: a review of physiology, pathophysiology and application of monitoring to diabetes. *Diabetes Metab. Res. Rev.* **15**, 412–426 (1999).

86. Morris, A. a. M. Cerebral ketone body metabolism. *J. Inherit. Metab. Dis.* **28**, 109–121 (2005).

87. Prins, M. L. Cerebral metabolic adaptation and ketone metabolism after brain injury. *J. Cereb. Blood Flow Metab.* **28**, 1–16 (2008).

88. Barañano, K. W. & Hartman, A. L. The ketogenic diet: uses in epilepsy and other neurologic illnesses. *Curr Treat Options Neurol* **10**, 410–419 (2008).

89. Pasca, L. *et al.* The changing face of dietary therapy for epilepsy. *Eur. J. Pediatr.* **175**, 1267–1276 (2016).

90. Nabbout, R. *et al.* Efficacy of ketogenic diet in severe refractory status epilepticus initiating fever induced refractory epileptic encephalopathy in school age children (FIRES). *Epilepsia* **51**, 2033–2037 (2010).

91. Cahill, G. F. Fuel metabolism in starvation. *Annu. Rev. Nutr.* **26**, 1–22 (2006).

92. Tisdale, M. J. & Brennan, R. A. Loss of acetoacetate coenzyme A transferase activity in tumours of peripheral tissues. *Br. J. Cancer* **47**, 293–297 (1983).

93. Chang, H. T., Olson, L. K. & Schwartz, K. A. Ketolytic and glycolytic enzymatic expression profiles in malignant gliomas: implication for ketogenic diet therapy. *Nutr Metab (Lond)* **10**, 47 (2013).

94. Patel, M. S., Russell, J. J. & Gershman, H. Ketone-body metabolism in glioma and neuroblastoma cells. *Proc. Natl. Acad. Sci. U.S.A.* **78**, 7214–7218 (1981).

95. De Feyter, H. M. *et al.* A ketogenic diet increases transport and oxidation of ketone bodies in RG2 and 9L gliomas without affecting tumor growth. *Neuro-oncology* **18**, 1079–1087 (2016).

96. Zhou, W. *et al.* The calorically restricted ketogenic diet, an effective alternative therapy for malignant brain cancer. *Nutr Metab (Lond)* **4**, 5 (2007).

97. Seyfried, T. N. *et al.* Metabolic management of brain cancer. *Biochim. Biophys. Acta* **1807**, 577–594 (2011).

98. Jiang, Y.-S. & Wang, F.-R. Caloric restriction reduces edema and prolongs survival in a mouse glioma model. *J. Neurooncol.* **114**, 25–32 (2013).

99. Mukherjee, P., El-Abbadi, M. M., Kasperzyk, J. L., Ranes, M. K. & Seyfried, T. N. Dietary restriction reduces angiogenesis and growth in an orthotopic mouse brain tumour model. *Br. J. Cancer* **86**, 1615–1621 (2002).

100. Cancer Genome Atlas Research Network. Comprehensive genomic characterization defines human glioblastoma genes and core pathways. *Nature* **455**, 1061–1068 (2008).

101. Agnihotri, S. & Zadeh, G. Metabolic reprogramming in glioblastoma: the influence of cancer metabolism on epigenetics and unanswered questions. *Neuro-oncology* **18**, 160–172 (2016).

102. Mahajan, K. & Mahajan, N. P. PI3K-independent AKT activation in cancers: a treasure trove for novel therapeutics. *J. Cell. Physiol.* **227**, 3178–3184 (2012).

103. Wu, S.-H., Bi, J.-F., Cloughesy, T., Cavenee, W. K. & Mischel, P. S. Emerging function of mTORC2 as a core regulator in glioblastoma: metabolic reprogramming and drug resistance. *Cancer Biol Med* **11**, 255–263 (2014).

104. Castel, P. *et al.* PDK1-SGK1 Signaling Sustains AKT-Independent mTORC1 Activation and Confers Resistance to PI3Kα Inhibition. *Cancer Cell* **30**, 229–242 (2016).

105. Elstrom, R. L. *et al.* Akt stimulates aerobic glycolysis in cancer cells. *Cancer Res.* **64**, 3892–3899 (2004).

106. Holness, M. J. & Sugden, M. C. Regulation of pyruvate dehydrogenase complex activity by reversible phosphorylation. *Biochem. Soc. Trans.* **31**, 1143–1151 (2003).

107. Randle, P. J., Garland, P. B., Hales, C. N. & Newsholme, E. A. The glucose fatty-acid cycle. Its role in insulin sensitivity and the metabolic disturbances of diabetes mellitus. *Lancet* **1**, 785–789 (1963).

108. Samoilov, M., Plyasunov, S. & Arkin, A. P. Stochastic amplification and signaling in enzymatic futile cycles through noise-induced bistability with oscillations. *Proc. Natl. Acad. Sci. U.S.A.* **102**, 2310–2315 (2005).

109. King, A., Selak, M. A. & Gottlieb, E. Succinate dehydrogenase and fumarate hydratase: linking mitochondrial dysfunction and cancer. *Oncogene* **25**, 4675–4682 (2006).

110. Lai, A. *et al.* Evidence for sequenced molecular evolution of IDH1 mutant glioblastoma from a distinct cell of origin. *J. Clin. Oncol.* **29**, 4482–4490 (2011).

111. Turcan, S. *et al.* IDH1 mutation is sufficient to establish the glioma hypermethylator phenotype. *Nature* **483**, 479–483 (2012).

112. Saha, S. K. *et al.* Mutant IDH inhibits HNF-4α to block hepatocyte differentiation and promote biliary cancer. *Nature* **513**, 110–114 (2014).

113. Li, S. *et al.* Overexpression of isocitrate dehydrogenase mutant proteins renders glioma cells more sensitive to radiation. *Neuro-oncology* **15**, 57–68 (2013).

114. Tateishi, K. *et al.* Extreme Vulnerability of IDH1 Mutant Cancers to NAD+ Depletion. *Cancer Cell* **28**, 773–784 (2015).

115. Pope, W. B. *et al.* Non-invasive detection of 2-hydroxyglutarate and other metabolites in IDH1 mutant glioma patients using magnetic resonance spectroscopy. *J. Neurooncol.* **107**, 197–205 (2012).

116. Deng, G. *et al.* Selective inhibition of mutant isocitrate dehydrogenase 1 (IDH1) via disruption of a metal binding network by an allosteric small molecule. *J. Biol. Chem.* **290**, 762–774 (2015).

117. Rohle, D. *et al.* An inhibitor of mutant IDH1 delays growth and promotes differentiation of glioma cells. *Science* **340**, 626–630 (2013).

118. Izquierdo-Garcia, J. L. *et al.* Glioma cells with the IDH1 mutation modulate metabolic fractional flux through pyruvate carboxylase. *PLoS ONE* **9**, e108289 (2014).

119. Grassian, A. R. *et al.* IDH1 mutations alter citric acid cycle metabolism and increase dependence on oxidative mitochondrial metabolism. *Cancer Res.* **74**, 3317–3331 (2014).

120. Johnson, B. E. *et al.* Mutational analysis reveals the origin and therapy-driven evolution of recurrent glioma. *Science* **343**, 189–193 (2014).

121. Eckel-Passow, J. E. *et al.* Glioma Groups Based on 1p/19q, IDH, and TERT Promoter Mutations in Tumors. *N. Engl. J. Med.* **372**, 2499–2508 (2015).

122. Kanehisa, M. & Goto, S. KEGG: kyoto encyclopedia of genes and genomes. *Nucleic Acids Res.* **28**, 27–30 (2000).

123. Subramanian, A. *et al.* Gene set enrichment analysis: a knowledge-based approach for interpreting genome-wide expression profiles. *Proc. Natl. Acad. Sci. U.S.A.* **102**, 15545–15550 (2005).

124. Laks, D. R. *et al.* Large-scale assessment of the gliomasphere model system. *Neuro-oncology* **18**, 1367–1378 (2016).

125. Laks, D. R. *et al.* Inhibition of Nucleotide Synthesis Targets Brain Tumor Stem Cells in a Subset of Glioblastoma. *Mol. Cancer Ther.* **15**, 1271–1278 (2016).

126. Luchman, H. A. *et al.* An in vivo patient-derived model of endogenous IDH1-mutant glioma. *Neuro-oncology* **14**, 184–191 (2012).

127. Izquierdo-Garcia, J. L. *et al.* IDH1 Mutation Induces Reprogramming of Pyruvate Metabolism. *Cancer Res.* **75**, 2999–3009 (2015).

128. Li, F. *et al.* NADP(+)-IDH Mutations Promote Hypersuccinylation that Impairs Mitochondria Respiration and Induces Apoptosis Resistance. *Mol. Cell* **60**, 661–675 (2015).

129. Sasaki, M. *et al.* D-2-hydroxyglutarate produced by mutant IDH1 perturbs collagen maturation and basement membrane function. *Genes Dev.* **26**, 2038–2049 (2012).

130. Barker, C. A., Bishop, A. J., Chang, M., Beal, K. & Chan, T. A. Valproic acid use during radiation therapy for glioblastoma associated with improved survival. *Int. J. Radiat. Oncol. Biol. Phys.* **86**, 504–509 (2013).

131. Reitman, Z. J. *et al.* Cancer-associated isocitrate dehydrogenase 1 (IDH1) R132H mutation and d-2-hydroxyglutarate stimulate glutamine metabolism under hypoxia. *J. Biol. Chem.* **289**, 23318–23328 (2014).

132. Reitman, Z. J. *et al.* Profiling the effects of isocitrate dehydrogenase 1 and 2 mutations on the cellular metabolome. *Proc. Natl. Acad. Sci. U.S.A.* **108**, 3270–3275 (2011).

133. Chaumeil, M. M. *et al.* Hyperpolarized [1-13C] glutamate: a metabolic imaging biomarker of IDH1 mutational status in glioma. *Cancer Res.* **74**, 4247–4257 (2014).

134. Ohka, F. *et al.* Quantitative metabolome analysis profiles activation of glutaminolysis in glioma with IDH1 mutation. *Tumour Biol.* **35**, 5911–5920 (2014).

135. Sulkowski, P. L. *et al.* 2-Hydroxyglutarate produced by neomorphic IDH mutations suppresses homologous recombination and induces PARP inhibitor sensitivity. *Sci Transl Med* **9**, (2017).

136. Lu, Y. *et al.* Chemosensitivity of IDH1-Mutated Gliomas Due to an Impairment in PARP1-Mediated DNA Repair. *Cancer Res.* **77**, 1709–1718 (2017).

137. Sevilla, M. D., Becker, D., Kumar, A. & Adhikary, A. Gamma and Ion-Beam Irradiation of DNA: Free Radical Mechanisms, Electron Effects, and Radiation Chemical Track Structure. *Radiat Phys Chem Oxf Engl 1993* **128**, 60–74 (2016).

138. Tran, A. N. *et al.* Increased sensitivity to radiochemotherapy in IDH1 mutant glioblastoma as demonstrated by serial quantitative MR volumetry. *Neuro-oncology* **16**, 414–420 (2014).

139. Shaw, E. *et al.* Prospective randomized trial of low- versus high-dose radiation therapy in adults with supratentorial low-grade glioma: initial report of a North Central Cancer Treatment Group/Radiation Therapy Oncology Group/Eastern Cooperative Oncology Group study. *J. Clin. Oncol.* **20**, 2267–2276 (2002).

140. Mannava, S. *et al.* Direct role of nucleotide metabolism in C-MYC-dependent proliferation of melanoma cells. *Cell Cycle* **7**, 2392–2400 (2008).

141. Cancer Genome Atlas Research Network *et al.* Comprehensive, Integrative Genomic Analysis of Diffuse Lower-Grade Gliomas. *N. Engl. J. Med.* **372**, 2481–2498 (2015).

142. McKenna, A. *et al.* The Genome Analysis Toolkit: a MapReduce framework for analyzing next-generation DNA sequencing data. *Genome Res.* **20**, 1297–1303 (2010).

143. Li, H. & Durbin, R. Fast and accurate long-read alignment with Burrows-Wheeler transform. *Bioinformatics* **26**, 589–595 (2010).

144. Wang, K., Li, M. & Hakonarson, H. ANNOVAR: functional annotation of genetic variants from high-throughput sequencing data. *Nucleic Acids Res.* **38**, e164 (2010).

145. Hernandez-Ferrer, C. *et al.* affy2sv: an R package to pre-process Affymetrix CytoScan HD and 750K arrays for SNP, CNV, inversion and mosaicism calling. *BMC Bioinformatics* **16**, 167 (2015).

146. Wang, K. *et al.* PennCNV: an integrated hidden Markov model designed for high-resolution copy number variation detection in whole-genome SNP genotyping data. *Genome Res.* **17**, 1665–1674 (2007).

147. Sun, W. T. genoCN: genotyping and copy number study tools. In. R package version 1.28.0. (2010).

148. Mayrhofer, M., Viklund, B. & Isaksson, A. Rawcopy: Improved copy number analysis with Affymetrix arrays. *Sci Rep* **6**, (2016).

149. Derfus, G. E. *et al.* Cell culture monitoring via an auto-sampler and an integrated multi-functional off-line analyzer. *Biotechnol. Prog.* **26**, 284–292 (2010).

150. Thai, M. *et al.* Adenovirus E4ORF1-induced MYC activation promotes host cell anabolic glucose metabolism and virus replication. *Cell Metab.* **19**, 694–701 (2014).

151. Thai, M. *et al.* MYC-induced reprogramming of glutamine catabolism supports optimal virus replication. *Nat Commun* **6**, 8873 (2015).

152. Visnyei, K. *et al.* A molecular screening approach to identify and characterize inhibitors of glioblastoma stem cells. *Mol. Cancer Ther.* **10**, 1818–1828 (2011).

153. Wan, X. S., Zhou, Z. & Kennedy, A. R. Adaptation of the dichlorofluorescein assay for detection of radiation-induced oxidative stress in cultured cells. *Radiat. Res.* **160**, 622–630 (2003).

154. Yang, J. *et al.* Targeting PI3K in cancer: mechanisms and advances in clinical trials. *Mol. Cancer* **18**, 26 (2019).

155. Mecca, C., Giambanco, I., Donato, R. & Arcuri, C. Targeting mTOR in Glioblastoma: Rationale and Preclinical/Clinical Evidence. *Dis. Markers* **2018**, 9230479 (2018).

156. Tateishi, K. *et al.* Myc-Driven Glycolysis Is a Therapeutic Target in Glioblastoma. *Clin. Cancer Res.* **22**, 4452–4465 (2016).

157. Tanaka, K. *et al.* Compensatory glutamine metabolism promotes glioblastoma resistance to mTOR inhibitor treatment. *J. Clin. Invest.* **125**, 1591–1602 (2015).

158. Liu, D. D. *et al.* Effects of inhibiting PI3K-Akt-mTOR pathway on lipid metabolism homeostasis in goose primary hepatocytes. *Animal* **10**, 1319–1327 (2016).

159. Woolf, E. C., Syed, N. & Scheck, A. C. Tumor Metabolism, the Ketogenic Diet and β-Hydroxybutyrate: Novel Approaches to Adjuvant Brain Tumor Therapy. *Front Mol Neurosci* **9**, 122 (2016).

160. Molenaar, R. J., Maciejewski, J. P., Wilmink, J. W. & van Noorden, C. J. F. Wild-type and mutated IDH1/2 enzymes and therapy responses. *Oncogene* **37**, 1949–1960 (2018).

161. Núñez, F. J. *et al.* IDH1-R132H acts as a tumor suppressor in glioma via epigenetic up-regulation of the DNA damage response. *Sci Transl Med* **11**, (2019).

162. Vidali, S. *et al.* Mitochondria: The ketogenic diet--A metabolism-based therapy. *Int. J. Biochem. Cell Biol.* **63**, 55–59 (2015).

163. Rieger, J. *et al.* ERGO: a pilot study of ketogenic diet in recurrent glioblastoma. *Int. J. Oncol.* **44**, 1843–1852 (2014).

164. Nagarajan, A., Malvi, P. & Wajapeyee, N. Oncogene-directed alterations in cancer cell metabolism. *Trends Cancer* **2**, 365–377 (2016).

165. Guo, D. *et al.* EGFR signaling through an Akt-SREBP-1-dependent, rapamycin-resistant pathway sensitizes glioblastomas to antilipogenic therapy. *Sci Signal* **2**, ra82 (2009).

166. Yecies, J. L. *et al.* Akt stimulates hepatic SREBP1c and lipogenesis through parallel mTORC1-dependent and independent pathways. *Cell Metab.* **14**, 21–32 (2011).

167. Guo, D., Bell, E. H., Mischel, P. & Chakravarti, A. Targeting SREBP-1-driven lipid metabolism to treat cancer. *Curr. Pharm. Des.* **20**, 2619–2626 (2014).

168. Ricoult, S. J. H., Yecies, J. L., Ben-Sahra, I. & Manning, B. D. Oncogenic PI3K and K-Ras stimulate de novo lipid synthesis through mTORC1 and SREBP. *Oncogene* **35**, 1250–1260 (2016).

169. Sayre, N. L. *et al.* Stimulation of astrocyte fatty acid oxidation by thyroid hormone is protective against ischemic stroke-induced damage. *J. Cereb. Blood Flow Metab.* **37**, 514–527 (2017).

170. Spector, R. Fatty acid transport through the blood-brain barrier. *J. Neurochem.* **50**, 639–643 (1988).

171. Silver, I. A. & Erecińska, M. Extracellular glucose concentration in mammalian brain: continuous monitoring of changes during increased neuronal activity and upon limitation in oxygen supply in normo-, hypo-, and hyperglycemic animals. *J. Neurosci.* **14**, 5068–5076 (1994).

172. Skinner, R., Trujillo, A., Ma, X. & Beierle, E. A. Ketone bodies inhibit the viability of human neuroblastoma cells. *J. Pediatr. Surg.* **44**, 212–216; discussion 216 (2009).

173. Seyfried, T. N., Sanderson, T. M., El-Abbadi, M. M., McGowan, R. & Mukherjee, P. Role of glucose and ketone bodies in the metabolic control of experimental brain cancer. *Br. J. Cancer* **89**, 1375–1382 (2003).

174. Yang, C. *et al.* Glioblastoma cells require glutamate dehydrogenase to survive impairments of glucose metabolism or Akt signaling. *Cancer Res.* **69**, 7986–7993 (2009).

175. Buzzai, M. *et al.* The glucose dependence of Akt-transformed cells can be reversed by pharmacologic activation of fatty acid beta-oxidation. *Oncogene* **24**, 4165–4173 (2005).

176. Ye, F. *et al.* Protective properties of radio-chemoresistant glioblastoma stem cell clones are associated with metabolic adaptation to reduced glucose dependence. *PLoS ONE* **8**, e80397 (2013).

177. Salzillo, T. C. *et al.* Interrogating Metabolism in Brain Cancer. *Magn Reson Imaging Clin N Am* **24**, 687–703 (2016).

178. Weber, D. D., Aminazdeh-Gohari, S. & Kofler, B. Ketogenic diet in cancer therapy. *Aging (Albany NY)* **10**, 164–165 (2018).

179. Zhang, Y., Xu, J., Zhang, K., Yang, W. & Li, B. The Anticonvulsant Effects of Ketogenic Diet on Epileptic Seizures and Potential Mechanisms. *Curr Neuropharmacol* **16**, 66–70 (2018).

180. Youngson, N. A., Morris, M. J. & Ballard, J. W. O. The mechanisms mediating the antiepileptic effects of the ketogenic diet, and potential opportunities for improvement with metabolism-altering drugs. *Seizure* **52**, 15–19 (2017).

181. Simeone, T. A., Matthews, S. A., Samson, K. K. & Simeone, K. A. Regulation of brain PPARgamma2 contributes to ketogenic diet anti-seizure efficacy. *Exp. Neurol.* **287**, 54–64 (2017).

182. Lussier, D. M. *et al.* Enhanced immunity in a mouse model of malignant glioma is mediated by a therapeutic ketogenic diet. *BMC Cancer* **16**, 310 (2016).

183. Meidenbauer, J. J., Ta, N. & Seyfried, T. N. Influence of a ketogenic diet, fish-oil, and calorie restriction on plasma metabolites and lipids in C57BL/6J mice. *Nutr Metab (Lond)* **11**, 23 (2014).

184. Schwartz, K. *et al.* Treatment of glioma patients with ketogenic diets: report of two cases treated with an IRB-approved energy-restricted ketogenic diet protocol and review of the literature. *Cancer Metab* **3**, 3 (2015).

185. Zuccoli, G. *et al.* Metabolic management of glioblastoma multiforme using standard therapy together with a restricted ketogenic diet: Case Report. *Nutr Metab (Lond)* **7**, 33 (2010).

186. Nebeling, L. C., Miraldi, F., Shurin, S. B. & Lerner, E. Effects of a ketogenic diet on tumor metabolism and nutritional status in pediatric oncology patients: two case reports. *J Am Coll Nutr* **14**, 202–208 (1995).

187. Maroon, J. C., Seyfried, T. N., Donohue, J. P. & Bost, J. The role of metabolic therapy in treating glioblastoma multiforme. *Surg Neurol Int* **6**, 61 (2015).

188. Gopal, K., Grossi, E., Paoletti, P. & Usardi, M. LIPID COMPOSITION OF HUMAN INTRACRANIAL TUMORS: A BIOCHEMICAL STUDY. *Acta Neurochir (Wien)* **11**, 333–347 (1963).

189. Tugnoli, V. *et al.* Characterization of lipids from human brain tissues by multinuclear magnetic resonance spectroscopy. *Biopolymers* **62**, 297–306 (2001).

190. Srivastava, N. K., Pradhan, S., Gowda, G. A. N. & Kumar, R. In vitro, high-resolution 1H and 31P NMR based analysis of the lipid components in the tissue, serum, and CSF of the patients with primary brain tumors: one possible diagnostic view. *NMR Biomed* **23**, 113–122 (2010).

191. Mashimo, T. *et al.* Acetate is a bioenergetic substrate for human glioblastoma and brain metastases. *Cell* **159**, 1603–1614 (2014).

192. Fraser, D. D. *et al.* Elevated polyunsaturated fatty acids in blood serum obtained from children on the ketogenic diet. *Neurology* **60**, 1026–1029 (2003).

193. Taha, A. Y., Ryan, M. A. A. & Cunnane, S. C. Despite transient ketosis, the classic high-fat ketogenic diet induces marked changes in fatty acid metabolism in rats. *Metab. Clin. Exp.* **54**, 1127–1132 (2005).

194. Laks, D. R. *et al.* Neurosphere formation is an independent predictor of clinical outcome in malignant glioma. *Stem Cells* **27**, 980–987 (2009).

195. Divakaruni, A. S., Paradyse, A., Ferrick, D. A., Murphy, A. N. & Jastroch, M. Analysis and interpretation of microplate-based oxygen consumption and pH data. *Meth. Enzymol.* **547**, 309–354 (2014).

196. Divakaruni, A. S. *et al.* Thiazolidinediones are acute, specific inhibitors of the mitochondrial pyruvate carrier. *Proc. Natl. Acad. Sci. U.S.A.* **110**, 5422–5427 (2013).

197. Borch, L. *et al.* Normal Levels of Plasma Free Carnitine and Acylcarnitines in Follow-Up Samples from a Presymptomatic Case of Carnitine Palmitoyl Transferase 1 (CPT1) Deficiency Detected Through Newborn Screening in Denmark. *JIMD Rep* **3**, 11–15 (2012).

198. Cunnane, S. C. *et al.* Plasma and brain fatty acid profiles in mild cognitive impairment and Alzheimer's disease. *J. Alzheimers Dis.* **29**, 691–697 (2012).

199. Jensen, M. D., Haymond, M. W., Rizza, R. A., Cryer, P. E. & Miles, J. M. Influence of body fat distribution on free fatty acid metabolism in obesity. *J. Clin. Invest.* **83**, 1168–1173 (1989).

200. Azzam, E. I., Jay-Gerin, J.-P. & Pain, D. Ionizing radiation-induced metabolic oxidative stress and prolonged cell injury. *Cancer Lett.* **327**, 48–60 (2012).

201. Schmidt-Schweda, S. & Holubarsch, C. First clinical trial with etomoxir in patients with chronic congestive heart failure. *Clin. Sci.* **99**, 27–35 (2000).

202. Gugiatti, E. *et al.* A reversible carnitine palmitoyltransferase (CPT1) inhibitor offsets the proliferation of chronic lymphocytic leukemia cells. *Haematologica* **103**, e531–e536 (2018).